2014

PREDICTION OF STRUCTURE BORNE NOISE RADIATION AND PROPAGATION FROM OFFSHORE IMPACT PILE DRIVING

Huikwan Kim
University of Rhode Island, hkkim524@my.uri.edu

PREDICTION OF STRUCTURE BORNE NOISE RADIATION AND PROPAGATION FROM OFFSHORE IMPACT PILE DRIVING

BY

HUIKWAN KIM

A DISSERTATION SUBMITTED IN PARTIAL FULFILLMENT OF THE

REQUIREMENTS FOR THE DEGREE OF

DOCTOR OF PHILOSOPHY

IN

OCEAN ENGINEERING

UNIVERSITY OF RHODE ISLAND

2014

DOCTOR OF PHILOSOPHY IN OCEAN ENGINEERING DISSERTATION

OF

HUIKWAN KIM

APPROVED:

Dissertation Committee:

Major Professor JAMES H. MILLER

GOPU R. POTTY

DAVID G. TAGGART

NASSER H. ZAWIA

DEAN OF THE GRADUATE SCHOOL

UNIVERSITY OF RHODE ISLAND

2014

ABSTRACT

This study investigates prediction of structure borne noise radiation and propagation from offshore impact pile driving in shallow water environment. Noise generated by offshore impact pile driving radiates into and propagates through the air, water, and sediment medium. Predicting noise levels around the pile structure at sea is required to estimate the effects of the noise and vibration on marine life. This study used one of the commercial FE (Finite Element) code Abaqus 6.11 to calculate harmonic and transient response of the offshore wind turbine support structure and associated acoustic pressure amplitudes due to hydraulic hammer impact on top. First of all, the study focuses on long range prediction of acoustic pressure by utilizing the results from FE model to existing parabolic equation model as its starting field. In addition to numerical approach, a simple analytical solution has been developed based on the theory of free and forced vibration of thin cylindrical shell. It is useful to calculate structural response by inputting basic pile design parameters such as length, radius and material properties instead of developing numerical models. Then the study numerically investigated effects of noise and vibration along the water – ocean bottom interface because many benthic animals live on the seabed. The ocean bottom for this study was considered as elastic medium which supports propagation of shear and interface waves in addition to compressional waves. Finally, it is important how much we can reduce the noise to protect biological damages on marine life. This study quantitatively predicted noise attenuation of air bubble curtain by putting small size air bubbles in the water column.

ACKNOWLEDGEMENTS

I remember the moment Professor Miller and Potty suggested that we can work together for structure borne noise radiation and propagation as a pure scientific research topic. It was great opportunity handling acoustic-structure interaction problems because other professors in the Department have different interests in their field. My advisors drew a big picture in their mind and showed me how to make it successful by myself. Their insight for engineering problems made me surprised. This approach changed me actively investigate my topic and my advisors always respect any results from study even if it didn't look good to me. Whenever I finished meeting with them, I felt more responsibility and became independent. Frankly, I am used to following my senior officer's specific instruction and didn't try to do it better than his instruction. I became more creative as time spent with my advisors is increasing. This is big change in my mind in addition to the results of the study. Above all, I have obtained a capability to predict structure borne noise radiation and propagation in the ocean using numerical models while I have been doing so many trials of modeling and calculation. The understanding of acoustic-structure interaction problem from this study will be applicable to more practical problems of interest in the future.

I appreciate Kevin Smith and Georges Dossot in regard to technical support for long range propagation model, MMPE (Monterey-Miami Parabolic Equation). Kevin Smith suggested long range prediction of impact pile driving noise when I was presenting my first ASA (Acoustical Society of America) speech in San Diego. Georges Dossot helped me to modify the standard MMPE model for my study of interest.

I like to thank for Martin Sadd and David Taggart in regard to finite element modeling of impact pile driving in the ocean. Their courses were very helpful understanding wave propagation in continuous media and theoretical background of finite element model. David Taggart provided commercial finite element code Abaqus/CAE 6.11 (research license).

I appreciate financial supports from the Republic of Korea Navy, The Link Foundation Ocean Engineering & Instrumentation PhD Fellowship, and stipend from my advisors. Especially, I appreciate the Dean of Engineering, Raymond Wright who significantly helped me not to miss the Link Foundation Fellowship at the last minute.

In addition, I am happy to take many courses from Peter Stepanishen who taught underwater acoustics approximately 40 years in the University of Rhode Island. He was also my advisor before he decided to retire. I learned a lot for the fundamentals of sound and vibration which have been building blocks for this study.

Personally, I like Stephan Grilli even though he is strict in his lab or classroom because I know he is very generous and humane in person. I am motivated from his life actively doing research in his field and showing strong family bonds off his office building. I also like Gail Palino because she always told me something on my side and was trying to help me as possible as she can. She has really warm heart and is very generous to everybody. She is a treasure in the Department of Ocean Engineering.

Moving on to off Campus, I really like to call Suk C Nam's family, Sangmin An, Myunga Kim, Jinhui Han, and Julia Baek who shared beautiful and unforgettable

memory each other in RI, U.S. I couldn't overcome difficulties without their help and affection. We laughed a lot and we shared a lot and we will do that lifelong.

Finally, I like to thank to my wife, Junghee and daughter, Garam. At the beginning of life here in the U.S., Garam was seriously injured and it was very difficult to live day by day with many concerns. However, we helped each other to make it better and better and Garam grows well just like a normal girl overcoming her weakness with strong and warm heart. Junghee did her best for Garam's rehabilitation and I really appreciate her effort. Now, I wish she can find something she wanted to do in South Korea. I also promise that I will put Junghee and Garam as the first priority during my rest of life. Happiness is not far away but just besides me.

For Junghee and Garam!

PREFACE

The following dissertation is intended in part for the fulfillment of the requirements set forth by the University of Rhode Island Graduate School and the Department of Ocean Engineering for the degree of Doctorate of Philosophy in Ocean Engineering. The purpose of this work is better understanding on structure borne noise due to offshore impact pile driving using theoretical approach and numerical tools.

This dissertation is presented in manuscript format. Section headings, references, figures, tables, and other formatting choices follow the American Institute of Physics Style Manual.

Manuscript I is written for the Journal of the Acoustical Society of America. It focuses upon prediction of offshore impact pile driving noise using the coupled FE-MMPE model. The coupled model compliments each model's strengths because the FE model effectively calculate harmonic structural response of the pile and associated complex acoustic pressure amplitude on the surface of the pile and the MMPE model uses the FE outputs as its starting field to calculate SEL (Sound Exposure Level) up to several kilometer ranges. The manuscript I presents details about each numerical model and coupling procedures and the RWI (Response Weighted Index).

Manuscript II is written in a format specific to the Journal of the Acoustical Society of America Express Letter (JASA-EL). This format is mandated to be brief, and limits the author to a figure and page count. The goal of this study is developing theoretical model for impact pile driving. It is motivated calculating structural response of the pile not in the FE modeling GUI environment but inputting basic pile design parameters because

any commercial FE codes need to be licensed and to know strong theoretical backgrounds for reliable modeling and simulation results. The manuscript II describes specific steps from Donnell's governing equations for thin cylindrical shell and radial displacement outputs due to impact loading as function of time and space.

Manuscript III is written in a format specific to the Journal of the Acoustical Society of America Express Letter (JASA-EL). The study verified the FE model with the measured data in the published paper and developed new FE model with the ocean bottom considered as an elastic material to investigate noise and vibration due to interface waves.

Manuscript IV is also written in a format specific to the Journal of the Acoustical Society of America Express Letter (JASA-EL). It focuses on noise mitigation technology against impact pile driving noise using modeling and simulation of air bubble curtain in the water column. The Manuscript IV is describing the relationship between the location of the air bubble curtain and received SEL.

TABLE OF CONTENTS

LIST OF TABLES

Manuscript I

Manuscript II

Manuscript III

Manuscript IV

LIST OF FIGURES

Manuscript I

Manuscript II

Manuscript III

Manuscript IV

Appendix B

MANUSCRIPT – I

Intended for submission to the Journal of the Acoustical Society of America

Predicting long range propagation of underwater radiated noise due to offshore impact pile driving

Corresponding Author:

Huikwan Kim

Department of Ocean Engineering, University of Rhode Island, Narragansett, Rhode Island 02882, hkkim524@my.uri.edu

Contributing Authors:

James H. Miller, Gopu R. Potty

Department of Ocean Engineering, University of Rhode Island, Narragansett, Rhode Island 02882

Abstract: Offshore wind turbines have been installed throughout Europe and are expected to be built in the United States waters shortly. Pile driving is required for the installation of offshore wind turbines in water depths as deep as 30 m. Noise generated by offshore impact pile driving radiates into and propagates through the air, water, and sediment medium. Predicting noise levels around the pile at sea is required to estimate the effects of the noise and vibration on marine life. This study focuses on long range propagation of acoustic pressure and particle velocity using the coupled FE (Finite Element) – MMPE (Monterey Miami Parabolic Equation) model. The FE model (commercial code Abaqus/CAE 6.11) calculates harmonic response of the complex acoustic pressure on the surface of the pile interacting with water and sediment acoustic medium. The MMPE model accepts the complex acoustic pressure at each frequency along the pile as its starting field and calculates complex acoustic pressure field in water and sediment.

PACS numbers: 43.30.Jx, 43.30.Nb

1.1 INTRODUCTION AND BACKGROUND

A. Introduction

Offshore wind turbines are being used by a number of countries to harness the energy of strong, consistent winds that are found over the oceans. In the United States, 53% of the nation's population lives in coastal areas, where energy costs and demands are high and land-based renewable energy resources are often limited. Abundant offshore wind resources have the potential to supply immense quantities of renewable energy to major U.S. coastal cities, such as New York City and Boston. Offshore winds tend to be higher speed and steadier than on land. The potential energy produced from wind is directly proportional to the cube of the wind speed. As a result, increased wind speeds of only a few kilometers per hour can produce significantly larger amount of electricity. For instance, a turbine at a site with an average wind speed of 25.7 km/h would produce 50% more electricity than at a site with the same turbine and average wind speeds of 22.5 km/h. This is one reason that developers are interested in pursuing offshore wind energy resources [1].

However, acoustic energy is created when impact pile driving is used to construct offshore wind turbine platforms and the sound travels into the water along different paths: 1. from the top of the pile where the hammer hits, through the air, into the water; 2. from the top of the pile, down the pile, radiating into the air while travelling down the pile, from air into water; 3. From the top of the pile, down the pile, radiating directly into the water from the length of pile below the waterline; 4. down the pile radiating into the ground, travelling through the ground and radiating back into the water. Acoustic energy arriving from different paths with different phase and time lags creates a pattern of

destructive and constructive interference near the pile and water- (and ground-) borne energy prevails further away from the pile. Noise increases with pile size (diameter and wall thickness) and hammer energy [2-4]. Radiated noise is also affected by environmental parameters in the ocean such as sound speed profile, bathymetry and ocean bottom properties. Figure 1.1 shows how the level increases as one pile is driven from start to end. The pressure amplitude is relatively low at the beginning of piling and it increases as the pile is driven harder into the bottom. A previous study compared the source spectra of anthropogenic sources and pile driving noise is quite intensive in comparison to the other sources except an air gun array [3] as shown in Figure 1.2. Thus, predicting noise levels around offshore support structures is required to estimate the anthropogenic noise impacts upon marine life.

B. Background

Betke et al [5] and De Jong et al [6] investigated underwater radiated noise due to offshore impact pile driving by using measurements Elmer et al [7] also measured data and presented several types of noise reduction techniques such as air bubble curtains, coated tubes as sound barriers etc. It is desirable to develop reliable numerical model to predict the noise for different size of piles and environmental parameters both for environmental assessment and for engineering new noise reduction techniques. Reinhall and Dahl [8-10] contributed significant amount of work on the investigation of impact pile driving noise in regard to numerical modeling using one of the commercial FE code (Comsol Multiphysics) and compared the model results with the measured data within the range of up to 15 m from the pile. This study follows up on their efforts by reproducing their FE model using another commercial FE code (Abaqus/CAE 6.11) [11, 12].

Fundamentals of finite element method and theoretical development of finite element equation for acoustic-structure interaction problem are described in Appendix A. The results of the FE model from this study have been compared with Reinhall and Dahl's measured data and have been presented and published as conference proceedings [13-15]. This study focuses on simulation of the pile driving noise at long ranges for different sizes of piles and environmental parameters such as bathymetry, sound speed profile in water and properties of the ocean bottom. The FE method is ideal for short range calculations of acoustic pressure from a complex structure, but it becomes computationally unsustainable when the size of the model is increased due to the mesh size requirement for longer ranges. To achieve long range prediction of the noise, the FE code alone has difficulties handling large number of degrees of freedom for the longer range numerical domain. It is also difficult to handle environmental inputs such as depth dependent sound speed profile or range dependent bathymetry. In contrast, the Parabolic Equation (PE) model is ideal for long-range propagation, once a starting field and environmental data can be adequately defined. The PE model can handle range dependence of the environmental parameters. The standard Monterey-Miami Parabolic Equation (MMPE) model accepts input files for source depth, array length, center frequency, frequency bandwidth and number of frequencies with other environmental input files. It is well suited for conventional SONAR (Sound and Navigation and Ranging) applications for the Navy. Details and derivation of PE model are described in Appendix B.

However, a structure-borne noise is space-dependent and broadband and it can't be represented as single point source or line array. To couple the frequency dependent FE

outputs to the frequency and depth dependent MMPE starting field, the Matlab scripts have been generated and the Standard MMPE code has been modified to input vertical complex acoustic pressure amplitudes from the FE model instead of generating default point or line source. The Matlab scripts enable to run broadband calculation for the MMPE model by accepting the complex acoustic pressure outputs from the FE model at each frequency. Post processing techniques are applied to calculate the peak SPL (Sound Pressure Level) in decibels reference to $1\mu Pa$ and SEL (Sound Exposure Level) which is the total energy level for the time duration or frequency band of interest in units of decibels reference to 1 μPa^2. The modified MMPE model [16] provides the output options for the vertical and horizontal component of particle velocity. It has the additional capability for investigating particle velocity outputs along the water and sediment interface.

Section 1.2 describes the procedures to implement the FE model using the commercial FE code Abaqus/CAE 6.11 and section 1.3 describes the results from the FE model. The section 1.4 describes the methodology to couple FE and MMPE model in detail and presents the results of broadband calculation of the modified MMPE model. Finally section 1.5 investigates environmental impact on marine life using the RWI (Response Weighted Index) for specific species of animals.

1.2 FINITE ELEMENT MODELING OF OFFSHORE IMPACT PILE DRIVING

A. Geometry

According to the Ocean SAMP (Special Area Management Plan) report [17, 18] the foundation pile for the initial development of the wind farm off Block Island, Rhode Island has a 1.8 m diameter and a 0.05 m wall thickness. The length of the pile below seabed was extended up to six times the diameter in the finite element analysis to ensure adequate soil-structure interaction in the design. Water depth 4.8 km off Block Island is approximately 26 m based on the bathymetry data [19]. Figure 1.3 shows the geometry which is modeled using the Abaqus/CAE 6.11 GUI (Graphic User Interface) and Figure 1.4 shows how this acoustic-structure interaction problem is modeled using the axisymmetric element available in Abaqus/CAE 6.11. To help understanding the axisymmetric model, it is compared with the 3D model. Axisymmetric elements provide for the modeling of bodies of revolution under axially symmetric loading conditions assuming that the hammer evenly strikes at the top of the pile. A body of revolution is generated by revolving a plane cross-section about an axis (the symmetry axis) and is readily described in cylindrical coordinates r, z and θ.

B. Material property

The FE model of the impact pile driving off Block Island, RI consists of three different materials such as steel, water and sediment. The steel is elastic medium defined by appropriate value of density (ρ), Young's modulus (E), and Poisson's ratio (ν). The water and sediment are considered as acoustic media defined by bulk modulus (K) and density (ρ). To set proper values of material parameters, the SSP (Sound Speed Profile) and bottom properties from a previous study [17] have been used. Figure 1.5 shows the SSP off Block Island, Rhode Island in August 2009. Overall, the SSP is decreasing with increasing depth. The FE model has difficulty applying this SSP. Hence, the material

properties corresponding to homogeneous water are defined with the mean of the SSP of 1,517.1 m/s. To achieve average SSP of 1,517.1 m/s for the FE model, the bulk modulus is set to 2.358 GPa with density of salt water 1,025 kg/m^3. In the acoustic medium, the compressional wave speed can be expressed in terms of bulk modulus (K) and density (ρ) as shown in equation (1.1).

$$C_p = \sqrt{\frac{K}{\rho}} \tag{1.1}$$

The compressional wave speed and density in the bottom are 1,580 m/s and 1,200 kg/m^3 respectively and the bulk modulus for the bottom is 2.995 GPa. Material properties are summarized in the Table 1.1

C. Mesh

Inadequate mesh refinement is the most common source of errors in acoustic and vibration analysis. For reasonable accuracy, at least six representative inter-nodal intervals of the acoustic mesh should fit into the shortest acoustic wavelength present in the analysis; accuracy improves substantially if ten or more inter-nodal intervals are used at the shortest wavelength. An "inter-nodal interval" is defined as the distance from a node to its nearest neighbor in an element; that is, the element size for a linear element or half of the element size for a quadratic element. At a fixed inter-nodal interval, quadratic elements are more accurate than linear elements. The level of refinement chosen for the acoustic medium should be reflected in the solid medium as well: the solid mesh should be sufficiently refined to accurately model flexural, compressional, and shear waves [18].

In this study the highest frequency of interest is 1,024 Hz and associated wave length with speed of sound 1517 m/s is 1.48 m. The minimum mesh size is determined as 0.25 m by dividing the shortest wavelength of interest. To get better accuracy, mesh size of 0.2 m and quadratic element is chosen in all over the computational domain. The quadratic elements make the inter-nodal intervals half (which is 0.1 m). Approximately 15 elements exist within the shortest wave length of 1.48 m.

D. Steady state dynamic analysis

Abaqus/CAE 6.11's steady-state dynamic analysis provides the steady-state amplitude and phase of the response of a system due to harmonic excitation at a given frequency. Such analysis is done as a frequency sweep by applying the loading at a series of different frequencies and recording the response. When defining a direct-solution steady-state dynamic step, it needs to specify the frequency ranges of interest and the number of frequencies at which results are required in each range (including the bounding frequencies of the range). The maximum frequency of interest for this study is 1,024 Hz and frequency spacing is 0.5 Hz and total number of frequency points is 2,048.

In addition, it is also required to specify the type of frequency spacing (linear or logarithmic) to be used [19]. It is possible to get field output variables of interest for the post processing of the results of simulation by setting the "Field Output Requests" in the "Step Module". The complex acoustic pressure, acoustic partible velocity field outputs are defined on top of the default field output setting. The SPL (Sound Pressure Level) for the complex acoustic pressure with reference pressure can be calculated using the post processing toolbox. In this acoustic structure interaction problem, only mechanical loading which is the hydraulic hammer impact applied on top of the pile is considered.

Any other loading conditions such as surface waves, current, and wind are not considered for this FE model analysis. The equation for transient impact pressure amplitude is available in a previous paper by Reinhall and Dahl [8].

$$p(t) = 2.1 \times 10^8 e^{-\frac{t}{0.004}} (Pa) \tag{1.2}$$

For the steady state dynamic analysis, it is necessary to provide Fourier transformed transient loading as indicated in equation (1.2)

$$P(f) = \int_{-\infty}^{\infty} p(t) e^{-j\omega t} dt \tag{1.3}$$

Figure 1.6 shows the transient hammer impact pressure loading (calculated using equation (1.2)) on top of the pile and its Fourier Transformed pressure amplitude as function of frequency. In the "Step module", steady state dynamic analysis has been set to compute complex response i.e. real and imaginary part of acoustic pressure on the surface of the pile. The linear scale is applied to get equally spaced frequency points. This setting enables the FE model to iteratively calculate harmonic response in the steel pile and water and sediment acoustic media at 2,048 frequency points with associated pressure amplitudes. To extract complex acoustic pressure on the surface of the pile, the nodes along the pile length in contact with water and sediment acoustic media are defined and they record frequency dependent complex pressure amplitude at each harmonic loading.

E. Interaction and constraint

A numerical boundary of each part is considered as rigid boundary which enables the waves approaching the boundary to be reflected. It is therefore necessary to set a PML

(Perfectly Matched Layer) along the edge of the numerical boundary of water and sediment medium. It is also possible to use non-reflecting acoustic impedance available in the "Interaction Module". For the acoustic-structure interaction problem, it is important to define constraint to share the same outputs between the nodes on the structure and acoustic medium. Surface-based tie constraints can be used to make the translational and rotational motion as well as all other active degrees of freedom equal for a pair of surfaces. By default, nodes are tied only where the surfaces are close to one another. One surface in the constraint is designated to be the slave surface; the other surface is the master surface [20].

1.3 THE RESULT OF FINITE ELEMENT MODEL

A. FE outputs

It is possible to compute many different types of field/history outputs depending on the setting of "Field output request" and "History output request" in the step module. Abaqus/CAE 6.11 generates field output from data that are spatially distributed over the entire model or over a portion of it. The field output data using deformed shape, contour, or symbol plots can be viewed in the "Visualization module". Abaqus/CAE 6.11 writes every component of the selected variables to the output database [24]. For this study, complex acoustic pressure and acoustic particle velocity field outputs were added in addition to the default parameters of interest such as stress, strain, displacement/velocity/acceleration, and forces/reactions. Abaqus/CAE 6.11 generates history output from data at specific points in a model. The history output using X–Y plots can be displayed in the Visualization module [24]. To record complex acoustic pressure

on the 185 nodes along the pile, the history output request is set to record complex acoustic pressure on the pre-defined nodes sets.

The magnitudes of acoustic pressure field outputs for the frequencies of 108, 436, 480, 960 Hz are shown in Figure 1.7. These are a few examples out of 2048 field outputs. The acoustic energy inside pile is high compared to outside pile in water and bottom but it is observed that large enough acoustic pressure are radiated. Harmonic loading of lower frequency such as 108 Hz excites lower mode of pile structure coupled with acoustic media. As the frequency of harmonic loading is increasing, the coupled system's higher mode is excited. Acoustic pressure radiates along the horizontal direction. It is also possible to present horizontal and vertical components of acoustic particle velocity. Overall, we observed that the horizontal component of particle velocity reflects the field output of acoustic pressure. Contribution of vertical component of particle velocity is relatively small.

The goal of developing the FE model is to generate starting field for widely used long range propagation model, the MMPE, because of limitation of the FE model running large numerical domain due to restriction of mesh size requirement and difficulties inputting SSP data. To generate the MMPE starting field at each frequency, complex acoustic pressure along the pile from FE results are used as starting field in the MMPE propagation model. The frequency and depth dependent complex pressure source instead of conventional point or line source should be fit into the MMPE staring field.

B. Generation of acoustic pressure field for MMPE starting field

The MMPE model contains numerical domain larger than the FE model. It is necessary to extend the FE model output to fit into the MMPE model domain. Figure 1.8 shows the examples of FE outputs and associated MMPE starting field. The real and imaginary part of acoustic pressure amplitude along the pile length in water and sediment from the FE model for 100 Hz and 1024 Hz used to generate the MMPE starting field using Matlab Script. For the broadband complex acoustic pressure calculation, the frequency and space dependent starting fields are iteratively input as starting field for the MMPE's range marching algorithm. The frequency band of interest is identified from the result of the plot for the spatial average of the magnitude of complex acoustic pressure on the surface of the pile. Figure 1.9 shows the spectrum of spatial average of the magnitudes of the complex acoustic pressure defined by the equation (1.4).

$$\overline{P_i(f)} = \frac{1}{N}\sum_{i=1}^{N}|P_i(f)| \tag{1.4}$$

where, N=184 (total number of nodes on the pile)

A few dominant frequencies for the system of the pile structure interacting with water and bottom media are labeled as 108 Hz, 436 Hz, 480 Hz, and 960 Hz. To cover these dominant frequencies, the frequency band of the MMPE model is set to 55 Hz ~ 1,024 Hz.

1.4 MMPE MODELING

A. Input files

The input files can be classified as main input file (pefiles.inp), environmental data (pessp.inp, pebath.inp, pebotprop.inp, pedbath.inp, pedbotprop.inp), and source data (pesrc.inp). The main input file reads all other input files for the environmental and

source data and defines numerical domain of the MMPE model such as range and depth etc. Specific details about input file are described in the webpage [25]. The sound speed profile off Block Island, RI obtained in August 2009 and bottom property data as a part of Ocean SAMP project is used for the environmental input files (pessp.inp, pebotprop.inp, pedbotprop.inp). The SSP is shown in Figure 1.5. In regard to bathymetry, flat bottom with water depth 26 m is considered for the environmental input file. The range is 3 km and depth is 136.6 m for the MMPE numerical domain (pefiles.inp). The depth of the FE model and the MMPE model are different and it is necessary to generate the MMPE starting field by extending the FE complex acoustic pressure with zero padding up to 136.6 m shown in Figure 1.8.

B. The coupled FE-MMPE model

The goal of this study is to investigate the long range propagation from structure borne noise and vibration. It is required to input complex acoustic pressure at each frequency along the pile as a starting field for the MMPE. The standard MMPE model generates vertical complex acoustic pressure field in water as a starting field which can be defined in the input file (pesrc.inp). The structure-borne noise cannot be represented by simple point or line source and thus it is necessary to input frequency dependent vertical acoustic pressure amplitude obtained from the result of FE steady state dynamic analysis. In addition, this study focuses on the broadband analysis for the frequency band of 55 Hz ~ 1024 Hz with 0.5 Hz frequency spacing. It is necessary to run 1,938 iterative model runs inputting starting field (pesrc.inp) at each frequency and saving the range and depth dependent complex pressure outputs for post-processing. This study modified the MMPE input files and developed post processing Matlab Script files to accomplish

broadband calculation. The modified code enables the iterative broadband analysis with a single run. The standard MMPE calculates TL (Transmission Loss) in dB re 1m and it displays relative level in the field compared to source level. The coupled FE-MMPE model accepts actual complex pressure amplitude from the FE model as its starting field and calculates complex pressure in the field.

1.5 THE RESULT OF THE MMPE MODEL

A. acoustic pressure in water and bottom

The standard MMPE model calculates complex pressure field outputs in the domain of interest. A few example plots for the SPL in dB re 1μPa are shown in Figure 1.10 for the four dominant frequencies. Figure 1.10shows the SPL of approximately 200 dB re 1μPa close to the pile. This study mainly focuses on the range and depth dependent total energy and peak response in the frequency band from 55 Hz to 1024 Hz along water-sediment interface because benthic species such as ground fish and lobsters are living on the seabed. The total energy in the frequency band, SEL (Sound Exposure Level) in dB re 1μPa^2 can be approximated by the sum of the magnitude squared of complex acoustic pressure multiplied by frequency spacing.

$$SEL = 10\log_{10}\left(\frac{\int_{55}^{1024}|P(f)|^2 df}{{P_{ref}}^2}\right) = 10\log_{10}\left(\frac{\sum_{n=1}^{N}|P_n(f)|^2 \times df}{{P_{ref}}^2}\right) \quad (1.5)$$

Figure 1.11 shows cumulative SEL field outputs in dB re 1μPa^2 as function of depth and range and it is observed that the SEL remains high in the water column which means acoustic energy generated by offshore impact pile driving propagates in water and top of the bottom. The depth dependent SEL data are extracted at four different depths including

water-bottom interface as shown in Figure 1.12. The energy level at the mid-depth and the water-bottom interface are relatively high. Quantitatively, the SEL along water-bottom interface is higher than 200 dB re $1\mu Pa^2$ within 40 m from the piling spot and the SEL at mid-water depth at range 3 km is 167 dB re $1\mu Pa^2$ which is higher than general shipping noise levels.

The range dependent SEL enables to predict RWI (Response Weighted Index) with an input of the number of strikes of piling. RWI attempts to model the biological effects of pile driving. The effects of the intense noise on Chinook salmon which has a swim bladder have been investigated by Halvorsen et al [21]. In this case, we applied the RWI salmon paradigm to the one of the benthic animal, flounder because no published work on this species. The RWI in equation (1.6) ranges from 1 (mild trauma) to 3 (moderate injury) to 5 (mortal injury, dead within an hour) and higher.

$$\text{RWI} = \exp(-30.050 + 0.149 \times SEL - 0.000171 \times N_{strikes}) - 1 \qquad (1.6)$$

Specifically, physiological impact of each observed injury was assessed and then assigned to weighted trauma categories [21, 22]. The mortal trauma category, weighted 5, included injuries that were severe enough to lead to death. The moderate trauma category, weighted 3, included injuries likely to have an adverse impact on fish health but might not lead directly to mortality. Finally, mild trauma category, weighted 1, referred to injuries of minimal to no physiological cost to fish.

Figure 1.13 shows RWI along the water-bottom interface predicted as a function of range from the pile installation for 960 and 1920 pile strikes. These number of strikes

were used in Halvorsen et al work [21]. The range to the mortality RWI is about 250 m for 960 pile strikes and 300 m for 1920 pile strikes.

In addition the range to morality RWI, it is necessary to investigates effects of marine life by peak acoustic pressure. The peak response in equation (1.7) is obtained by taking inverse Fourier Transform of the frequency dependent complex acoustic pressure.

$$p(t)_{peak} = max\left|\int_{55}^{1024} P(f)e^{j2\pi ft}df\right| \tag{1.7}$$

$$SPL_{peak} = 20\log_{10}\left(\frac{p(t)_{peak}}{P_{ref}}\right) \tag{1.8}$$

Figure 1.14 shows the Peak SPL (dB re 1μPa) as function of range compared with SEL (dB re 1μPa^2). The peak SPL is approximately 10 dB higher than the SEL which means marine life are instantaneously exposed to 10 dB higher acoustic pressure when the first arrival of Mach wave [8] approaches them. Quantitatively, 200 dB re 1μPa within the range approximately 250 m on marine life can cause serious injury due to the impact pile driving.

B. Particle velocity along water bottom interface

The MMPE model is capable of calculating horizontal and vertical component of acoustic particle velocity in addition to the acoustic pressure. This study can be extended to explore the effects of vertical component of particle velocity. This can be achieved by using the binary files, apvr.bin (acoustic particle velocity – radial direction) or apvz.bin (acoustic particle velocity – vertical direction) from the MMPE result at each frequency. Figure 1.15 shows the comparison between horizontal and vertical component of particle

velocities. The MMPE model does not support shear and interface waves in the bottom because the bottom is considered as an equivalent acoustic medium. In practice, impact pile driving can generate shear waves in the bottom and Sholte waves along the water-bottom interface in addition to the compressional waves propagating along the radial direction. The MMPE model only calculates vertical/horizontal component of particle velocity which act on marine life on the sea floor contributed by compressional waves. It is necessary to investigate the effects by the other wave types.

1.6 CONCLUSIONS

We have successfully coupled a FE model to the MMPE model by incorporating the starting field from the FE model into the MMPE model. The coupled FE-MMPE model is advantageous because the FE and the MMPE model compliment their strength. The FE model is ideal for short range calculation of complex acoustic pressure from the complex structure. For this study, we used a simple hollow pile for the structure but it is possible to do similar analysis by importing 3D CAD model of offshore structures or ships for further application. However, the FE model becomes computationally unsustainable when the size of the model is increased due to the mesh size requirement for longer range. The FE model itself has difficulties modeling inhomogeneous acoustic medium reflecting a measured SSP in the water column. In contrast, the MMPE model is ideal for long range propagation, once a starting field can be adequately defined. It is also easy to apply measured SSP and bathymetry data in the model. However the standard MMPE model only accept point or line source with source depth in water which is different from frequency and space dependent structure borne source.

We modeled the coupled FE-MMPE model for offshore impact pile driving off Block Island RI where five jacket type offshore wind farms are planned to be constructed shortly. We assumed that the pile with the length 46.8 m, the radius 1.8 m, and the thickness 0.05 m is driven to 10.8 m in the bottom. The FE axisymmetric element makes the model computationally efficient assuming the loading the associated responses have no variation along azimuthal direction. One of the commercial FE code, Abaqus/CAE 6.11's steady state dynamic analysis calculates complex acoustic pressure along the length of the pile in contacted with water and bottom acoustic medium. The frequency band for the FE model spanned 1Hz-1024Hz with 0.5Hz frequency spacing. The frequency dependent exponentially decaying pressure amplitudes are applied at each frequency using frequency sweep method. The loading is Fourier Transformed transient impact pressure model developed by Reinhall and Dahl. The FE results on the surface of the pile are considered as source in the MMPE numerical domain. The associated starting fields for the source at each frequency are inputted with other input field in the MMPE model. The MMPE model calculates complex acoustic pressure in the predefined numerical domain and we applied post processing techniques to get range dependent SEL and peak SPL to predict what range will be seriously affected by the offshore impact pile driving. From our mortality RWI plot, we can expect marine life within the range 250 m from piling location are exposed to intensive noise and vibration. It is generally known that the amplitude of shear and interface waves are larger than compressional waves. The ocean bottom maintains rigidity to support shear waves in the bottom and interface waves along the water – bottom interface. We investigated vertical component of particle velocity along the interface which is small compare to horizontal component of particle

velocity because there is only contribution by compressional waves. In reality, the vertical velocity by interface waves is higher than the results from the MMPE model only. It is necessary to explore the effects on marine life due to interface waves propagating along the water-bottom interface in the future.

ACKNOWLEDGEMENTS

I would like to acknowledge the financial support of the Republic of Korea Navy and the Link Foundation Ocean Engineering and Instrumentation PhD Fellowship Program which enabled me to carry out this work at the University of Rhode Island.

TABLES

Table 1.1 Material properties of the FE model

Parameters	Water	Bottom	Steel
Density ($\rho, kg/m^3$)	1,025	1,200	7900
Bulk Modulus (K, GPa)	2.358	2.995	-
Young's Modulus (E, GPa)	-	-	200
Poisson's Ratio(ν)	-	-	0.3

FIGURES

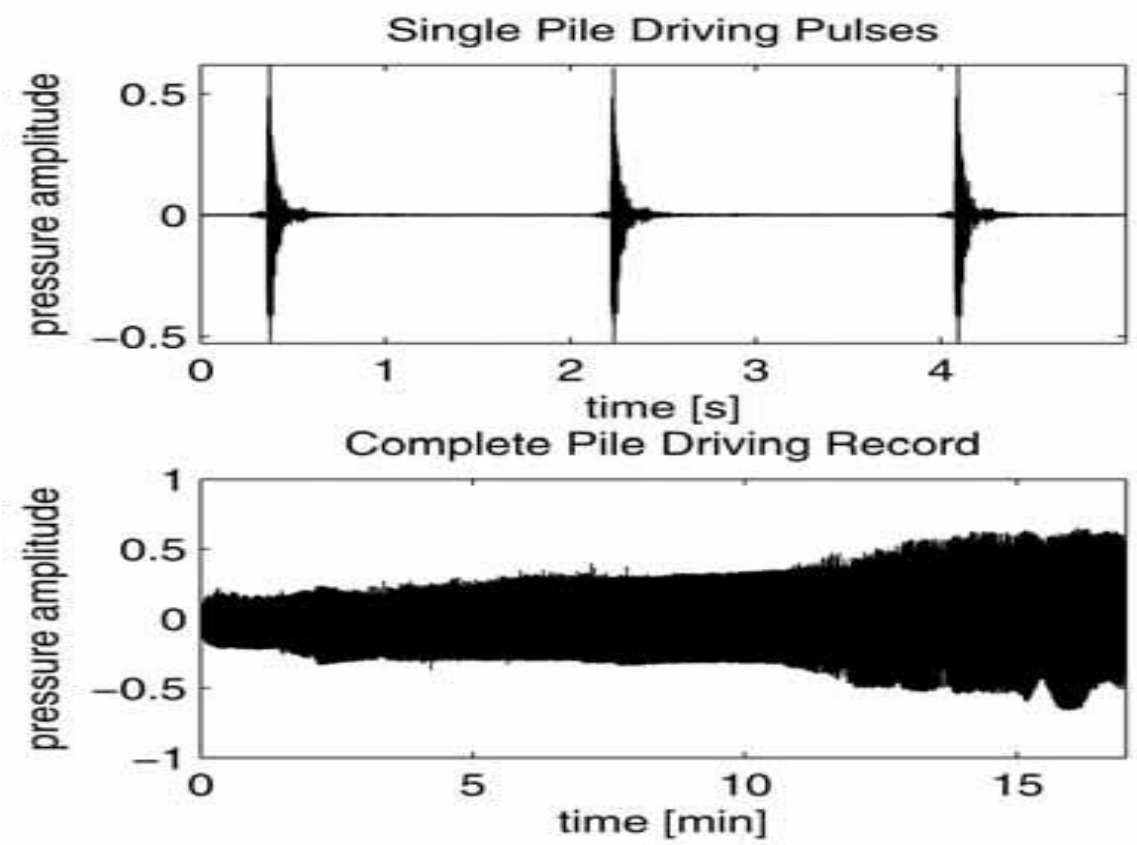

Figure 1.1 **Waveform of impact pile driving recorded at 320 m range. Water depth 3 m, hollow steel pile, diameter 0.8 m, wall thickness 1.3 cm, driven to 25 m below ground, into sandstone bedrock, hydraulic hammer of 12 ton weight and 180 kJ energy rating [2].**

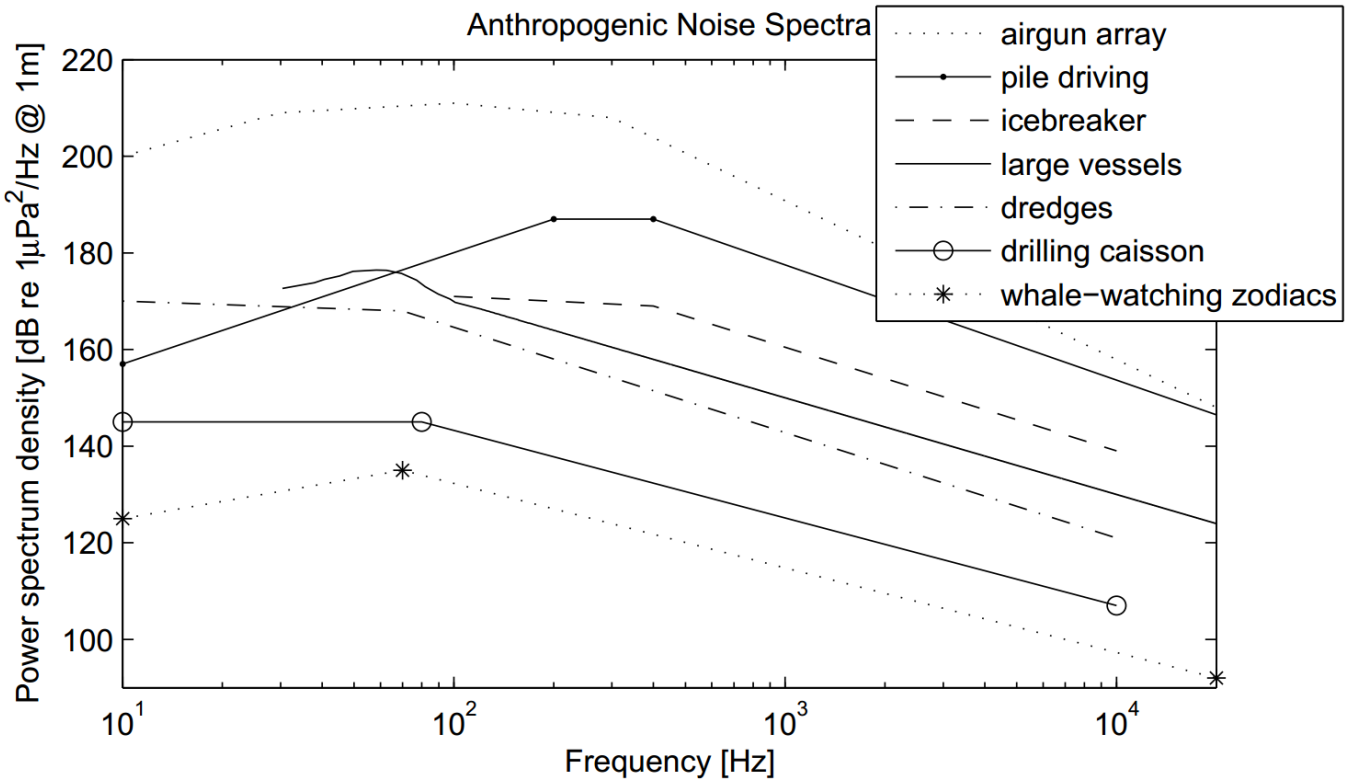

Figure 1.2 **Source spectra of anthropogenic noise source in the ocean. The power spectral density for the airgun array (dotted line) shows the highest level and the one for pile driving keeps level high for approximate frequency band 100 Hz to 1000 Hz. The other power spectrums for shipping are relatively small compared to airgun array and pile driving [2].**

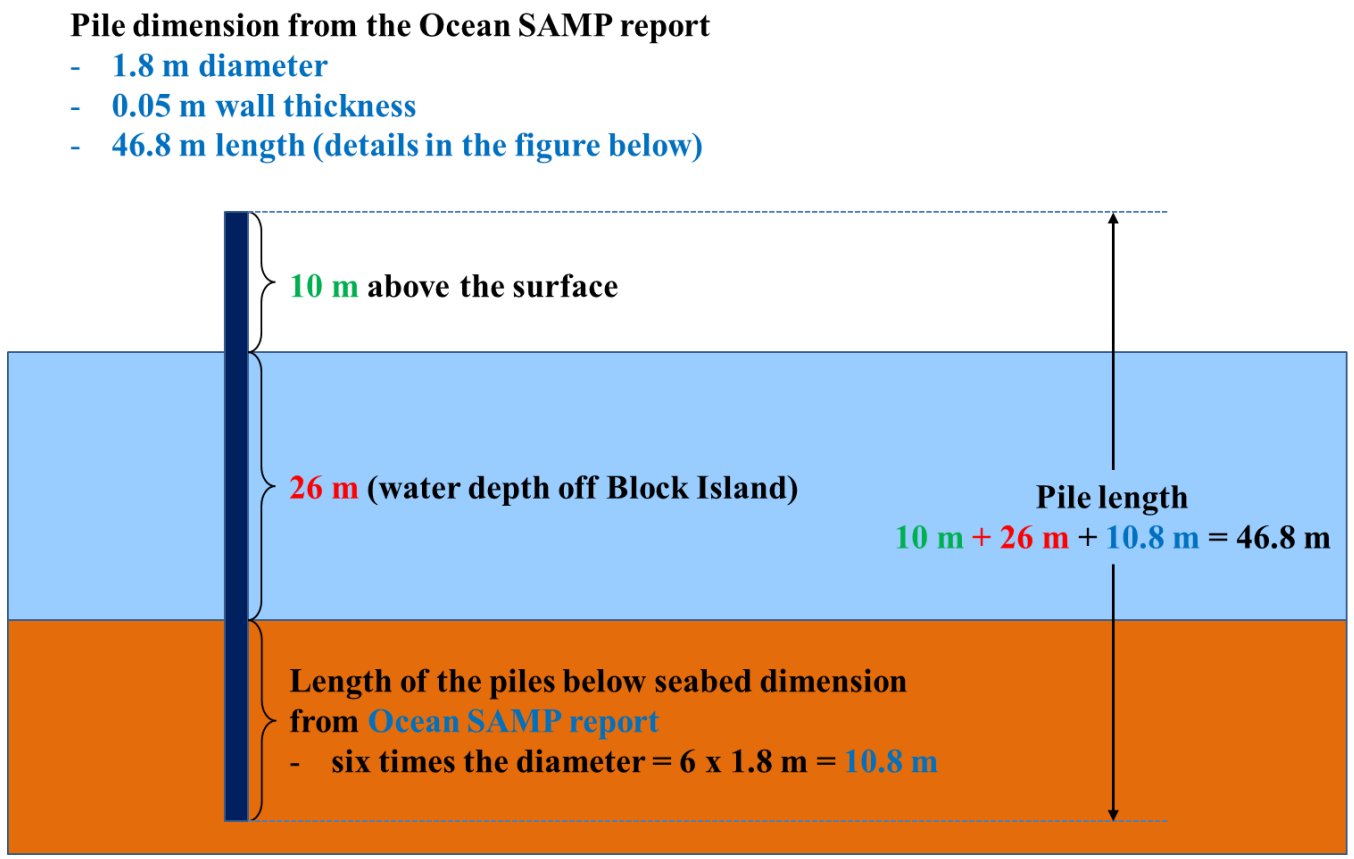

Figure 1.3 **Determination of pile dimension and water depths for the FE model. The approximated water depth three miles off Block Island RI is 26 *m* [23] and the pile diameter and thickness are given in the Ocean SAMP report. The length of the pile driven below seabed is six times the diameter.**

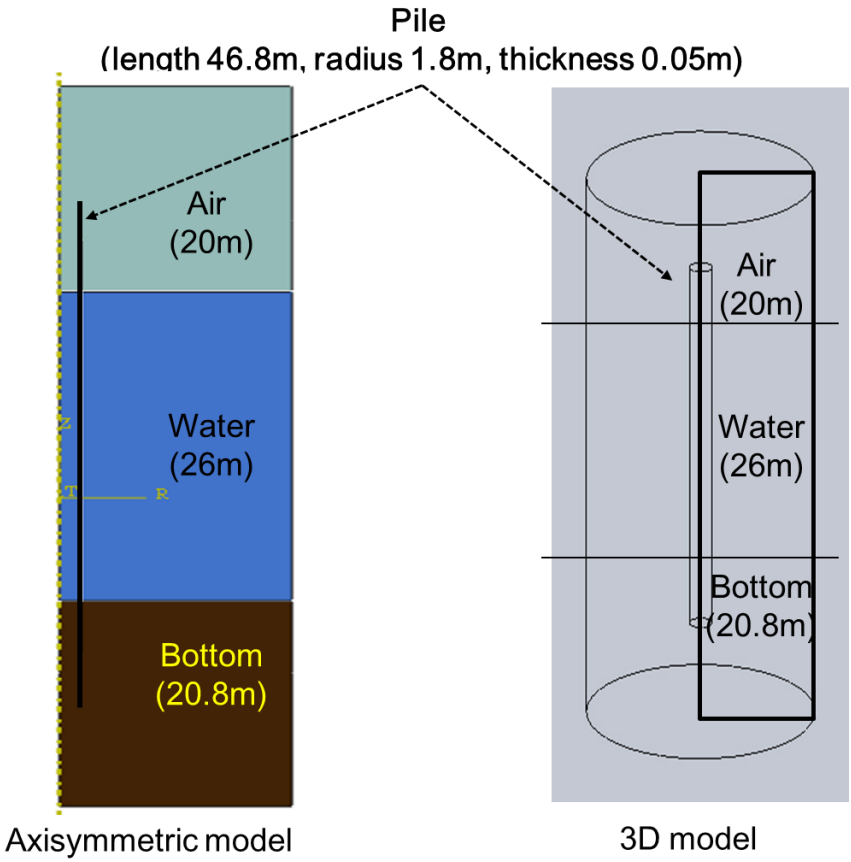

Figure 1.4 **Axisymmetric geometry of FE model and 3D representation. The pile has length 46.8 m, radius 1.8 m, and thickness 0.05 m. The pile is hollow and is filled with same acoustic medium as the one outside the pile. The axisymmetric geometry in the Abaqus/CAE 6.11 (left panel) is the section indicated in the 3D geometry (right panel).**

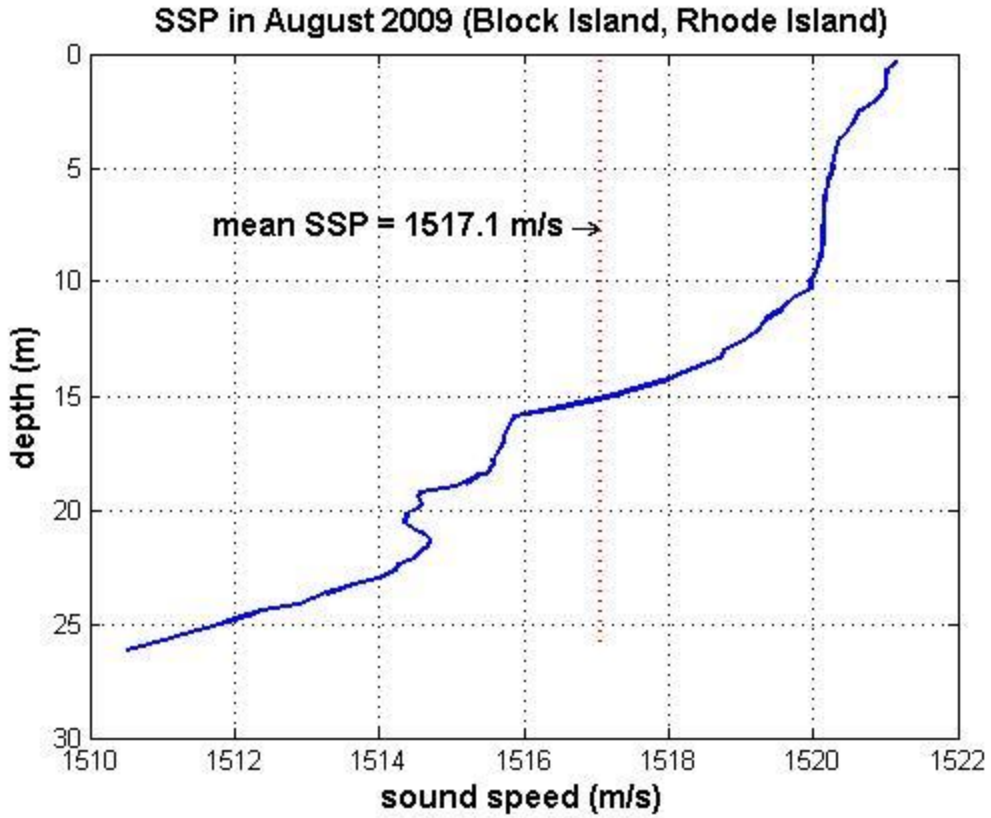

Figure 1.5 **The SSP (Sound Speed Profile) in August 2009 (Block Island, Rhode Island). Overall, the SSP is decreasing with increasing depth. The FE model has difficulty applying this SSP. Hence, the material properties for homogeneous water are defined to make the mean of the SSP of 1517.1 m/s.**

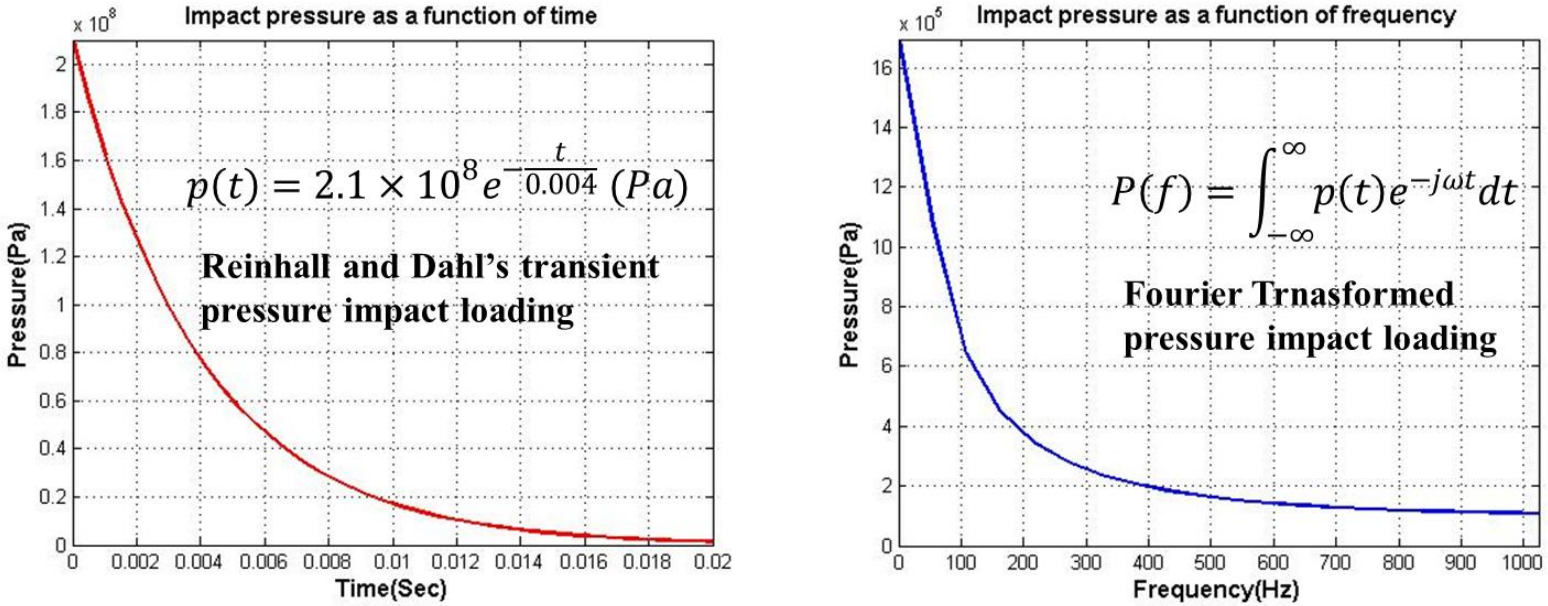

Figure 1.6 **Mathematical expression for the transient hammer impact pressure loading on top of the pile (left panel) and its Fourier Transformed pressure amplitude as function of frequency which is loading condition for steady state dynamic analysis (right panel).**

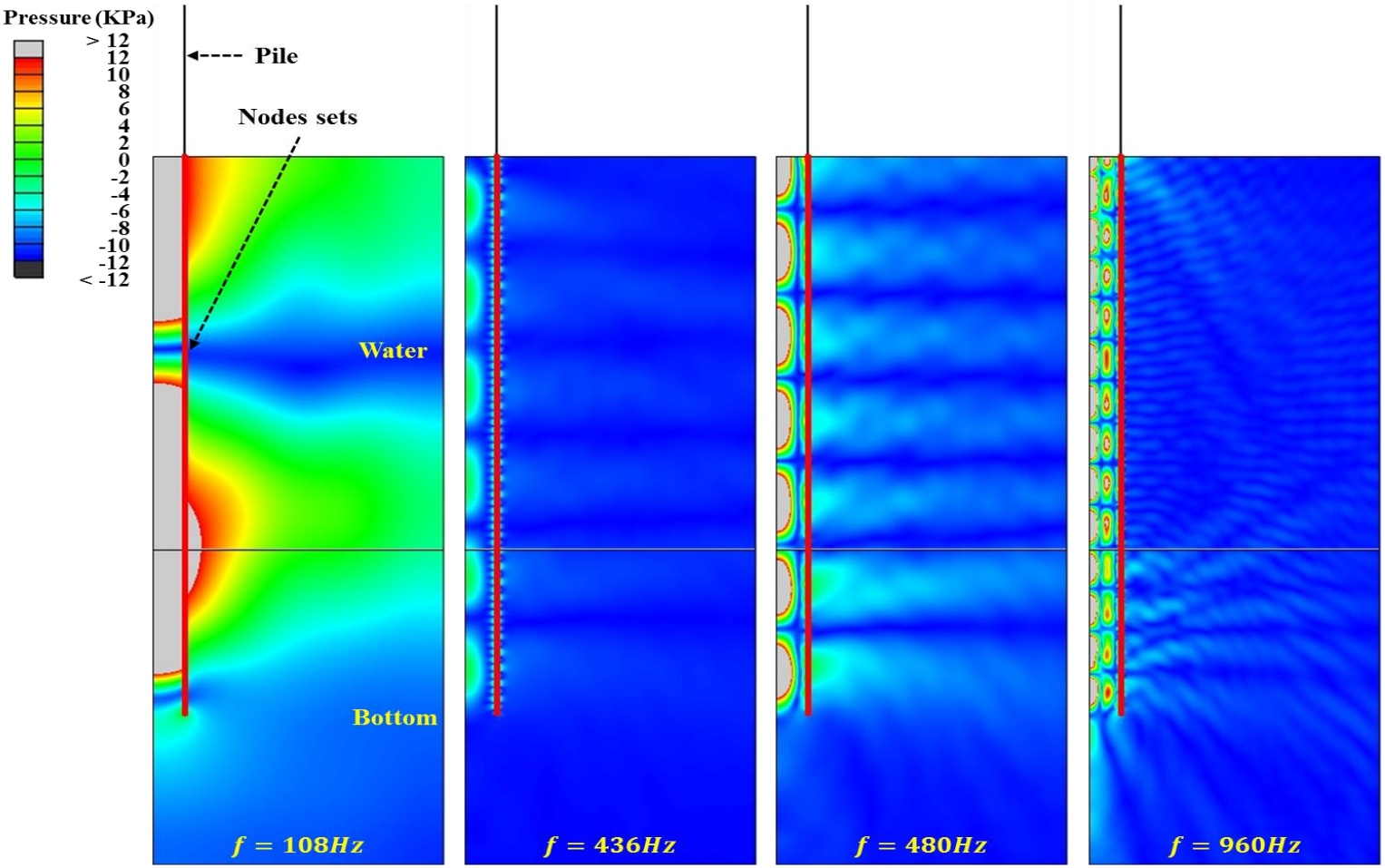

Figure 1.7 **A few examples of the magnitudes of acoustic pressure field output due to impact pile driving. Harmonic loading with 4 dominant frequencies of 108, 436, 480, 960 Hz.**

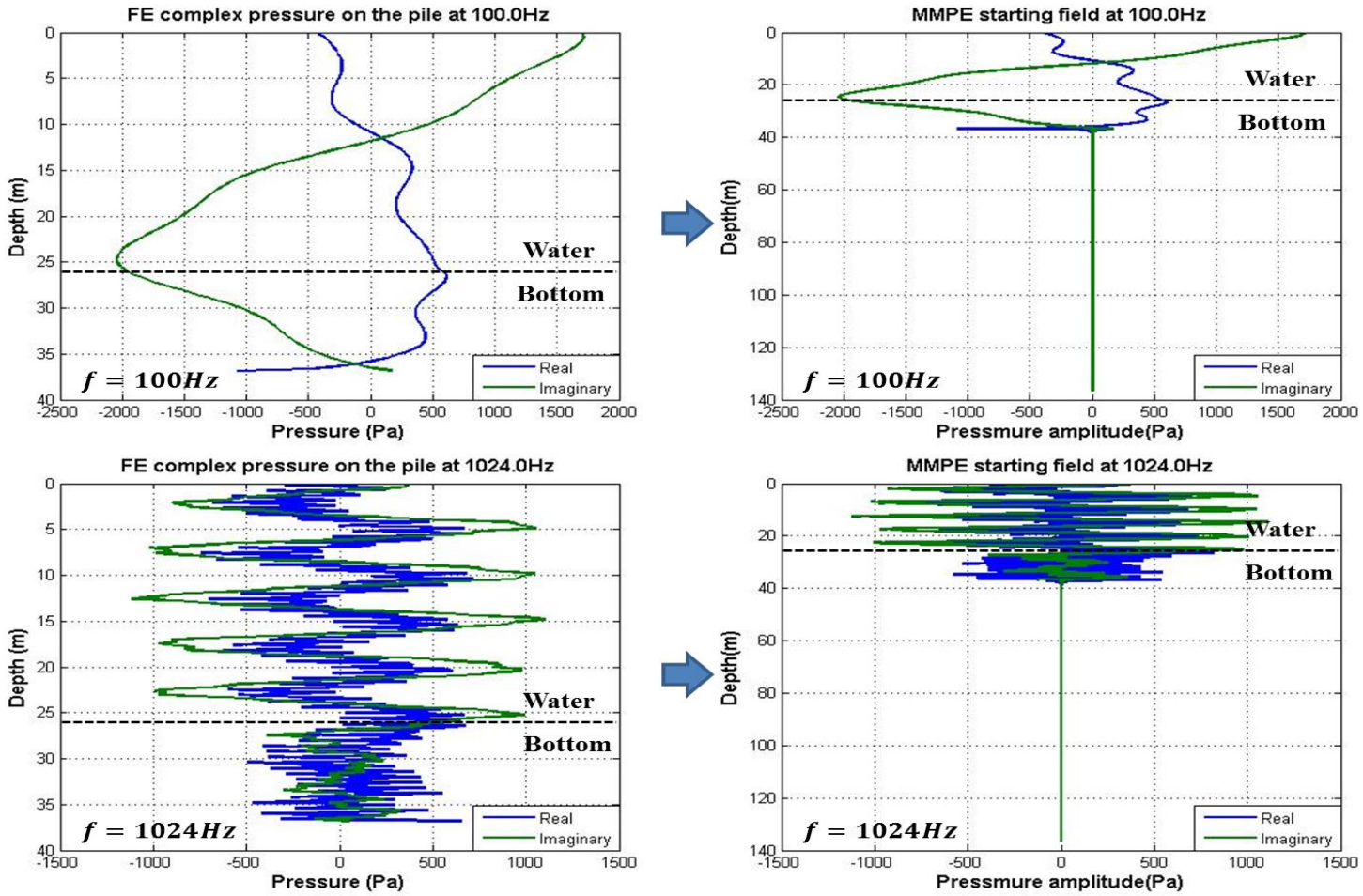

Figure 1.8 **Complex acoustic pressure along the pile length in water and sediment from the FE model for 100 Hz and 1024 Hz (left panels) and the associated MMPE staring field developed using the Matlab Script (right panels).**

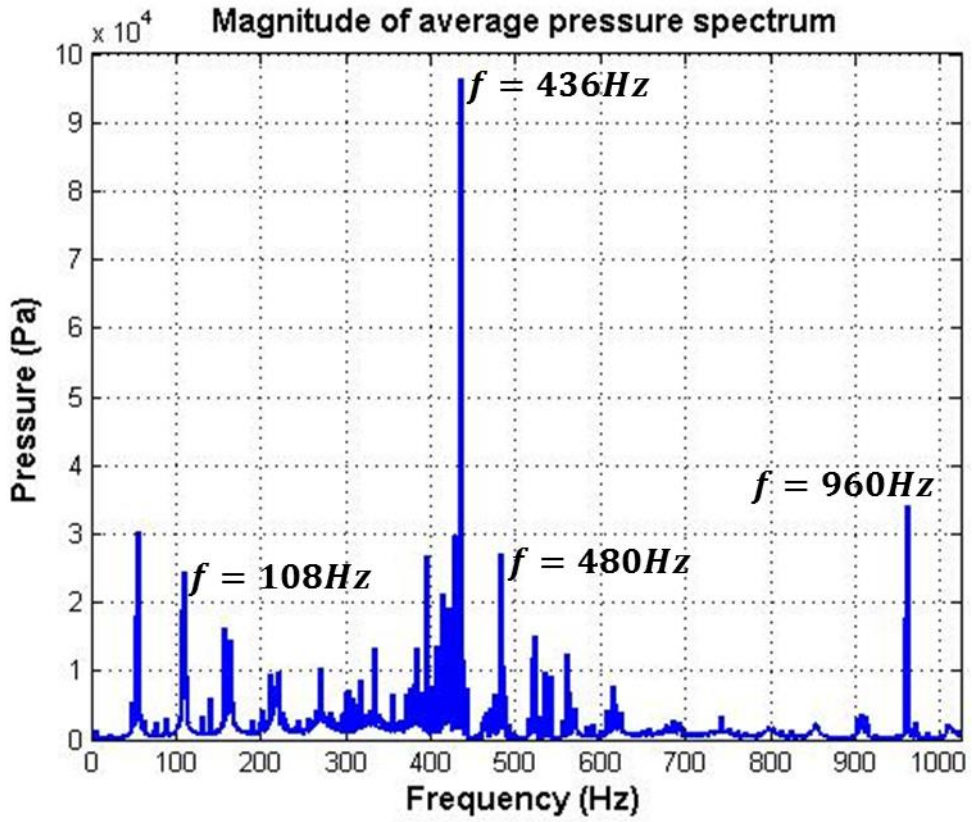

Figure 1.9 **The spectrum of spatial average of the magnitudes of the complex acoustic pressure. A few dominant frequencies of the pile structure interacting with water, bottom media are labeled as 108 Hz, 436 Hz, 480 Hz, and 960 Hz. To cover these dominant frequencies, the frequency band of the MMPE model is set to 55 Hz ~ 1,024 Hz**

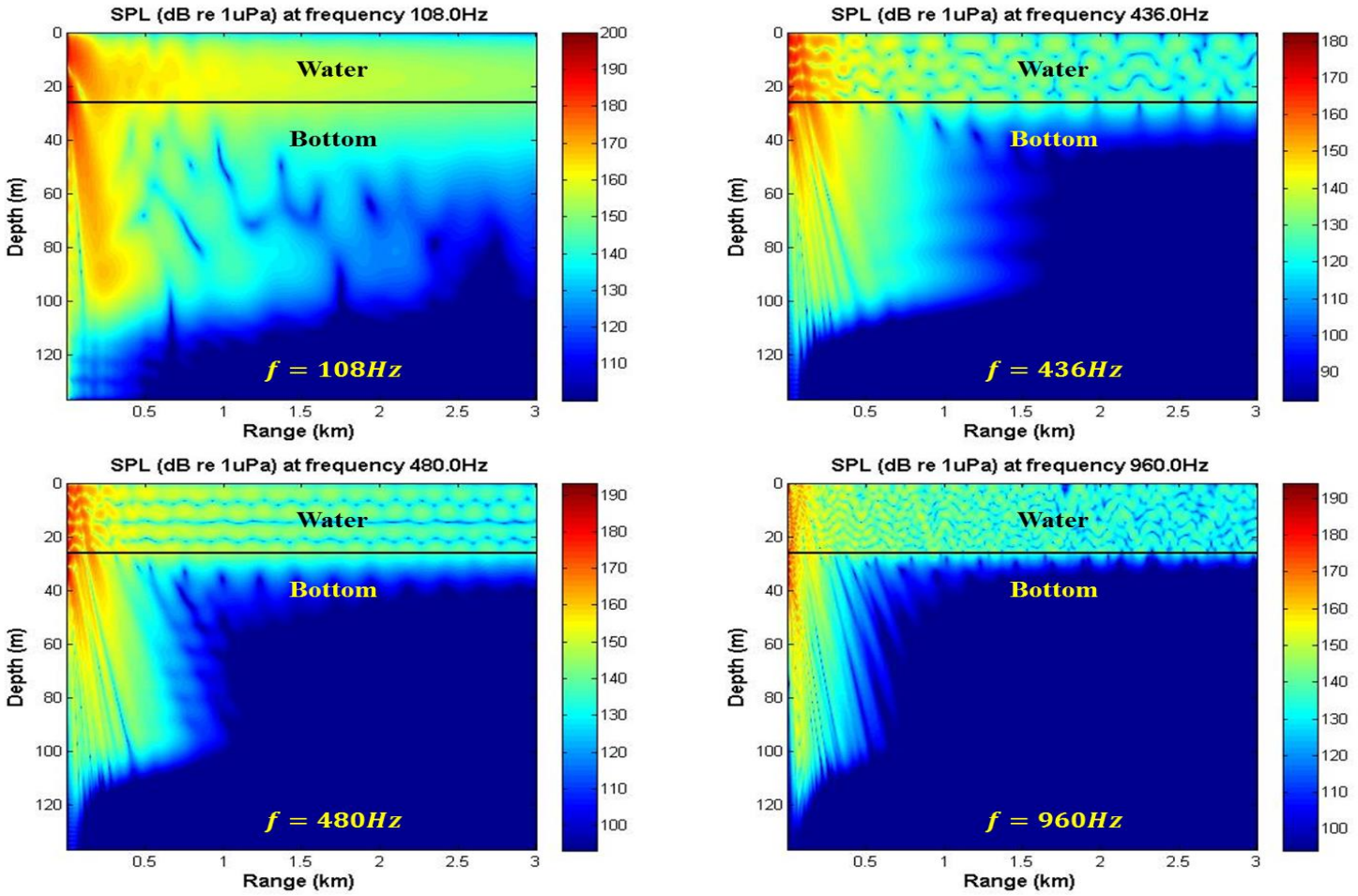

Figure 1.10 **The SPL in dB re 1μPa for the starting fields at frequencies of 108, 436, 480 960 Hz respectively. Four panels show SPL in dB re 1μPa instead of TL in dB re 1m standard MMPE model's default representation.**

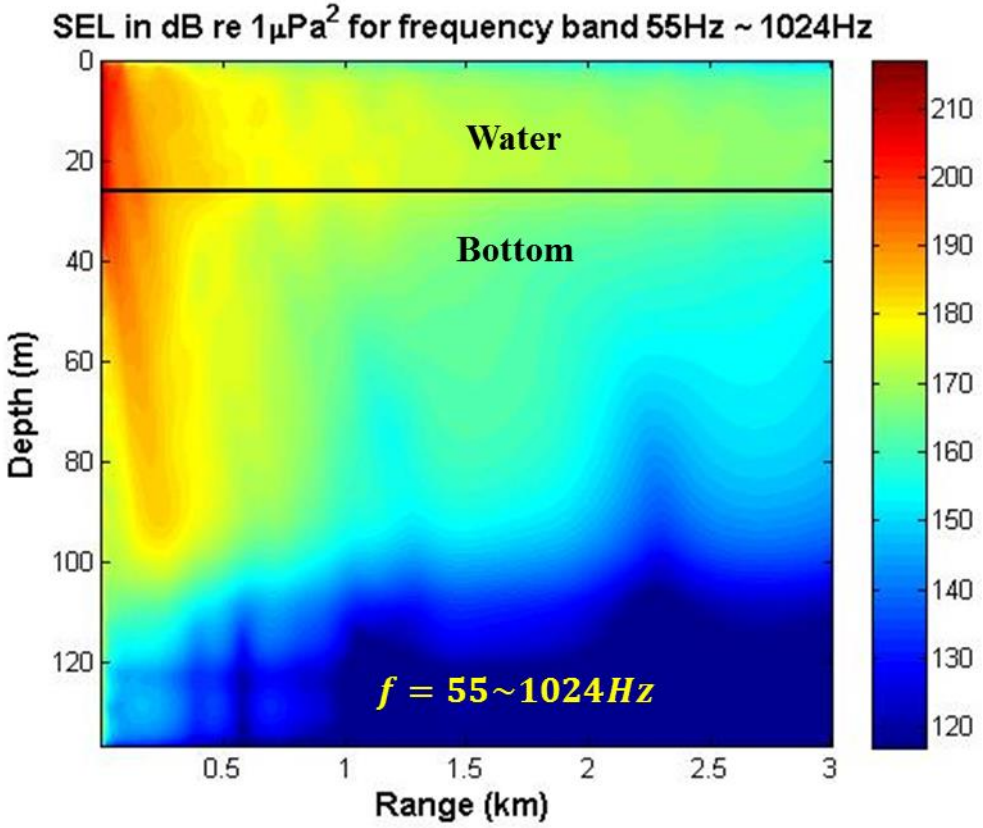

Figure 1.11 The SEL (dB re 1μPa^2) as function of depth and range. The black solid line indicates water-bottom interface.

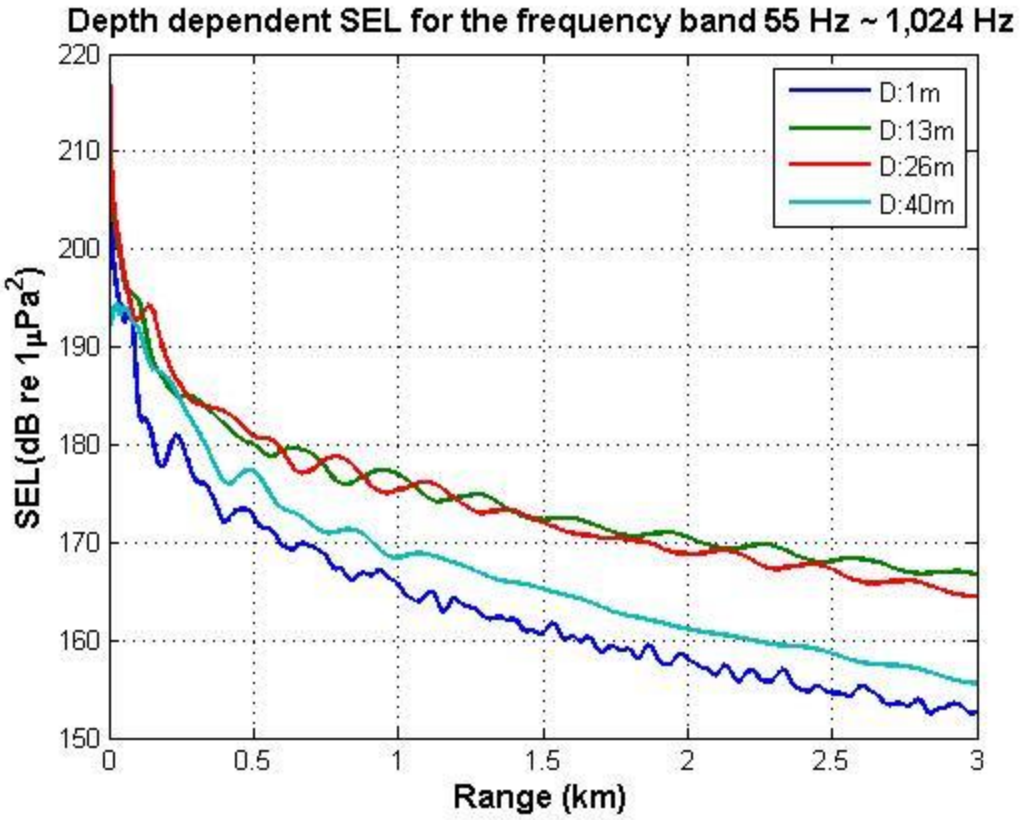

Figure 1.12 **Depth dependent SEL (dB re 1μPa^2) as function of range (km). The energy levels are high at water depth 13 m (mid**-depth) and 26 m (water-bottom interface).

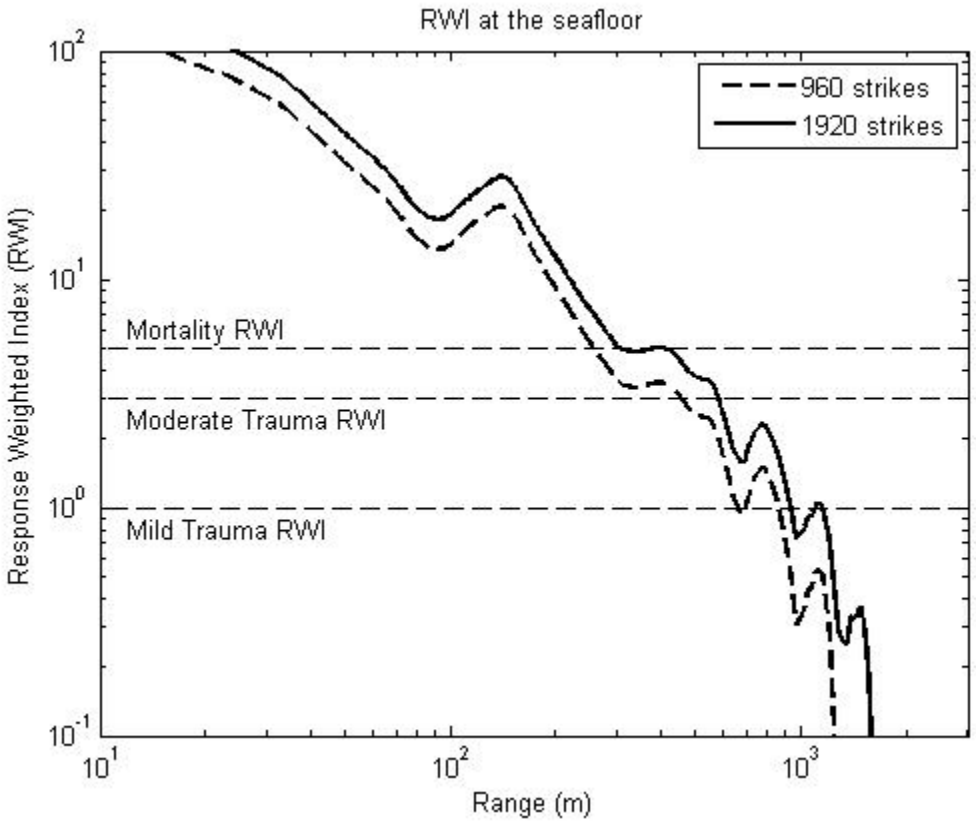

Figure 1.13 Response weighted index (RWI) predicted as a function of range from the pile installation for 960 and 1920 pile strikes [24]. Also indicated on the graph are the fish mortality RWI of 5, moderate trauma RWI of 3 and the mild trauma RWI of 1 as suggested by Halvorsen et al [25].

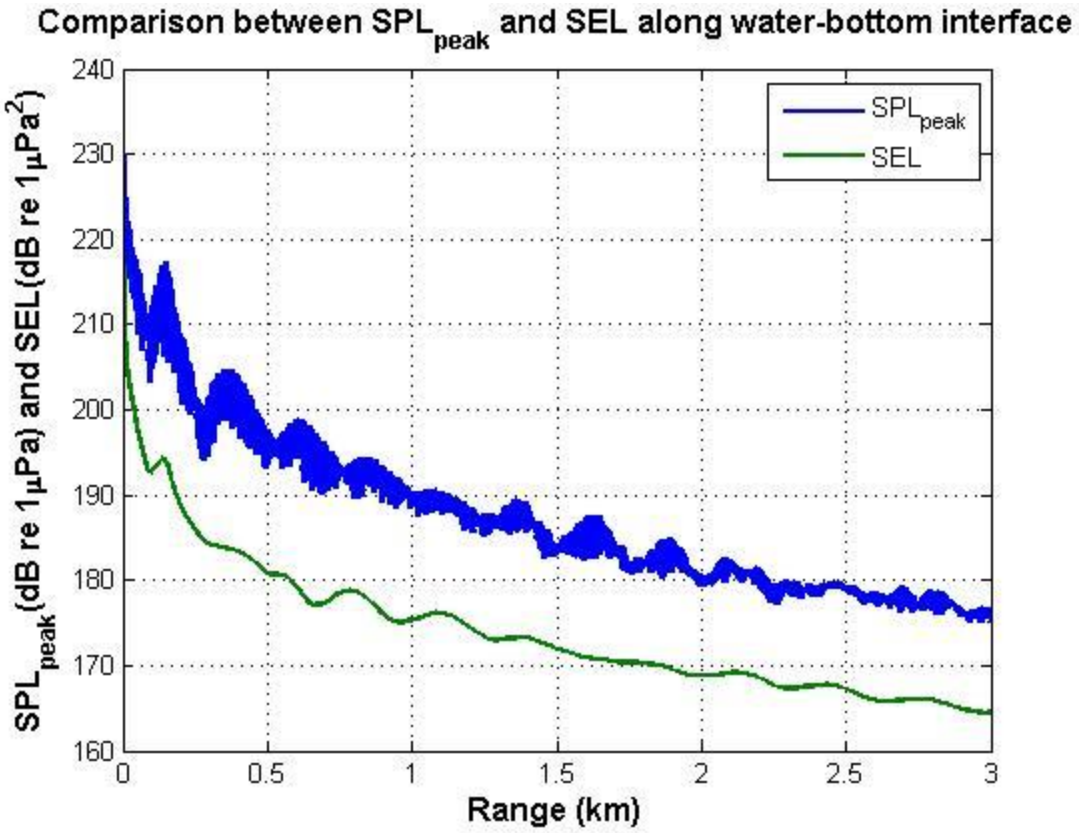

Figure 1.14 Comparison between the peak SPL (dB re 1μPa) and SEL (dB re 1μPa^2) as function of range (km).

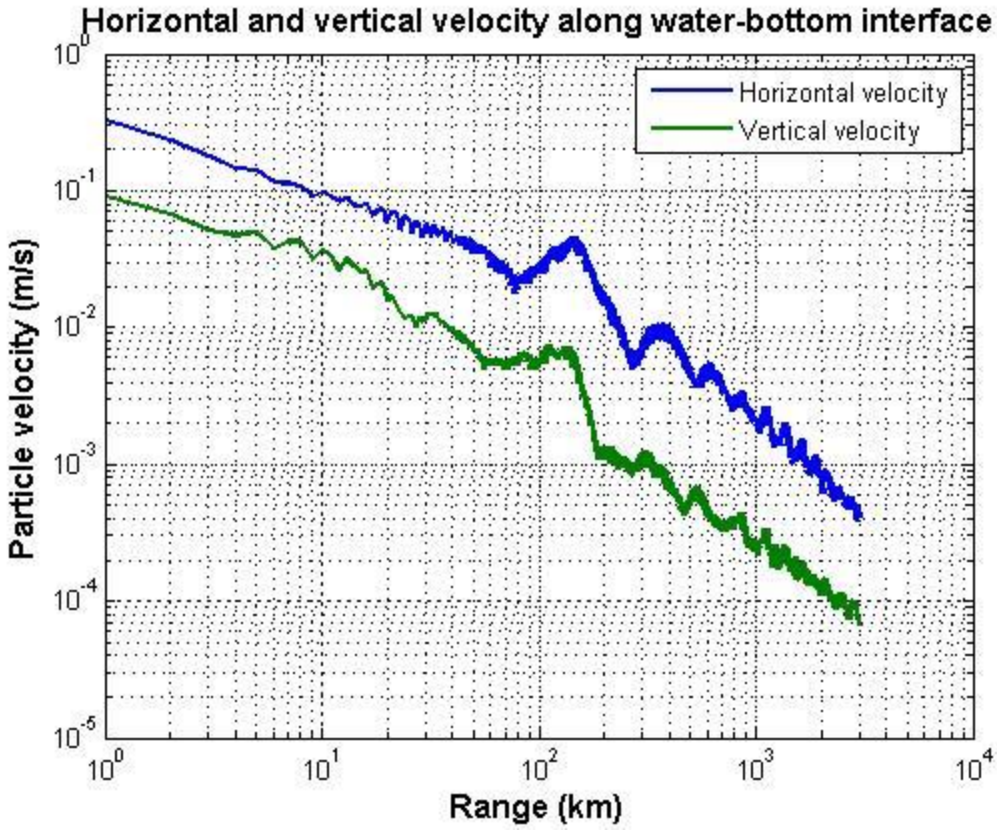

Figure 1.15 Horizontal and vertical component of particle velocities along the water-bottom interface

REFERENCES AND LINKS

1. ***Bureau of Ocean Energy Management*. Offshore Wind Energy Resources; Available from: http://www.boem.gov/Renewable-Energy-Program/Renewable-Energy-Guide/Offshore-Wind-Energy.aspx.**

2. **Erbe, C., *UNDERWATER NOISE FROM PILE DRIVING IN MORETON BAY, QLD.* Acoustics Australia;Dec2009, Vol. 37 Issue 3, p87, 2009.**

3. **Erbe, C., *Underwater acoustics: Noise and the effects on marine mammals, 3rd edn. Pocketbook*2010: JASCO Applied Sciences.**

4. **Erbe, C., *Effects of Underwater Noise on Marine Mammals*, in *The Effects of Noise on Aquatic Life*, A. Popper and A. Hawkins, Editors. 2012, Springer New York.**

5. **Betke, K., M.S.-v. Glahn, and R. Matuschek, *Measurement and Reduction of Offshore Wind Turbine Construction Noise.* 2004.**

6. **Jong, C.A.F.D. and M.A. Ainslie. *Underwater radiated noise due to the piling for the Q7 offshore wind park*. in *Acoustic 08 Paris*. 2008.**

7. **Elmer, K.H., et al., *Measurement and Reduction of Offshore Wind Turbine Construction Noise*, in *DEWI Magazin Nr. 30, Februar 2007*.**

8. **Reinhall, P.G. and P.H. Dahl, *Underwater Mach wave radiation from impact pile driving: Theory and observation.* The Journal of the Acoustical Society of America, 2011. 130(3): p. 1209-1216.**

9. **Reinhall, P.G. and P.H. Dahl. *Acoustic radiation from a submerged pile during pile driving*. in *OCEANS 2010*. 2010.**

10. **Reinhall, P.G. and P.H. Dahl, *Acoustic radiation during marine pile driving.* The Journal of the Acoustical Society of America, 2011. 129(4): p. 2460.**

11. **Kim, H., et al., *Modeling of offshore wind turbine noise radiation and propagation.* The Journal of the Acoustical Society of America, 2011. 130(4): p. 2332.**

12. **Potty, G.R., K. Huikwan, and J.H. Miller.** ***Acoustic radiation from offshore wind farms*****. in** ***Ocean Electronics (SYMPOL), 2011 International Symposium on*****. 2011.**

13. **Kim, H., J.H. Miller, and G.R. Potty,** ***Predicting underwater radiated noise levels due to the first offshore wind turbine installation in the U.S.*** **The Proceedings of Meetings on Acoustics, 2013. 19: p. 040067.**

14. **Kim, H., et al.** ***Long range propagation modeling of offshore wind turbine construction noise using Finite Element and Parabolic Equation models*****. in** ***OCEANS, 2012 - Yeosu*****. 2012.**

15. **Kim, H., et al.,** ***Long range propagation modeling of offshore wind turbine noise using finite element and parabolic equation models.*** **The Journal of the Acoustical Society of America, 2012. 131(4): p. 3392.**

16. **Smith, K.B.,** ***Convergence, Stability, and Variability of Shallow Water Acoustic Predictions Using a Split-Step Fourier Parabolic Equation Model.*** **Journal of Computational Acoustics, 2001. 9(1): p. 243.**

17. **Crocker, S.E.,** ***Geoacoustic inversion using the vector field,*** **in** ***Ocean Engineering*****2011, University of Rhode Island: Narragansett.**

18. **Simulia,** ***6.10.1 Acoustic, shock, and coupled acoustic-structural analysis,*** **in** ***Abaqus 6.11 PDF Documentation Analysis User's Manual Volume II: Analysis*****2011.**

19. **Simulia,** ***6.3.4 Direct-solution steady-state dynamic analysis,*** **in** ***Abaqus 6.11 PDF Documentation Analysis User's Manual Volume II: Analysis*** **2011.**

20. **Simulia,** ***33.3.1 Mesh tie constraints,*** **in** ***Abaqus 6.11 PDF Documentation Analysis User's Manual Volume V: Prescribed Conditions, Constraints & Interactions*** **2011.**

21. **Halvorsen, M.R., et al.,** ***Threshold for onset of injury in Chinook Salmon from exposure to impulsive pile driving sound, PLOS One, vol. 7, no. 6,*** **2012.**

22. Chawda MN, H.F., Pape HC, Giannoudis PV, *Predicting outcome after multiple trauma: which scoring system? Injury: Internaltion.* Journal of the Care of the Injured, 2004. 35: p. 347–358.

23. OceanSAMP GIS Data Download: Bathymetry. Available from: http://www.narrbay.org/physical_data.htm.

24. Miller, J.H., G.R. Potty, and H. Kim, *Pile driving pressure and particle velocity at the seabed: Quantifying effects on crustaceans and ground fish.* The 3rd International Conference on the Effects of Noise on Aquatic Life, 2013.

25. Halvorsen, M.R., et al., Predicting and mitigating hydroacoustic impacts on fish from pile installations, Washington, DC: NCHRP Research Digest 263, Transportation Research Board, 2011.

MANUSCRIPT – II

Intended for submission to the Journal of the Acoustical Society of America-Express Letter

Analysis of the transient structural response of finite length cylindrical shell due to impact pile driving

Corresponding Author:

Huikwan Kim

Department of Ocean Engineering, University of Rhode Island, Narragansett, Rhode Island 02882, hkkim524@my.uri.edu

Contributing Authors:

James H. Miller, Gopu R. Potty

Department of Ocean Engineering, University of Rhode Island, Narragansett, Rhode Island 02882

Abstract: Underwater noise is generated by vibration of pile structure due to hydraulic hammer impact on top of the pile. This study has been initiated to provide simple analytic solution for structural response as function of basic pile design parameters such as length, radius, etc. The acoustic pressure amplitude calculated by this approach can be used starting field to calculate broadband SPL (Sound Pressure Level) at a distance from the pile using parabolic equation methods such as MMPE (Monterey-Miami Parabolic Equation). This study focuses on the calculation of transient structural responses of finite cylindrical shell using the method of normal modes. It starts from the Donnell's equations of motion for radial and axial and tangential displacement of thin cylindrical shell. The coupled equations are decoupled and are simplified assuming the loading and associated outputs are independent of azimuthal angle. Also, we assume the pile has membrane shell which support only transverse wave propagating along pile length. We present the overall process calculating natural frequencies, mode shapes and forced vibration response using normal modes superposition approach.

PACS numbers: 43.40.Ey, 43.40.Dx, 43.40.Cw, 43.40.Kd

2.1 INTRODUCTION AND BACKGROUDN

A. Introduction

This study has been initiated from the motivation that there is no simple analytical model available for prediction of noise impact on marine life due to impact pile driving. The goal of this study is to develop an efficient method for calculating transient structural response of the pile with given pile design parameters such as length, radius and material properties of the pile. The displacement amplitudes in the radial direction along the pile length can be used to calculate associated acoustic pressure amplitude using the well-known MMPE ocean acoustics propagation model's starting field. It is advantageous because the method allows the study of the effects of pile design parameters efficiently as compared to the computationally expensive approaches such as Finite Elements.

B. Background

Over five decades, a number of researchers have investigated wave propagation problems in thin wall elastic shell structures in vacuum or in contact with acoustic medium. The latter problem is called acoustic-structure interaction problem. Junger and Feit made contributions that predominately dealt with the harmonic response of coupled acoustic-structural system [1-5] by solving the Helmholtz integral equation. They considered infinite and finite length thin wall cylindrical shell structure. Stepanishen considered transient response of the structure submerged in an acoustic medium [6-11] by solving Kirchhoff integral equation. Kraus described static and dynamic response of general shape and cylindrical/spherical thin elastic shell structure [12, 13]. His book includes specific procedure for calculating transient structural response due to space and time dependent force on the structure which is good benchmark procedure to this study.

These investigators did not directly consider offshore impact pile driving problems but included two major solution approaches for solving acoustic-structure interaction problems. Recently, researchers have used computationally expensive numerical approaches for predicting offshore impact pile driving noise. Reinhall and Dahl used one of the commercial FE (Finite Element) code, Comsol Multiphysics and compared their simulation results with measured data [14, 15]. Kim et al [16-20] also used another commercial FE code, Abaqus/CAE 6.11 to predict transient and harmonic response (acoustic pressure amplitude) for a mono pile considering air, water, and ocean bottom acoustic medium. Any numerical approaches need adequate theoretical background and technical skill for FE modeling and post-processing of raw results. Hence this study presents overall procedures for calculating a forced vibration solution for a finite length membrane cylindrical shell structure without complicated FE modeling. The method only needs to input pile design parameters of interest and can make predictions of pile vibrations quickly and efficiently.

2.2 CALCULATION OF STRUCTURAL RESPONSE OF SHELL-OVERVIEW

To calculate radial displacement on the surface of the pile duo to impact pile driving on top of the pile, we used the classical method of spectral representation (also called normal mode superposition) where in the dependent variables of the theory of shells are expanded in infinite series of the normal modes of free vibration as described in Kraus's previous work [13]. It is necessary to calculate the normal modes and associated natural frequencies and each normal mode is multiplied by an unknown time dependent coefficient. The unknown coefficients can be determined using orthogonal property and

variation of parameters. This approach is not only applicable to thin cylindrical shell but can also be applied to calculation of space and time dependent displacement for string, beam and plate using appropriate governing equations and boundary conditions. The equations of motion are different in each case and it is needless to say the governing equations for finite length cylindrical shell is more complicated involving three dependent variables (axial (u_x), tangential (u_θ), and radial displacement (w)) which are coupled due to curvature effect in contrast to circular or rectangular plate problems. Direct solution for three coupled governing equations of cylindrical shell is difficult and requires some assumptions simplifying the equations and reducing calculation steps. The major assumption is azimuthal independence which enables us to use axisymmetric loading applied on top of the pile and the responses are also axisymmetric. This cancels all partial derivatives with respect to azimuthal angle (θ) in the governing equations. We also applied Yu's assumption [13, 21] that the length (l) of the pile is large compared to the radius (a) of the pile. This cancels many terms in the modified governing equations too. Lastly, we assumed that the pile is membrane cylindrical shell and this transforms the decoupled 8th order PDE (Partial Differential Equation) to 4th order. The boundary conditions applied are clamped – free condition and the clamped end ($x = 0$) at lower end of pile assuming the pile is driven at the fixity depth in the ocean bottom and upper end ($x = l$) at free condition. The following sections describe details of calculation with the boundary conditions of interest.

2.3 GOVERNING EUQAIONS FOR A THIN CYLINDRICAL SHELL

Our analytic solution for the calculation of radial displacement for thin cylindrical shell due to transient impact loading on one end of finite cylinder starts from Donnell's

equations of motion as expressed in the equation (2.1), (2.2), and (2.3) respectively [12, 13].

$$\frac{\partial^2 u_x}{\partial x^2} + \frac{1-\nu}{2a^2}\frac{\partial^2 u_x}{\partial \theta^2} + \frac{1+\nu}{2a}\frac{\partial^2 u_\theta}{\partial x \partial \theta} + \frac{\nu}{a}\frac{\partial w}{\partial x} - \frac{1-\nu^2}{E}\rho\frac{\partial^2 u_x}{\partial t^2} = 0 \qquad (2.1)$$

$$\frac{1+\nu}{2a}\frac{\partial^2 u_x}{\partial x \partial \theta} + \frac{1-\nu}{2}\frac{\partial^2 u_\theta}{\partial x^2} + \frac{1}{a^2}\frac{\partial^2 u_\theta}{\partial \theta^2} + \frac{1}{a^2}\frac{\partial w}{\partial \theta} - \frac{1-\nu^2}{E}\rho\frac{\partial^2 u_\theta}{\partial t^2} = 0 \qquad (2.2)$$

$$\frac{\nu}{a}\frac{\partial u_x}{\partial x} + \frac{1}{a^2}\frac{\partial u_\theta}{\partial \theta} + \frac{w}{a^2} + \frac{h^2}{12}\nabla^4 w + \frac{1-\nu^2}{E}\rho\frac{\partial^2 w}{\partial t^2} = 0 \qquad (2.3)$$

where, u_x: axial displacement, u_θ: tangential displacement, w: radial displacement, a : radius of finite cylinder, E: Young's modulus, ν: Poisson's ratio, h: thickness of finite cylinder, ρ: density of finite cylinder

These equations governs the displacements in the direction of axial (u_x), tangential (u_θ), and radial (w) and this study focuses on the radial displacement because radial component of particle velocity on the surface of the pile pushes acoustic media such as air, water, and ocean bottom. In contrast to the case of beam or plate, displacement output of cylindrical shell in each direction are dependent and three equations are coupled each other due to curvature of the cylindrical shell. These governing equations can be decoupled with some operations in series and the final result gives the 8th order decoupled PDE with a dependent variable w (radial displacement).

2.4 CALCULATION OF MODE SHAPES AND NATURAL FREQUENCIES

A. Calculation of mode shapes

It is necessary to decouple the equations of motion and Kraus [13] provided details about decoupling procedures for Donnell's equations of motion which are reproduced in the following equations (2.4) – (2.7). First of all, it is recommended to operate on equation (2.1) successively with $\partial^2/\partial x^2$, $\partial^2/\partial\theta^2$ and $\partial^2/\partial t$ and solve in each case for the term involving u_θ. Then these expression are substituted into the equation that is obtained by operating on equation (2.2) with $\partial^2/\partial x\partial\theta$ to give

$$\nabla^4 u_x + \frac{\nu}{a}\frac{\partial^3 w}{\partial x^3} - \frac{1}{a^3}\frac{\partial^3 w}{\partial x \partial\theta^2} = -\frac{2(1+\nu)}{E}\,\rho\frac{\partial^2}{\partial t^2}\left\{\frac{1-\nu^2}{E}\rho\frac{\partial^2 u_x}{\partial t^2} - \frac{3-\nu}{2}\nabla^2 u_x - \frac{\nu}{a}\frac{\partial w}{\partial x}\right\} \tag{2.4}$$

Then, operating on equation (2.2) with $\partial^2/\partial x^2$, $\partial^2/\partial\theta^2$ and $\partial^2/\partial t$ and solving in each case for the term involving u_x and substituting these expressions into the equation obtained by operating on equation (2.1) with $\partial^2/\partial x\partial\theta$ gives

$$\nabla^4 u_\theta + \frac{2+\nu}{a^2}\frac{\partial^3 w}{\partial x^2\partial\theta} + \frac{1}{a^4}\frac{\partial^3 w}{\partial\theta^3} = -\frac{2(1+\nu)}{E}\,\rho\frac{\partial^2}{\partial t^2}\left\{\frac{1-\nu^2}{E}\rho\frac{\partial^2 u_\theta}{\partial t^2} - \frac{3-\nu}{2}\nabla^2 u_\theta - \frac{1}{a^2}\frac{\partial w}{\partial\theta}\right\} \tag{2.5}$$

A third equation is obtained by operating on equation (2.4) and (2.5) with $\nu\partial/a\partial x$ and $\partial^2/a^2\partial\theta^2$, respectively, and adding the results. This gives

$$\nabla^4\left(\frac{\nu}{a}\frac{\partial u_x}{\partial x}+\frac{1}{a^2}\frac{\partial u_\theta}{\partial\theta}\right)+\frac{\nu^2}{a^2}\frac{\partial^4 w}{\partial x^4}+\frac{2}{a^4}\frac{\partial^4 w}{\partial x^2\partial\theta^2}+\frac{1}{a^6}\frac{\partial^4 w}{\partial\theta^4}$$
$$=-\frac{2(1+\nu)}{E}\rho\frac{\partial^2}{\partial t^2}\left[\frac{1-\nu^2}{E}\rho\frac{\partial^2}{\partial t^2}\left(\frac{\nu}{a}\frac{\partial u_x}{\partial x}+\frac{1}{a^2}\frac{\partial u_\theta}{\partial\theta}\right)\right] \quad (2.6)$$
$$-\frac{3-\nu}{2}\nabla^2\left(\frac{\nu}{a}\frac{\partial u_x}{\partial x}+\frac{1}{a^2}\frac{\partial u_\theta}{\partial\theta}\right)-\frac{\nu^2}{a^2}\frac{\partial^2 w}{\partial x^2}+\frac{1}{a^4}\frac{\partial^2 w}{\partial\theta^2}$$

The quantity in parentheses in equation (2.6) can be expressed in terms of w from equation (2.3). This final operation gives decoupled 8th order PDE with dependent variable w as follows

$$\frac{h^2}{12}\nabla^8 w+\frac{1-\nu^2}{a^2}\frac{\partial^4 w}{\partial x^4}$$
$$=-\frac{2(1+\nu)}{E}\rho\frac{\partial^2}{\partial t^2}\left[\left(\frac{1-\nu^2}{E}\rho\frac{\partial^2}{\partial t^2}-\frac{3-\nu)}{2}\nabla^2\right)\right.$$
$$\times\left(\frac{1-\nu^2}{E}\rho\frac{\partial^2 w}{\partial t^2}+\frac{w}{a^2}+\frac{h^2}{12}\nabla^4 w\right)+\frac{1-\nu}{2}\nabla^4 w \quad (2.7)$$
$$\left.+\frac{\nu^2}{a^2}\frac{\partial^2 w}{\partial x^2}+\frac{1}{a^4}\frac{\partial^2 w}{\partial\theta^2}\right]$$

Kraus also provided general solution for the space and time dependent displacement in three directions and these satisfy Donnell's equations of motion. These equations are

$$u_{xmn}(x,\theta,t) = \sum_{i=1}^{8} A_i exp\left(\frac{\lambda_i x}{l}\right) cos\, n\theta cos\omega_{mn} t \tag{2.8}$$

$$u_{\theta mn}(x,\theta,t) = \sum_{i=1}^{8} B_i exp\left(\frac{\lambda_i x}{l}\right) sin\, n\theta cos\omega_{mn} t \tag{2.9}$$

$$w_{mn}(x,\theta,t) = \sum_{i=1}^{8} C_i exp\left(\frac{\lambda_i x}{l}\right) cos\, n\theta cos\omega_{mn} t \tag{2.10}$$

Equation (2.10) is substituted into the equation (2.7) which is the 8th order decoupled equation and Yu's assumption that the pile length is large radius is then applied.

$$\frac{\left|\lambda_i{}^2\right| a^2}{n^2 l^2} \ll 1 \tag{2.11}$$

The result is shown in the following equation and can be more simplified with assumption that the loading and response of the pile is independent of azimuthal angle. All terms including n are canceled because it is dependent by $\partial/\partial\theta$.

$$
\begin{aligned}
&(1-\nu)(1-\nu^2)\left(\frac{\lambda_i a}{l}\right)^4 \\
&\qquad = 2\Delta^3 \\
&\qquad - \Delta^2\left[2 + (3-\nu)\cancel{n^2}\left(1 - \frac{\cancel{\lambda_i^2 a^2}}{\cancel{n^2 l^2}}\right)\right. \\
&\qquad \left. + \frac{2\cancel{n^4}}{\xi}\left(1 - \frac{\cancel{\lambda_i^2 a^2}}{\cancel{n^2 l^2}}\right)^2\right] \\
&\qquad + \Delta\left[(3-\nu)\cancel{n^2}\left(1 - \frac{\cancel{\lambda_i^2 a^2}}{\cancel{n^2 l^2}}\right) - 2\cancel{n^2}\left(1 - \nu^2\frac{\cancel{\lambda_i^2 a^2}}{\cancel{n^2 l^2}}\right)\right. \\
&\qquad \left. + (1-\nu)\cancel{n^4}\left(1 - \frac{\cancel{\lambda_i^2 a^2}}{\cancel{n^2 l^2}}\right)^2 + (3-\nu)\frac{\cancel{n^6}}{\xi}\left(1 - \frac{\cancel{\lambda_i^2 a^2}}{\cancel{n^2 l^2}}\right)^3\right] \\
&\qquad - (1-\nu)\frac{\cancel{n^8}}{\xi}\left(1 - \frac{\cancel{\lambda_i^2 a^2}}{\cancel{n^2 l^2}}\right)^4
\end{aligned}
\tag{2.12}
$$

where, a : radius of finite cylinder, E: Young's modulus, ν: Poisson's ratio, h: thickness of finite cylinder, ρ: density of finite cylinder, $\Delta = \rho a^2(1-\nu^2)\frac{\omega^2}{E}$, $\frac{1}{\xi} = \frac{h^2}{12a^2}$

Finally, equation (2.12) simplifies to:

$$
\begin{aligned}
&(1-\nu)(1-\nu^2)\left(\frac{\lambda_i a}{l}\right)^4 \\
&\qquad = 2\left\{\rho a^2(1-\nu^2)\frac{\omega^2}{E}\right\}^3 - 2\left\{\rho a^2(1-\nu^2)\frac{\omega^2}{E}\right\}^2
\end{aligned}
\tag{2.13}
$$

The values for λ_i in the equation (2.13) will be of the form

$$\lambda_1 = K, \qquad \lambda_2 = -K, \qquad \lambda_3 = jK, \qquad \lambda_4 = -jK \tag{2.14}$$

The values for K are related to the boundary conditions of interest and we applied clamped condition at $x = 0$ with zero displacement and slope and free condition at $x = l$ with zero shear and moment as expressed in the following equation

$$\begin{aligned} w(x=0) = \frac{dw(x=0)}{dx} = 0 \\ \frac{d^2w(x=l)}{dx^2} = \frac{d^3w(x=l)}{dx^3} = 0 \end{aligned} \tag{2.15}$$

Applying four boundary conditions for the general form of radial displacement, equation (2.10) gives

$$\begin{aligned} &\sum_{i=1}^{4} C_i = C_1 + C_2 + C_3 + C_4 = 0 \\ &\sum_{i=1}^{4} C_i e^{\lambda_i} = C_1 e^{\lambda_1} + C_2 e^{\lambda_2} + C_3 e^{\lambda_3} + C_4 e^{\lambda_4} \\ &\qquad = C_1 e^{K} + C_2 e^{-K} + C_3 e^{jK} + C_4 e^{-jK} = 0 \\ &\sum_{i=1}^{4} C_i \lambda_i = C_1\lambda_1 + C_2\lambda_2 + C_3\lambda_3 + C_4\lambda_4 = C_1K - C_2K + jC_3K - jC_4K \\ &\qquad = 0 \end{aligned} \tag{2.16}$$

$$\sum_{i=1}^{4} C_i \lambda_i e^{\lambda_i} = C_1 \lambda_1 e^{\lambda_1} + C_2 \lambda_2 e^{\lambda_2} + C_3 \lambda_3 e^{\lambda_3} + C_4 \lambda_4 e^{\lambda_4}$$

$$= C_1 K e^{K} - C_2 K e^{-K} + jC_3 K e^{jK} - jC_4 K e^{-jK} = 0$$

Matrix form of the homogeneous system equation as follows

$$\begin{bmatrix} 1 & 1 & 1 & 1 \\ e^{K} & e^{-K} & e^{jK} & e^{-jK} \\ K & -K & jK & -jK \\ Ke^{K} & -Ke^{-K} & jKe^{K} & -jKe^{-jK} \end{bmatrix} \begin{Bmatrix} C_1 \\ C_2 \\ C_3 \\ C_4 \end{Bmatrix} = \begin{Bmatrix} 0 \\ 0 \\ 0 \\ 0 \end{Bmatrix} \tag{2.17}$$

To avoid non-trivial solution, the determinant of the matrix in the equation (2.17) should be zero.

$$det \begin{bmatrix} 1 & 1 & 1 & 1 \\ e^{K} & e^{-K} & e^{jK} & e^{-jK} \\ K & -K & jK & -jK \\ Ke^{K} & -Ke^{-K} & jKe^{K} & -jKe^{-jK} \end{bmatrix} = 0 \tag{2.18}$$

An analytical solution for equation (2.18) has been calculated using Matlab's symbolic operation. To make the determinant of homogeneous system matrix zero, there are infinite numbers of roots for K which are related to number of modes for axial waves along the pile length. To determine the roots for K, we used Matlab built in command "fzero". The left panel in Figure 2.1 shows the results of roots for K values.

The next step in calculating mode shapes for axisymmetric membrane cylindrical shell is finding relationship among the values of C_i from the equation (2.17). In regard to homogeneous system equation the four C_i are not independent and it is possible to solve

for three of them in terms of fourth. Matlab's symbolic operation is used again to apply Gauss-Elimination approach on the system matrix. The values for C_1, C_2, C_3 can be expressed as multiplication of C_4 as shown in equation (2.19)

$$C_1 = \alpha C_4, \quad C_2 = \beta C_4, \quad C_3 = \gamma C_4 \tag{2.19}$$

These expressions are substituted into the general solution form for radial displacement and mode shapes are obtained as shown in equation (2.20).

$$w_m(x,t) = \left\{\alpha C_4 \exp\left(\frac{\lambda_{1m}x}{l}\right) + \beta C_4 \exp\left(\frac{\lambda_{2m}x}{l}\right) + \gamma C_4 \exp\left(\frac{\lambda_{3m}x}{l}\right) + C_4 \exp\left(\frac{\lambda_{4m}x}{l}\right)\right\} cos\omega_m t \tag{2.20}$$

To obtain mode shapes for axial displacement ($u_{xm}(x,t)$), the general solution in the equation (2.8) is substituted into the equation (2.4) with the same assumption we applied in the equation (2.12)

$$\frac{A_i}{C_i}\left\{\frac{2}{1-\nu}\Delta^2 - \frac{3-\nu}{1-\nu}\Delta n^2\left(1 - \frac{\lambda_i^2 a^2}{n^2 l^2}\right) + n^4\left(1 - \frac{\lambda_i^2 a^2}{n^2 l^2}\right)^2\right\} = -\frac{\lambda_i a}{l}\left\{\frac{2\nu}{1-\nu}\Delta + n^2\left(1 + \nu\frac{\lambda_i^2 a^2}{n^2 l^2}\right)\right\} \tag{2.21}$$

The coefficients A_i can be expressed as factor of C_i as shown in equation (2.22)

$$A_i = -\frac{C_i \lambda_i a}{l} \frac{\frac{2\nu}{1-\nu}\Delta}{\frac{2}{1-\nu}\Delta^2} = -\frac{C_i \lambda_i a}{l}\frac{\nu}{\Delta} = \frac{C_i \lambda_i a}{l} M \tag{2.22}$$

where, $M = -\frac{\nu}{\Delta} = -\frac{\nu}{\rho a^2 (1-\nu^2)\frac{\omega^2}{E}}$

The values of coefficient A_i can be determined with known values for C_i and λ_i and substituting these expression into the general solution for axial displacement

$$u_{xm}(x,t) = \left\{\alpha' A_4 \exp\left(\frac{\lambda_{1m} x}{l}\right) + \beta' A_4 \exp\left(\frac{\lambda_{2m} x}{l}\right) + \gamma' A_4 \exp\left(\frac{\lambda_{3m} x}{l}\right) + A_4 \exp\left(\frac{\lambda_{4m} x}{l}\right)\right\} cos\omega_m t \tag{2.23}$$

Kraus [13] also provided the expression for mode shapes of axial displacement ($u_{xm}(x,t)$) with given information of radial displacement ($w_m(x,t)$) as shown in the equation (2.24)

$$u_{xm}(x,t) = Ma \frac{\partial w_m(x,t)}{\partial x} \tag{2.24}$$

We used equation (2.24) to obtain the mode shapes for axial displacement ($u_{xm}(x,t)$).

Figure 2.2 shows mode shapes for the first five modes of radial ($w_m(x,t)$) and axial displacement ($u_{xm}(x,t)$). It shows mode shapes with, $x = 0$ clamped and $x = l$ free, are the applied boundary conditions.

B. Calculation of natural frequencies

In addition to the calculation of mode shapes for radial and axial direction, it is necessary to obtain natural frequencies associated with modes shapes to solve free and forced vibration problems of interest using normal mode superposition technique. The natural frequencies are obtained from the equation (2.13) by substituting numerical values of K. The third order polynomial in regard to ω^2 with all known input parameters. We used Matlab built in command "fzero" again to determine out ω^2. The bottom panel in Figure 2.1 shows natural frequencies for clamped-free axisymmetric membrane cylindrical shell as function of number of half axial waves.

2.5 NORMAL MODE SUPERPOSITION APPROACH

A. Overview of normal mode superposition using string vibration

It is easier to explain normal mode superposition approach for the simplest example such as the response of a fixed-fixed string with point loading in the middle. Then we extend the approach to our problem of interest, impact pile driving on top of the pile.

The governing equation for finite string with fixed-fixed boundary condition is wave equation with a dependent variable, transverse displacement $y(x,t)$ and space and time dependent loading condition $q(x,t)$ as shown in the equation (2.25).

$$\frac{\partial^2 y(x,t)}{\partial x^2} - \frac{1}{{c_o}^2}\frac{\partial^2 y(x,t)}{\partial t^2} + q(x,t) = 0 \tag{2.25}$$

where, $c_0 = \sqrt{\frac{T}{\rho}}$: Phase velocity, T: tension, ρ_L: linear mass density

The solution in the form of transient response by normal mode superposition can be expressed as in the equation (2.26). $q_m(t)$ is unknown time dependent coefficients which

governs transient forced vibration problems of interest and $Y_m(x)$ is mode shapes for the fixed-fixed string.

$$y(x,t) = \sum_{m=1}^{\infty} q_m(t) Y_m(x) \tag{2.26}$$

Substituting the equation (2.26) into the governing equation for string with forcing function equation (2.25)

$$\sum_{n=1}^{\infty} \{\ddot{q_m}(t) + \omega_m^2 q_m(t)\} Y_m(x) = \frac{1}{\rho} q(x,t) \tag{2.27}$$

where, $\omega_m = \frac{m\pi c_o}{l}$: angular natural frequencies

Multiplying $Y_n(x)$ on both sides and integrated over the length of finite string gives

$$\sum_{m=1}^{\infty} \{\ddot{q_m}(t) + \omega_m^2 q_m(t)\} \int_0^l Y_m(x) Y_n(x)\, dx = \frac{1}{\rho} \int_0^l q(x,t)\, Y_n(x) dx \tag{2.28}$$

Using orthogonal property in the equation (2.28)

$$\ddot{q_m}(t) + {\omega_m}^2\, q_m(t) = \frac{1}{\rho \int_0^l Y_m(x)^2 dx} \int_0^l q(x,t)\, Y_n(x) dx \\ = Q_m(t) \tag{2.29}$$

The unknown time dependent coefficients can be determined using variation of parameters [22]

$$q_m(t) = \frac{1}{\omega_m} \int_0^t Q_m(t) sin\big(\omega_m(t-\tau)\big) d\tau \\ = \frac{1}{\omega_m} Q_m(t) \otimes sin(\omega_m t) \tag{2.30}$$

Transient response of fixed-fixed finite string can be determined by substituting $q_m(t)$ in the equation (2.30) into the general solution form for normal mode superposition in the equation (2.26) with associated mode shapes and natural frequencies.

B. Forced vibration of membrane cylindrical shell

We expanded this classical approach to clamped-free membrane cylindrical shell structure by setting normal mode superposition for radial displacement (w)

$$\begin{Bmatrix} u_x(x,t) \\ w(x,t) \end{Bmatrix} = \sum_{m=1}^{\infty} q_m(t) \begin{Bmatrix} u_{xm}(x) \\ w_m(x) \end{Bmatrix} \tag{2.31}$$

Referring to the end result shown in the equation (9.6a) in Kraus [13] , we can obtain

$$\sum_{m=1}^{\infty}\{\rho h\ddot{q_m}(t)+\rho h\omega_m^2 q_m(t)\}\begin{Bmatrix}u_{xm}(x)\\ w_m(x)\end{Bmatrix}=\begin{Bmatrix}p_x(x,t)\\ -p_w(x,t)\end{Bmatrix} \tag{2.32}$$

where, $q_m(t)$: unknown time dependent coefficients, $u_m(x)$: mode shapes for axial displacement, $w_m(x)$: mode shapes for radial displacement, $p_x(x,t)$: loading in axial direction, $p_w(x,t)$: loading in radial direction, ω_m: angular natural frequencies, ρ: density of the pile, h: thickness of the pile

Multiplication of each of equation (2.32) by $u_n(x)$ and $w_n(x)$, respectively, addition of two resulting equations and integration over the length of the pile gives

$$\begin{aligned}\int_{x=0}^{x=l}\sum_{m=1}^{\infty}\{\rho h\ddot{q_m}(t)+\rho h\omega_m^2 q_m(t)\}\{u_{xm}(x)u_{xn}(x)\\ +w_m(x)w_n(x)\}dx\\ =\int_{x=0}^{x=l}\{p_x(x,t)u_{xn}(x)-p_w(x,t)w_n(x)\}\,dx\end{aligned} \tag{2.33}$$

Using orthogonal property, the integral of the products of the displacement components will be non-zero for the case of m=n

$$\begin{aligned}\{\rho h\ddot{q_m}(t)+\rho h\omega_m^2 q_m(t)\}\{u_{xm}(x)^2+w_m(x)^2\}\\ =\int_{x=0}^{x=l}\{p_x(x,t)u_{xm}(x)-p_w(x,t)w_n(x)\}dx\end{aligned} \tag{2.34}$$

Rearranging equation (2.34)

$$\ddot{q_m}(t) + \omega_m^2 q_m(t) = \frac{1}{\rho h} Q_m(t) \tag{2.35}$$

where, $Q_m(t) = \frac{1}{\{u_{xm}(x)^2 + w_m(x)^2\}} \int_{x=0}^{x=l} \{p_x(x,t) u_{xm}(x) - p_w(x,t) w_m(x)\} dx$

$Q_m(t)$ relates space-time dependent forcing functions for axial (p_x)and radial (p_w) directions. We are considering force in the axial direction (p_x) as loading condition because actual impact pile driving involving vertically applied load on top of the pile structure. We ignore the surface loading (p_w) applied on the surface of the pile due to ocean waves, winds, and radiation loading by acoustic media. The unknown time dependent coefficients can be determined using variation of parameters again [12, 13]

$$\begin{aligned} q_m(t) &= \frac{1}{\rho h \omega_m} \int_0^t Q_m(t) sin\big(\omega_m(t-\tau)\big) d\tau \\ &= \frac{1}{\rho h \omega_m} Q_m(t) \otimes sin(\omega_m t) \end{aligned} \tag{2.36}$$

Finally, transient response of axial and radial displacements due to impact pile driving on top of the pile with clamped-free boundary condition can be obtained by substituting time dependent coefficients $q_m(t)$ in equation (2.36) into general form of normal mode expansion in equation (2.31). We generated Matlab code for entire procedures for transient structural response.

2.6 RESULTS

We applied example input parameters as indicated in the Table 2.1. The length of 10 m and radius of 1 m for the pile has been assumed. To check propagation speed of the

radial component of waves, we theoretically calculated compression and transverse wave speeds using the equation (2.37) - (2.40).

$$Bulk\ Modulus\ (\bar{K}) = \frac{E}{3(1-2\nu)} \tag{2.37}$$

$$Shear\ Modulus\ (\bar{G}) = \frac{E}{2(1+\nu)} \tag{2.38}$$

$$Compressional\ wave\ speed\ (c_p) = \sqrt{\frac{1}{\rho}\left(\bar{K} + \frac{4}{3}\bar{G}\right)} \tag{2.39}$$

$$Transeverse\ wave\ speed\ (c_s) = \sqrt{\frac{\bar{G}}{\rho}} \tag{2.40}$$

We focuses on the transverse wave speed because of the membrane cylindrical shell which supports only transverse wave propagation along the pile. The wave speed is 3,187 m/s using the material parameters in Table 2.1 and equation (2.38) and (2.40). Travel times to $L/4$, $L/2$ and $3L/4$ are 0.0000784, 0.0016, and 0.0024 second respectively. Figure 2.3 shows snap shots for the corresponding times. We also plotted the radial and axial displacement time history at the location of x $= L/2$ as shown in Figure 2.4 . These plots show the transient radial and axial displacement generated by impact loading applied in the axial direction as a result of simple analytical model. Velocity is then obtained by taking the derivative of the displacement. Harmonic pressure amplitude on the surface of the pile can be determined by taking Fourier Transform and multiplying characteristic acoustic impedance (ρc) of acoustic medium with the assumption that the spatial domain of pile is discretized finely enough and this enable us to use plane wave approximation. This post processing from the result of simple analytical model

constitutes a starting field for the MMPE model's broadband calculation we have done in the coupled FE-MMPE approach.

2.7 CONCLUSIONS

We have developed a relatively simple semi-analytical model for the structural response of finite length membrane cylindrical shell due to impact pile driving. We set clamped end at $x = 0$ and free end at $x = L$ assuming the pile is driven deep enough in the ocean bottom. Starting from Donnell's equations of motion for thin cylindrical shell (which is coupled 4th order PDE). We followed decoupling procedure as described in the Kraus [13] and then applied our assumption simplifying the complicated decoupled 8th PDE for the dependent variable of radial displacement. The first assumption is that the loading and associated outputs are axisymmetric and independent of azimuthal angle (θ) which enable us to cancel all the terms partial derivative with respect to azimuthal angle (θ). Other assumptions are that the finite length cylinder is membrane shell and large aspect ratio which is related to the Yu's assumption [21]. We took advantage of Matlab functions for finding determinant of homogeneous system equation for solving for mode shapes for radial and axial displacement and associated natural frequencies. To handle forced vibration problem of cylindrical shell, we used normal mode superposition approach and the results show that radial displacement propagates with theoretical transverse wave speed. The outputs with some post-processing can be used as a starting field of the ocean acoustics propagation model MMPE as we did our previous study.

ACKNOWLEDGEMENTS

I would like to acknowledge the financial support of the Republic of Korea Navy and the Link Foundation Ocean Engineering and Instrumentation PhD Fellowship Program which enabled me to carry out this work at the University of Rhode Island.

TABLES

Table 2.1 Input parameters for analytical model

Contents	Parameters	
Material parameters	Density ($\rho, kg/m^3$)	7831
	Young's Modulus (E, GPa)	206.8
	Poisson's Ratio(ν)	0.3
Geometric parameters	Length (m)	10
	Radius (m)	1
	Thickness (m)	0.001
Propagation speed	Compressional wave speed (c_p, m/s)	5,962
	Transverse wave speed (c_s, m/s)	3,187

FIGURES

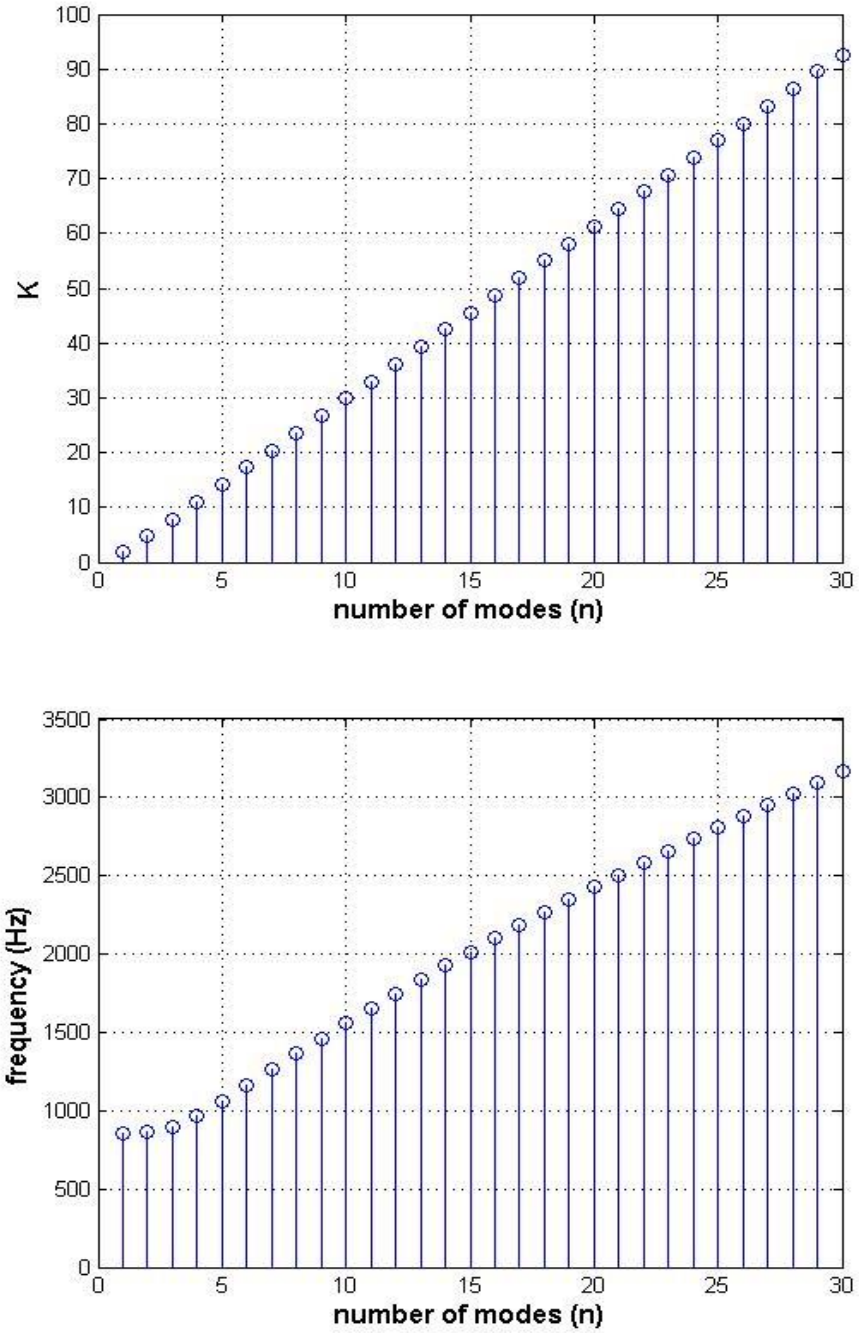

Figure 2.1 **Values of K (top panel) and associated natural frequencies (bottom panel) as function of number of modes**

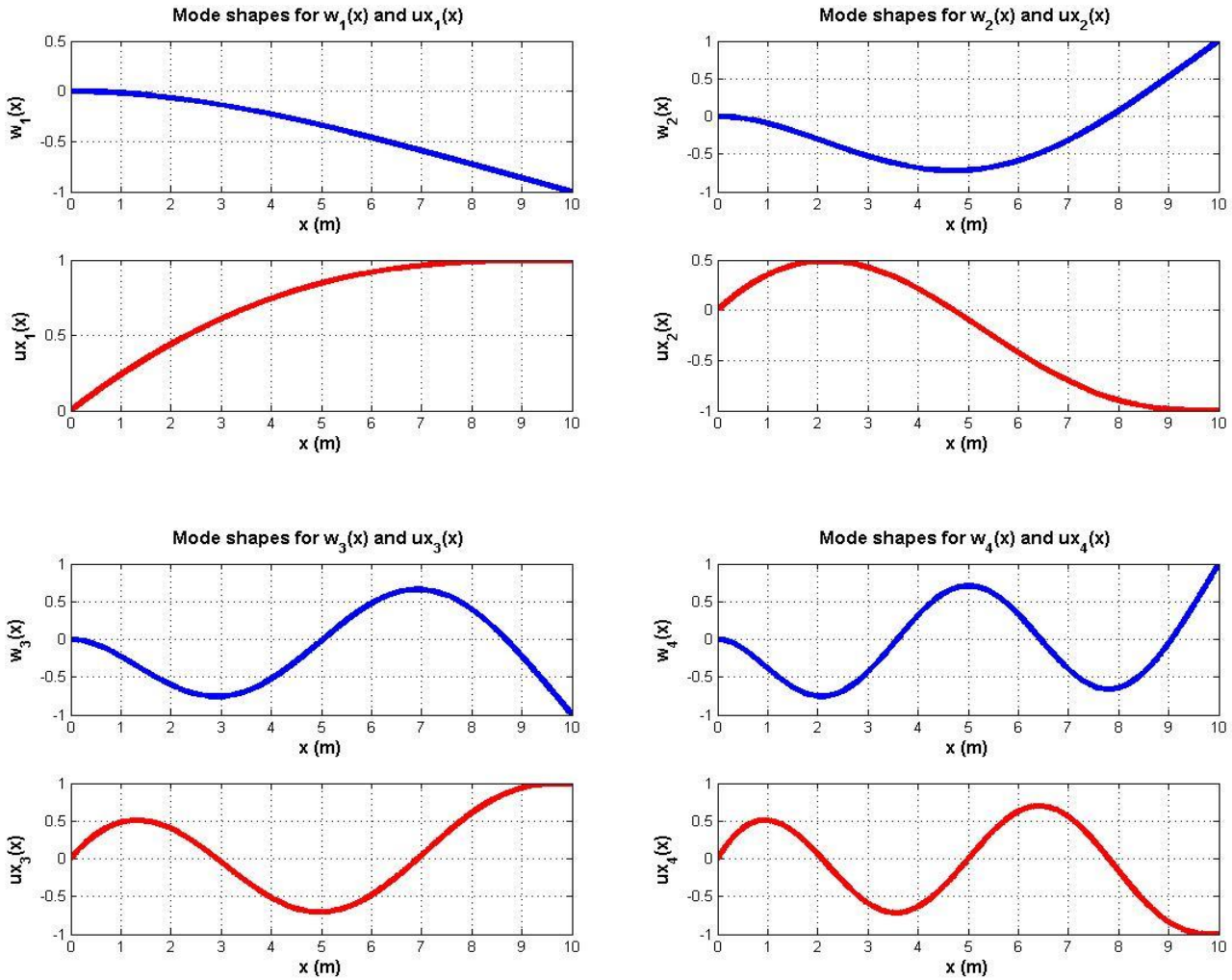

Figure 2.2 **Mode shapes for the first 4 modes of radial ($w_m(x,t)$) and axial ($u_{xm}(x,t)$) displacement**

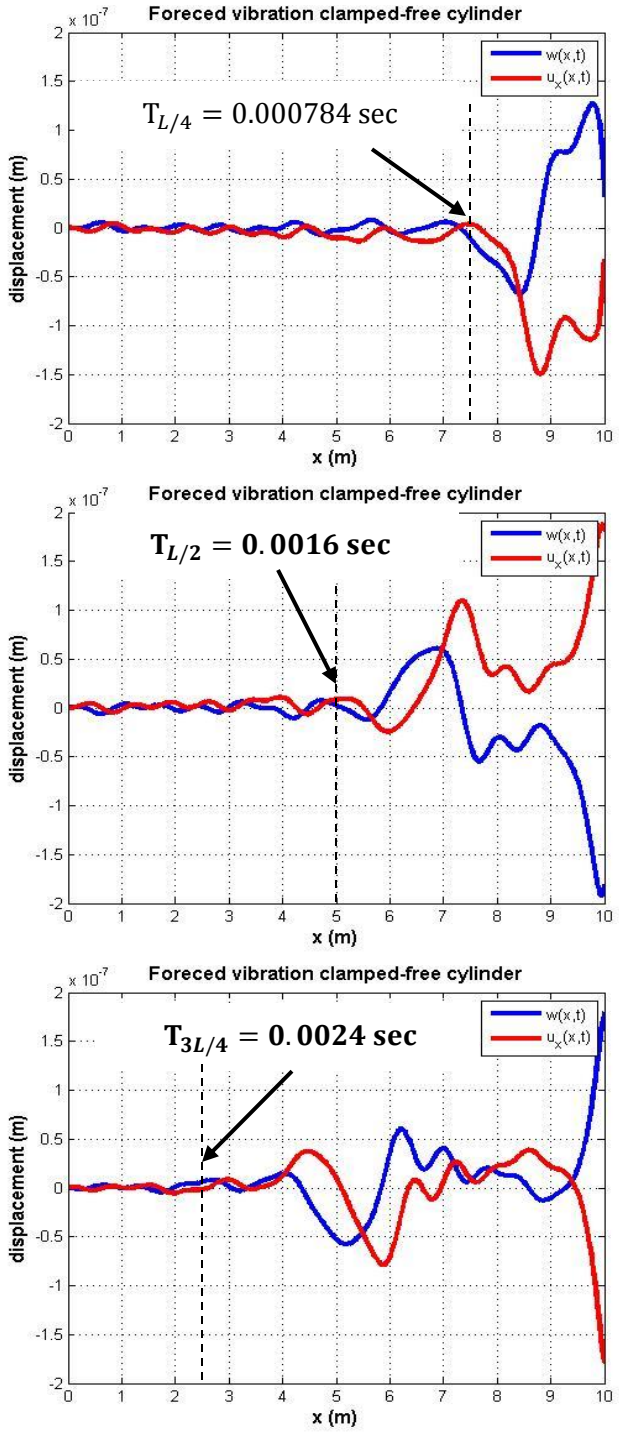

Figure 2.3 **The radial ($w(x,t)$) and axial ($u_x(x,t)$) displacement at time, $T_{L/4} = 0.000784$ sec (top), $T_{L/2} = 0.0016$ sec (middle), $T_{3L/4} = 0.0024$ sec (bottom)**

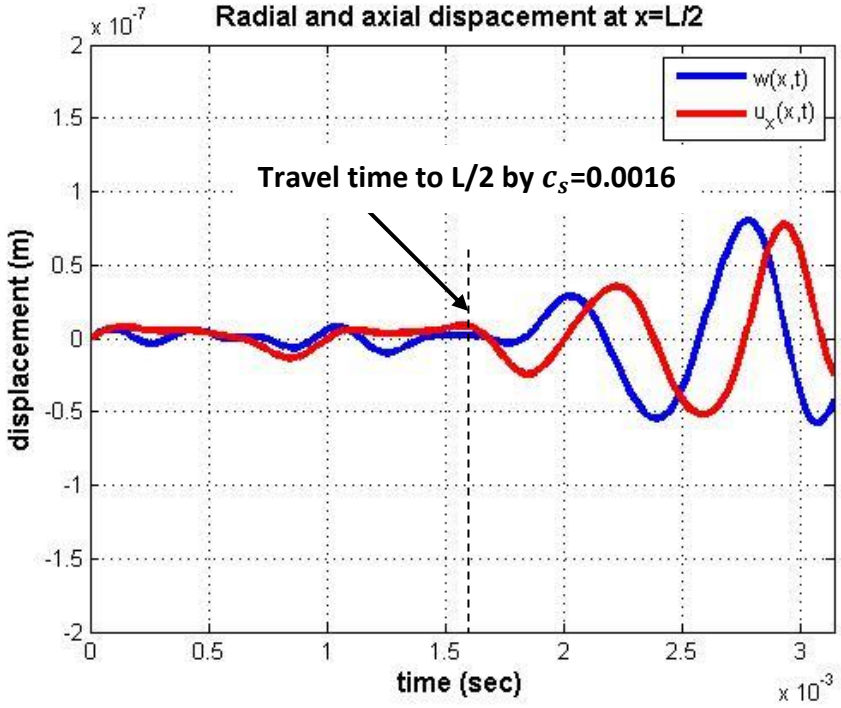

Figure 2.4 **The radial ($w(x,t)$) and axial ($u_x(x,t)$) displacement time history at x=L/2**

REFERENCES AND LINKS

1. **Junger, M.C. and F.J. Rosato, *The Propagation of Elastic Waves in Thin-Walled Cylindrical Shells*. The Journal of the Acoustical Society of America, 1954. 26(5): p. 709-713.**

2. **Junger, M.C., *Approaches to acoustic fluid--elastic structure interactions.* The Journal of the Acoustical Society of America, 1987. 82(4): p. 1115-1121.**

3. **Junger, M.C. and J.M. Garrelick, *Multiple modal resonances of thin cylindrical shells vibrating in an acoustic medium.* The Journal of the Acoustical Society of America, 1984. 75(5): p. 1380-1382.**

4. **Junger, M.C., D. Feit, and J.E. Greenspon, *Sound, Structures, and Their Interaction,* 2nd edition by Miguel C. Junger and David Feit. The Journal of the Acoustical Society of America, 1987. 82(4): p. 1466.**

5. **Junger, M.C., *Vibrations of simply supported cylindrical shells isolated from an ambient acoustic medium by a compliant layer.* The Journal of the Acoustical Society of America, 1992. 92(4): p. 1994-1997.**

6. **Stepanishen, P.R., *Radiated power and radiation loading of cylindrical surfaces with nonuniform velocity distributions.* The Journal of the Acoustical Society of America, 1978. 63(2): p. 328-338.**

7. **Stepanishen, P.R., *Modal coupling in the vibration of fluid-loaded cylindrical shells.* The Journal of the Acoustical Society of America, 1982. 71(4): p. 813-823.**

8. **Stepanishen, P.R. and S.E. Hassan, *Harmonic response of finite cylindrical shells coupled to interior fluid regions.* The Journal of the Acoustical Society of America, 1991. 90(4): p. 2343.**

9. **Stepanishen, P.R. and H.-W. Chen, *Acoustic harmonic radiation and scattering from shells of revolution using finite element and internal source density methods.* The Journal of the Acoustical Society of America, 1992. 92(6): p. 3343-3357.**

10. **Stepanishen, P.R. and H.-W. Chen, *Surface pressure and harmonic loading on shells of revolution using an internal source density method.* The Journal of the Acoustical Society of America, 1992. 92(4): p. 2248-2259.**

11. **Stepanishen, P.R., *Acoustic transient radiation and scattering from fluid-loaded elastic shells using convolution methods.* The Journal of the Acoustical Society of America, 1997. 102(1): p. 110-119.**

12. **Kraus, H. and A. Kalnins, *Transient Vibration of Thin Elastic Shells.* The Journal of the Acoustical Society of America, 1965. 38(6): p. 994-1002.**

13. **Kraus, H., Thin elastic shells; *An introduction to the theoretical foundations and the analysis of their static and dynamic behavior 1967:* John Wiley & Sons, Inc.**

14. **Reinhall, P.G. and P.H. Dahl. *Acoustic radiation from a submerged pile during pile driving.* in OCEANS 2010. 2010.**

15. **Reinhall, P.G. and P.H. Dahl, *Underwater Mach wave radiation from impact pile driving: Theory and observation.* The Journal of the Acoustical Society of America, 2011. 130(3): p. 1209-1216.**

16. **Kim, H., et al., *Modeling of offshore wind turbine noise radiation and propagation.* The Journal of the Acoustical Society of America, 2011. 130(4): p. 2332.**

17. **Huikwan, K., et al. *Long range propagation modeling of offshore wind turbine construction noise using Finite Element and Parabolic Equation models.* in OCEANS, 2012 - Yeosu. 2012.**

18. **Kim, H., et al., *Long range propagation modeling of offshore wind turbine noise using finite element and parabolic equation models.* The Journal of the Acoustical Society of America, 2012. 131(4): p. 3392.**

19. **Kim, H., J.H. Miller, and G.R. Potty, *Predicting underwater radiated noise levels due to the first offshore wind turbine installation in the U.S.* The Proceedings of Meetings on Acoustics, 2013. 19: p. 040067.**

20. **Miller, J.H., G.R. Potty, and H. Kim, *Pile driving pressure and particle velocity at the seabed: Quantifying effects on crustaceans and ground fish.* The 3rd International Conference on the Effects of Noise on Aquatic Life, 2013.**

21. **Yu, Y.Y., *Free vibrations of thin cylindrical shells having finite lengths with freely supported and clamped edges.* Journal of applied mechanics, 1955: p. 547-552.**

22. **Graff, K.F., *Wave motion in elastic solids* p. 49-51 1975: Oxford University Press.**

MANUSCRIPT – III

Intended for submission to the Journal of the Acoustical Society of America-Express

Letter

Finite element acoustic modeling of offshore impact pile driving with fluid and elastic ocean bottoms

Corresponding Author:

Huikwan Kim

Department of Ocean Engineering, University of Rhode Island, Narragansett, Rhode Island 02882, hkkim524@my.uri.edu

Contributing Authors:

James H. Miller, Gopu R. Potty

Department of Ocean Engineering, University of Rhode Island, Narragansett, Rhode Island 02882

Abstract: There is concern that sound from offshore impact pile driving may be intense enough to harm marine life. Reinhall and Dahl [1] used one of the commercial FE (Finite Element) code, Comsol Multiphysics and PE (Parabolic Equation) to model offshore impact pile driving noise and they modeled the ocean bottom as fluid half space. We benchmarked their measurement set up using another FE code, Abaqus/CAE 6.11 and verified our model with their measured data. We extended our model by considering the ocean bottom as elastic medium and that enables the prediction of the interface wave (Sholte wave) propagating along the water and ocean bottom interface. Thus, the effects of particle velocity of the acoustic field due to impact pile driving on the seabed on benthic species such as crustaceans and ground fish. In our FE model, we used implicit dynamic analysis and presented acoustic pressure and particle velocity field outputs and received levels at the pre-defined nodes of interest.

PACS numbers: 43.30.Jx, 43.30.Ky, 43.30.Nb

3.1 INTRODUCTION

Offshore wind turbines are being used by a number of countries to harness the energy of strong, consistent winds that are found over the oceans[2]. However, sound generated by offshore impact pile driving for wind turbine construction radiates into and propagates through the air, water, and ocean bottom. Noise and vibration increase with pile size (diameter and wall thickness) and hammer energy [3-5]. Researchers have investigated acoustic impact due to this noise in the water column by analyzing measured data and numerical modeling and simulation. We initiated this study by developing a benchmark model with the bottom considered as fluid half-space. Then, we verified our FE model by comparing with the measured data Reinhall and Dahl [1]. We modeled the ocean bottom as elastic medium and observed that the particle velocity amplitudes by interface waves are relatively high compared to the compressional and shear waves in the ocean bottom.

Offshore wind farms are being planned and construction could begin in the near future along the east coast of the U.S. and one of the offshore wind turbines project, Block Island Wind Farm is a 30-megawatt offshore wind farm to be located approximately three miles southeast of Block Island Rhode Island consisting of 5 turbines. The company will begin transmission construction as early as 2014 and offshore construction in 2015 [6].

3.2 BENCHMARK MODEL

Following Reinhall and Dahl [1, 7], we modeled the Vashon pile which was driven using a Delmag D62-22 Diesel Hammer with an impact weight of 6,200 kg and energy of 180 kNm. The initial downward velocity of weight is 7.6 m/s and the equation for the

average pressure across the top of the pile during impact was approximated by $p(t) = 2.1 \times 10^8 \exp\left(-\frac{t}{\tau}\right)$ Pa, where t is time after impact and time constant τ is equal to 0.004 second [1]. This loading condition was used in our entire FE model. The measurement set up for impact pile driving by Reinhall and Dahl is shown in Figure 3.1. The depth of water is 12.5m and 30.2 m length of pile is driven into the sediment by 10 m. The speed of sounds in the water and sediment are 1485 m/s and 1625 m/s respectively. The associated material properties such as bulk modulus and density are set to achieve these sound speeds. To simulate transient noise radiation from a submerged pile, we used implicit dynamic analysis with pressure impact loading as function of time on top of the pile. A compressional wave in the pile caused by the hammer strike produces an associated radial displacement motion due to the Poisson effect. The radial displacement propagates downwards. Since the speed of sound in the steel pile is higher than in water, the rapidly downward propagating wave produces an acoustic field in the shape of an axisymmetric cone which is called Mach wave. The cone's apex travels concurrently with the pile deformation wave front. When the Mach wave reaches the pile's terminal end, it is reflected upwards. This phenomenon is shown in Figure 3.2. The first Mach wave in the water column propagates with the Mach angle and the pre-defined nodes at the distance of 8, 12, and 15 m which correspond to the Reinhall and Dahl's measurement set up recorded time history of acoustic pressure amplitude. The dynamic range for pressure unit of KPa in the first panel applies to all other panels consistently for direct comparison. The results in Figure 3.3 obtained by calculating SPL of first arrival Mach wave from our FE analysis compared well with the measured data by the VLA (Vertical Line Array) located at 8, 12, 15 m from the pile in the published paper by

Reinhall and Dahl [1]. The FE results at pre-defined nodes are shown as solid line with different color and the results using red square, black triangle, and blue circle represent measured data. The valued for the these measured SPL data were picked from Reinhall and Dahl's previous work [1] to overlay our FE results and their measured data.

3.3 MODELING OF IMPACT PILE DRIVING OFF BLOCK ISLAND RI

We extended our FE model to the offshore impact pile driving noise off Block Island Rhode Island based on the results of the benchmark model. According to the Ocean SAMP (Special Area Management Plan) report [8, 9] the foundation pile has 1.8m diameter and 0.05m wall thickness. The length of the pile below seabed was set to 10 m in the FE analysis to ensure some incorporation of ocean bottom - pile structure interaction in the design. Water depth three miles off Block Island is approximately 26 m based on the bathymetry data [10]. We used measured SSP as part of the Ocean SAMP project. Overall, the SSP is decreasing with depth. The FE model has difficulty applying the depth dependent SSP. Hence, the material properties for homogeneous water are defined to make the mean of the SSP, 1,517.1 m/s. To achieve average SSP of 1,517.1 m/s for the FE model, the bulk modulus is set to 2.359 GPa with density of salt water 1,025 kg/m^3. In the acoustic medium, the compressional wave speed can be expressed in terms of bulk modulus (K) and density (ρ) as shown in equation (3.1)

$$C_{p\_acoustic} = \sqrt{\frac{K}{\rho}} \tag{3.1}$$

We considered the ocean bottom as fluid and elastic material because fluid bottom only support propagation of compressional waves but elastic bottom support shear and interface waves in addition to compressional waves. The focus of this study is quantitatively predicting particle velocity due to interface wave on the seabed. We set pre-defined nodes on the seabed with 1 m spacing and these nodes are supposed to record acoustic pressure and velocity time history.

A. Fluid bottom FE model

For this model, the ocean bottom is considered as acoustic medium by inputting density (ρ) and bulk modulus (K) in the property module of Abaqus/CAE 6.11. The compressional wave speed in the bottom is set to 1746 m/s. We used implicit dynamic analysis and maximum time duration was set to 0.0377 second and time increment was set to 6.7535e-5 second. The field output request was defined to calculate acoustic pressure units in Pascal in addition to default setting such as displacement, velocity, acceleration and so on. The history output was set to record acoustic pressure and vertical and horizontal component of velocity time series at the predefined nodes. The virtual HLA is located at water depth 26 m (water-bottom interface). We used 8-node quadratic axisymmetric acoustic quadrilateral element for the air, water, and bottom domain and 8-node biquadratic axisymmetric quadrilateral element for steel pile domain. To prevent reflection from the numerical boundaries from air, water, and bottom domain, non-reflecting boundary condition was defined along the boundary. The boundary conditions for pile structure are set to free top end and fixed lower end assuming the lower end of pile reaches to the fixity depth. This is an acoustic structure interaction problem and the velocity outputs at the nodes on the pile structure in contact with acoustic medium can be

converted associated acoustic pressure at the nodes in the acoustic medium. Specific details about FE theory are well described in the manual [11]. To solve this interaction problem, tie constraints were applied all the contacts in the FE model. For example, the surface of the steel pile interacts with three acoustic media and acoustic media interact at the air-water and water-bottom interface region.

B. Elastic bottom FE model

On top of the same FE modeling set up, we tried to model the ocean bottom as elastic medium by inputting Young's modulus (E), Poisson's ratio (ν), and density (ρ) because this modeling supports propagation of shear and interface waves due to impact pile driving in addition to compressional waves. We observed this phenomenon in our previous work [12] and we assumed that vertical component of particle velocity of ground rolling interface waves due to offshore impact pile driving affect animals living on the ocean bottom like flounders and lobsters. For the elastic bottom FE model, we set the pile is driven to 10 m in the ocean bottom. The locations of pre-defined nodes are the same as the setting in the fluid bottom FE model. The compressional wave speed (1,746 m/s) in the elastic bottom is the same as in the fluid bottom FE model. Using equation (3.2), we applied Young's modulus of 1,147,000,000 Pa and Poisson's ratio of 0.463 and density of 1886 kg/m^3 for the elastic sediment to achieve corresponding compressional wave speed.

$$C_{p\_elastic} = \sqrt{\frac{E(1-\nu)}{\rho(1+\nu)(1-2\nu)}} \tag{3.2}$$

The material properties of each part are summarized in the Table 3.1. Lastly, we applied attenuation in the elastic ocean bottom by defining Rayleigh damping coefficient. We tested the relationship between Rayleigh damping coefficient and attenuation coefficient in the ocean bottom of our interest. We set the bottom attenuation to 0.025 dB/m based on the figure 24 in which reproduced from Potty et al [13]. Structures and foundations damping plays an important role in dynamic analysis. One of the ways to treat damping within modal analysis is to consider the damping value as an equivalent Rayleigh Damping in form of

$$[C] = \alpha[M] + \beta[K] \tag{3.3}$$

where, $[C]$ = damping matrix of the physical system; $[M]$ = mass matrix of the physical system; $[K]$ = stiffness matrix of the system; α and β are pre-defined constants. Modal damping ratios (ζ_i) can be expressed as following with angular frequencies (ω_i)

$$\zeta_i = \frac{\alpha}{2\omega_i} + \frac{\beta\omega_i}{2} \tag{3.4}$$

We assumed the first term in equation (3.4) which is inversely related to angular frequency is small and considered damping ratio is linearly related to angular frequency with Rayleigh damping coefficient β. To find out appropriate value of β, We carried out parametric study for β in our FE model to achieve this attenuation in the ocean bottom. The specific values for these coefficients are $\alpha = 0$ and $\beta = 5 \times 10^{-6}$.

3.4 RESULTS FOR FLUID AND ELASTIC BOTTOM FE MODEL

This section discusses the results of prediction for offshore impact pile driving noise. The acoustic pressure and velocity field outputs are plotted to visualize the evolution of Mach waves from the pile. In addition, we plotted SEL in dB re 1 μPa^2 and velocity amplitude in m/s on the seabed as function of range. The equation (3.5) is used for the calculation of SEL. $p(t)$ is pressure time history at the pre-defined nodes.

$$SEL = 10\log_{10}\left(\frac{\int_0^{T_0}|p(t)|^2 dt}{1\mu Pa^2}\right) \tag{3.5}$$

Figure 3.4 shows acoustic pressure output for the fluid bottom FE model. The four panels show evolution of Mach waves from the top of the pile due to exponentially decaying pressure impact on top. The pile is in contacted with three acoustic media, air, water, and bottom. The pile can be seen as straight line because axisymmetric model is used and same material properties for the acoustic media are defined inside and outside pile respectively. The dynamic range is set to the same for the four panels maintaining consistency. In the first panel, it is clearly observed that the Mach wave is propagating down the pile as radial displacement due to Poisson effect by compressional wave. The compressional wave speed in the steel pile is much faster than the one in the acoustic media and the Mach wave has wave front with the Mach angle defined by the equation (3.6)

$$\theta_{Mach} = \sin^{-1}\left(\frac{c_{p\_medium}}{c_{p\_pile}}\right) \tag{3.6}$$

As time increases (the second panel), the Mach wave is incident on the ocean bottom and it has bigger Mach angle in the bottom due to higher compressional wave speed in the bottom. When the Mach wave reaches the lower end of the pile it is reflected and propagates back to the top of the pile with associated Mach wave angle as shown in the third panel.

In contrast to the fluid bottom FE model, Figure 3.5 shows offshore impact pile driving noise with the ocean bottom considered as elastic medium. We applied compressional wave attenuation of 0.025 dB/m in the bottom based on the result of previous study by Potty et al [13]. To accomplish the attenuation we defined the Rayleigh damping coefficient $\alpha = 0$ and $\beta = 5 \times 10^{-6}$ in the property module in Abaqus/CAE. There are legends for acoustic pressure in air and water and velocity in the bottom. When the Mach wave meets the ocean bottom, the magnitude of velocity field outputs show wave family of compressional, shear, and interface waves. Each wave has different propagation speed and separation is clearer as the time evolves. In the fourth panel, the compressional wave reaches the horizontal end of the numerical model and slowly propagates as ground rolling wave, interface wave, which has higher amplitude compared to shear and compressional waves.

We focus on the effect of this wave on marine life living on the seabed and investigated the contribution of the interface wave by comparing acoustic pressure amplitudes at pre-defined nodes on the seabed. These nodes are seen as red dots on all of the panels in Figure 3.4 and Figure 3.5.

We calculated SEL as function of range up to 10 m for this study and it will be possible to get longer range if we increase the size of the FE model. The left panel in Figure 3.6 shows two SEL curves for fluid and elastic bottom FE models. Overall SEL is higher than 200 dB at range 10 m and the SEL of the elastic bottom FE model is approximately 4 dB higher than in fluid bottom FE model due to the contribution of interface wave. The difference between two models is bigger in the near field and it decreases with range because the amplitude of interface wave decays fast.

Finally we investigated the peak velocity propagating along the water-bottom interface. The right panel in Figure 3.6 shows vertical and horizontal component of peak particle velocity as function of range up to a range of 10 m. The combination of vertical and horizontal component of particle velocities constitute ground rolling interface wave and crustaceans and ground fish are exposed to consecutive interface waves due to reflections from lower and top end of the pile for single impact. It is estimated that each pile requires 10,000 strike per pile [12].

3.5 CONCLUSIONS

We have successfully modeled offshore impact pile driving noise using one of the commercial FE code Abaqus/CAE 6.11. The goal of this study is quantitative prediction of noise and vibration impact on the seabed due to interface wave generated by the impact pile driving. It is important to know the impact of pile driving on the animals living on the seabed. We started from development of benchmark model for Reinhall and Dahl's measurement set up to compare the result of our model with the measured data in the published paper [1]. Even though we are assuming axisymmetric condition and

homogeneous speed of sound in water and flat ocean bottom with water depth of 12.5 m and flat water surface, the calculation of SPL of first arrival Mach wave on to the virtual VLA at 8, 12, and 15 m is well matched to the SPL of measured data. Based on the satisfactory modeling and simulation result of our benchmark model, we extended similar modeling with the scenario of Block Island Wind Farm Project with fluid and elastic bottom FE models. To make our model practically useful, we tested the relationship between Rayleigh damping coefficients for elastic bottom and the attenuation coefficient we want to apply in the piling spot of interest. We observed slowly propagating high velocity amplitude which is interface wave in our crude elastic bottom FE model. It is necessary to investigate the velocity impact on marine in addition to the acoustic impact. Thus we compared SEL outputs for fluid and elastic bottom FE models on the seabed as function of range and the SEL in the elastic bottom has approximately 4 dB higher and the contribution of interface wave decreases quickly with the. The prediction of vertical and horizontal components of velocity on the seabed will be useful in investigating the vibration impact from the biological point of view. We also found the possibility developing inversion scheme using the elastic bottom FE model. Based on the Sholte wave arrivals, it is possible to pose an inverse problem estimate ocean bottom properties.

ACKNOWLEDGEMENTS

I would like to acknowledge the financial support of the Republic of Korea Navy and the Link Foundation Ocean Engineering and Instrumentation PhD Fellowship Program which enabled me to carry out this work at the University of Rhode Island.

TABLES

Table 3.1 Material properties of the fluid and elastic bottom FE model

Parameters	Air	Water	fluid bottom	Elastic bottom	Steel
Density ($\rho, kg/m^3$)	1.21	1,025	1,866	1,866	7,831
Bulk Modulus (K, Pa)	117,650	2,358,821,225	5,750,315,938	-	-
Young's Modulus (E, Pa)	-	-	-	1,147,000,000	206,800,000,000
Poisson's Ratio(ν)	-	-	-	0.463	0.3
Compressional wave speed (m/s)	311	1517.1	1,746	1,746	5,962
Shear wave speed (m/s)	-	-	-	458	3,187

FIGURES

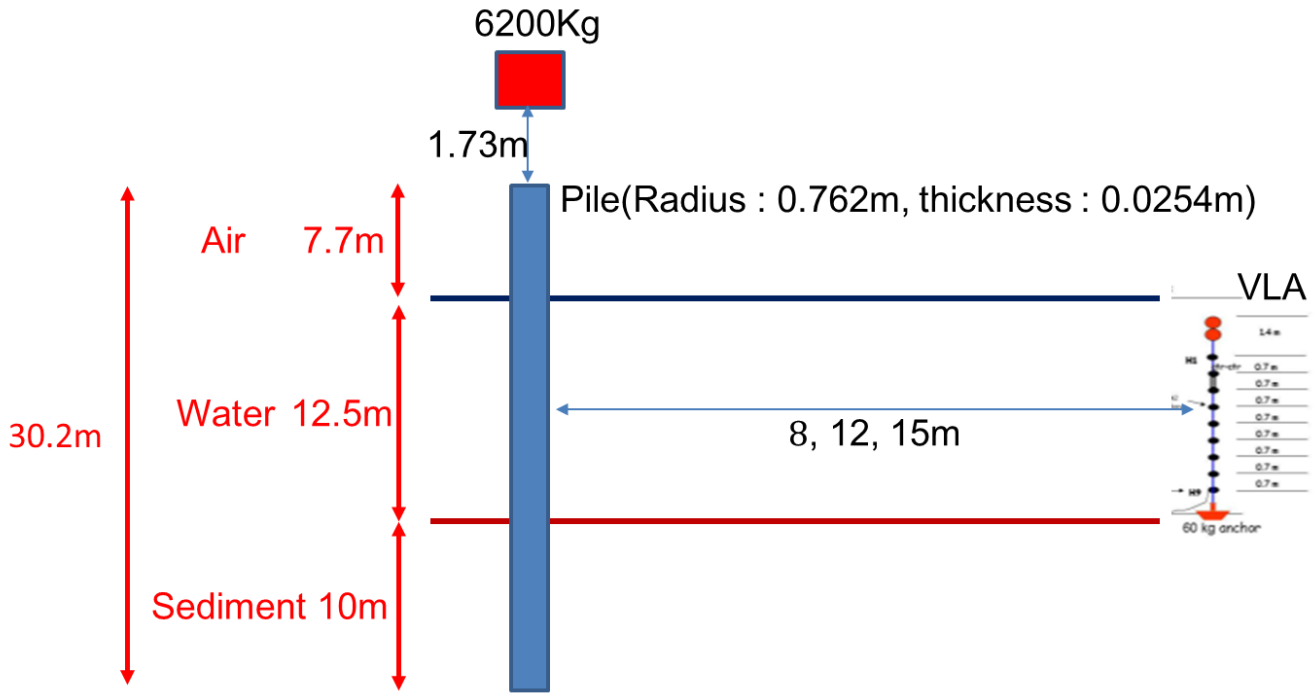

Figure 3.1 Measurement set up for impact pile driving by Reinhall and Dahl [1, 7]

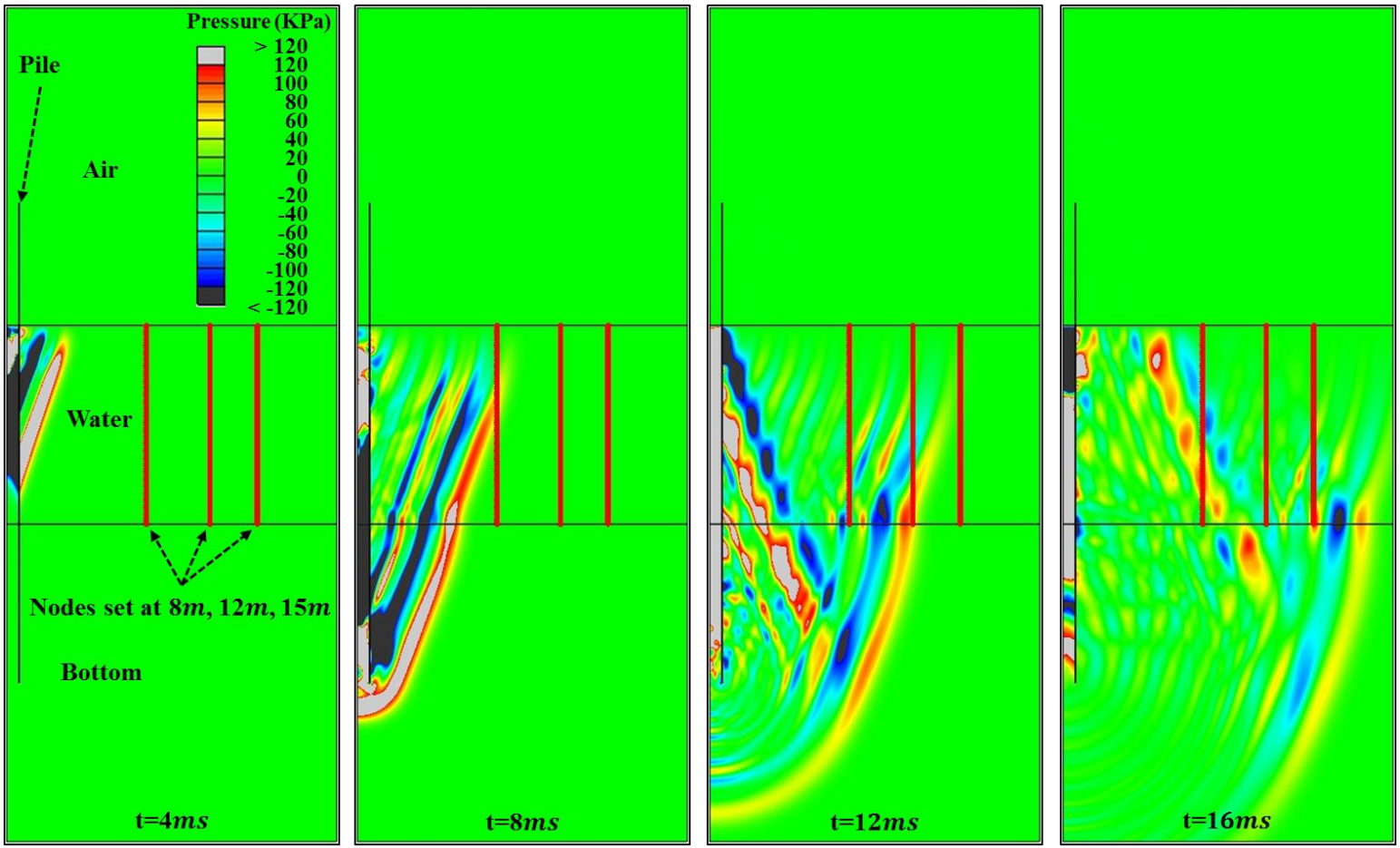

Figure 3.2 **Acoustic wave generated by the pile hammer impact for the case of fluid bottom. The four panels show the evolution of the waves at time t=4, 8, 12, 16 milliseconds. The red dots simulating the VLA at 8, 12, and 15 m are recording acoustic pressure time history (all panels have same dynamic ranges)**

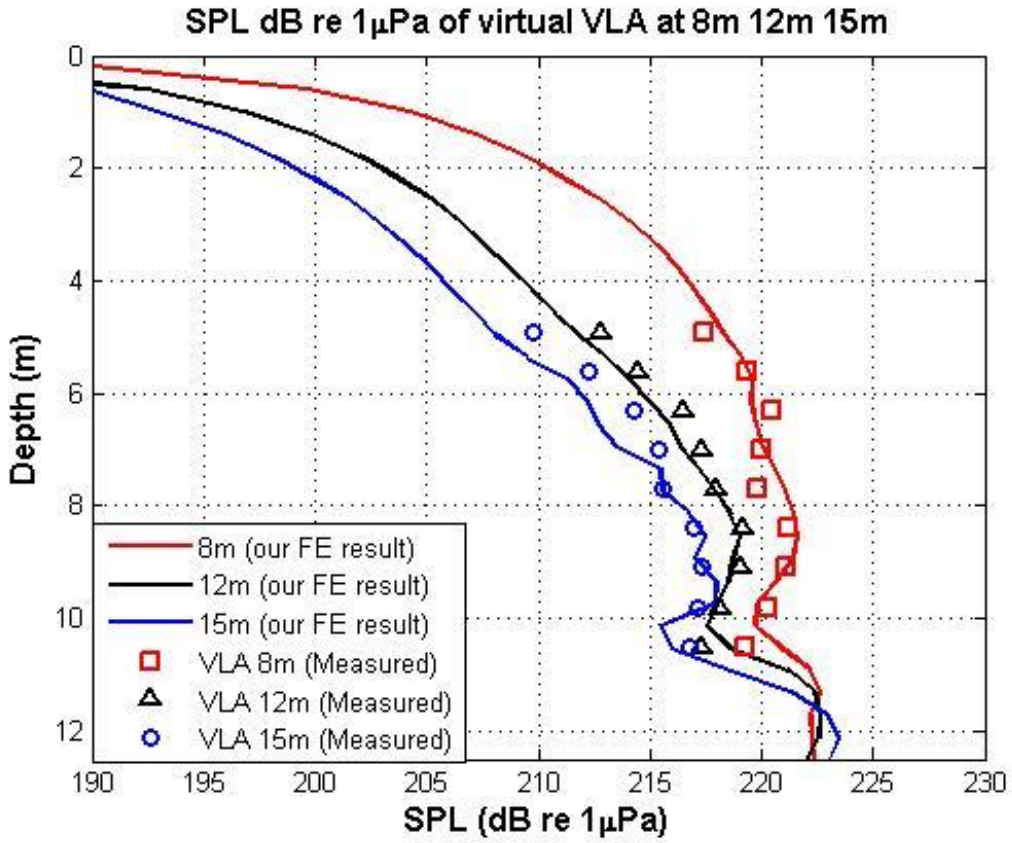

Figure 3.3 **The first-arrival pressure amplitude in dB re 1μPa as a function of depth. The solid lines with different color represent the result of our FE model and the representation of 'rectangle', 'triangle', 'circle' shows measured data from VLA at 8m, 12m, 15m respectively**

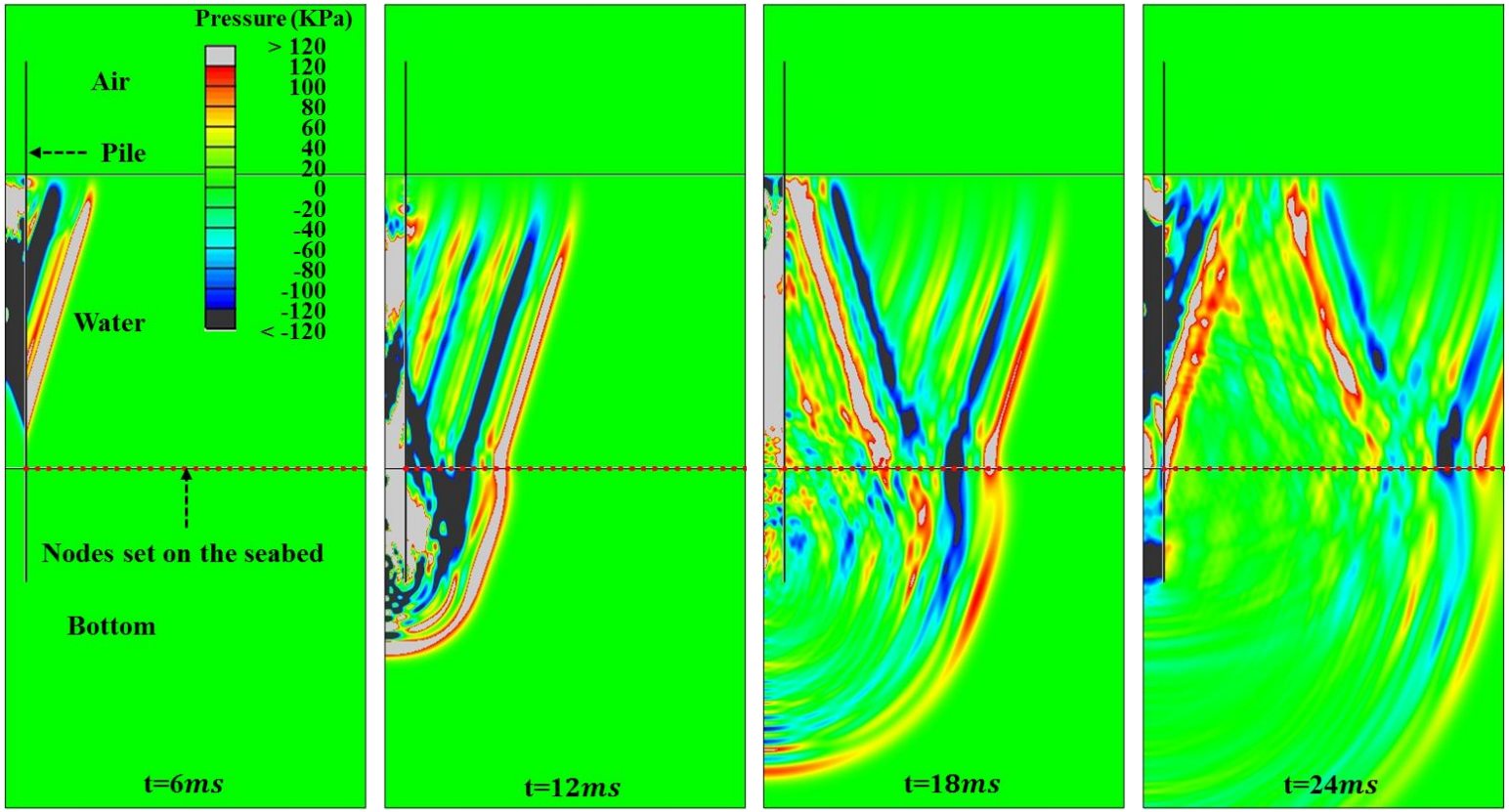

Figure 3.4 **Acoustic wave generated by the pile hammer impact for the case of fluid bottom FE model. The four panels show the evolution of the waves at time t=6, 12, 18, 24 milliseconds. The air, water, and bottom domain only support propagation of compressional waves. The red dots on the seabed are pre-defined nodes to record acoustic pressure and velocity time history**

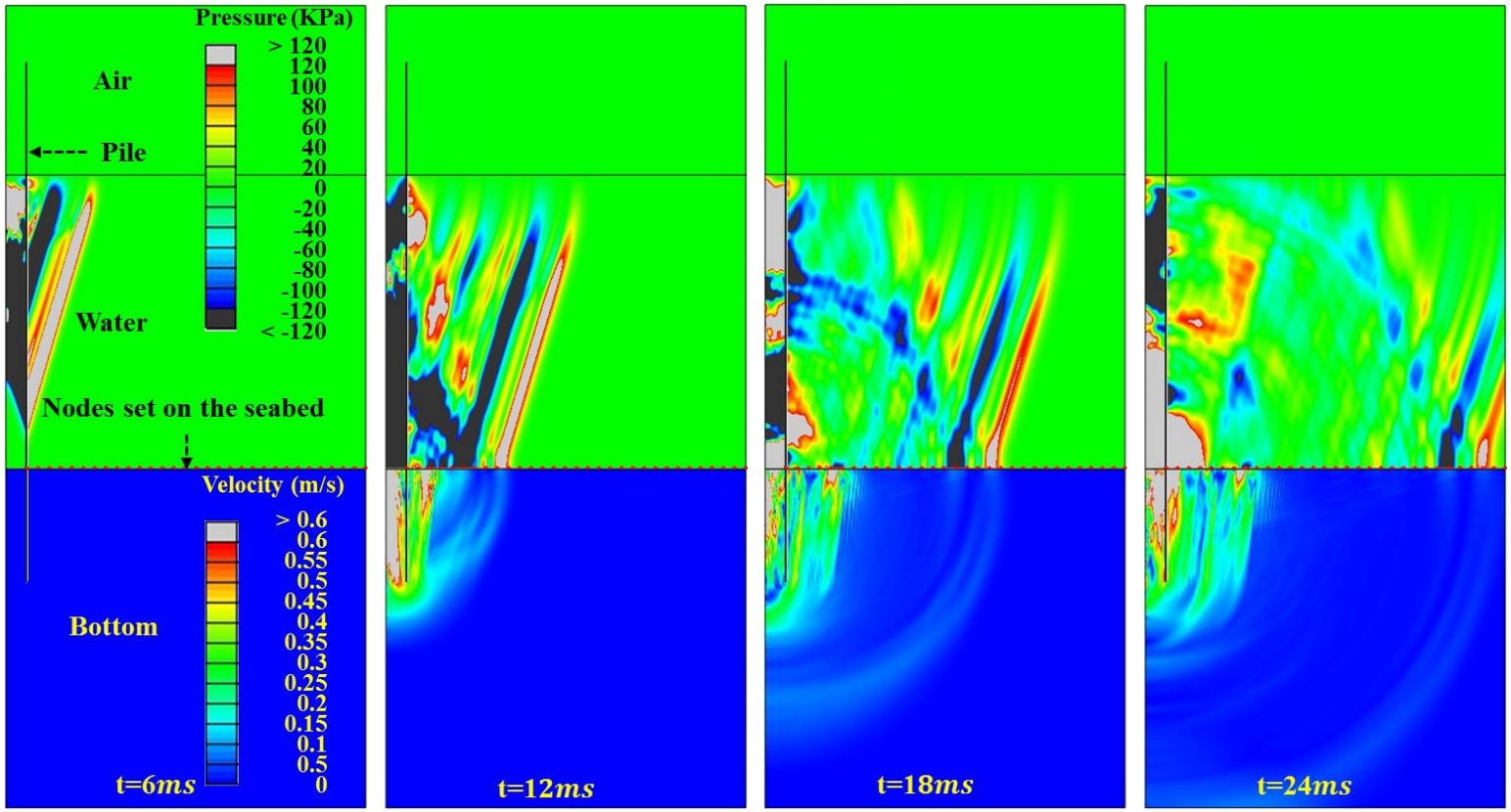

Figure 3.5 **Acoustic wave generated by the pile hammer impact for the case of elastic bottom FE model. The four panels show the evolution of the waves at time t=6, 12, 18, 24 milliseconds. The air and water domain only support propagation of compressional waves and the elastic bottom support compressional, shear, and interface waves.**

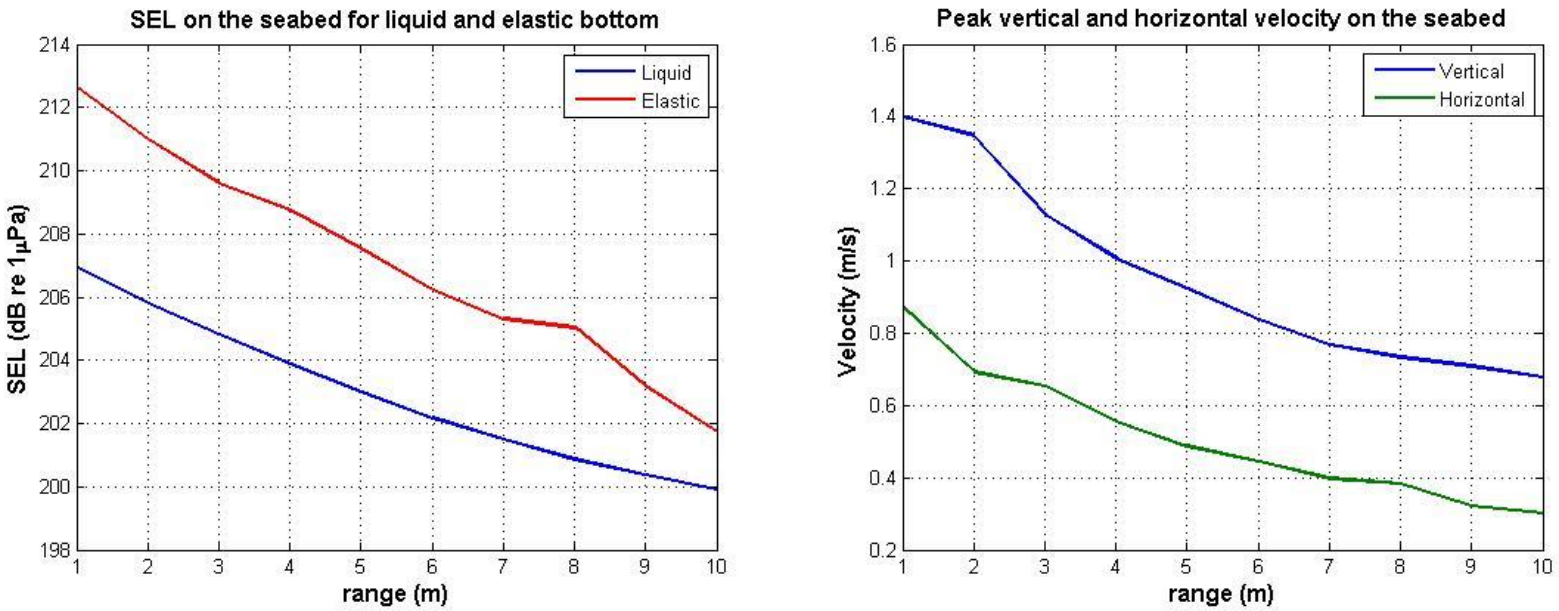

Figure 3.6 **Left panel shows SEL for the fluid and elastic ocean bottom output as function of range up to 10 *m*. Approximately 4 dB higher in elastic bottom FE model due to interface wave effect. The gap of between fluid and elastic bottom is decreasing with decay of interface wave amplitude. Right panel shows vertical and horizontal component of peak particle velocity on the seabed.**

REFERENCES AND LINKS

1. **Reinhall, P.G. and P.H. Dahl, *Underwater Mach wave radiation from impact pile driving: Theory and observation.* The Journal of the Acoustical Society of America, 2011. 130(3): p. 1209-1216.**

2. **Bureau of Ocean Energy Management. *Offshore Wind Energy Resources;* Available from: http://www.boem.gov/Renewable-Energy-Program/Renewable-Energy-Guide/Offshore-Wind-Energy.aspx.**

3. **Erbe, C., *UNDERWATER NOISE FROM PILE DRIVING IN MORETON BAY, QLD.* Acoustics Australia; Dec 2009, Vol. 37 Issue 3, p87, 2009.**

4. **Erbe, C., *Underwater acoustics: Noise and the effects on marine mammals,* 3rd ed. Pocketbook2010: JASCO Applied Sciences.**

5. **Erbe, C., *Effects of Underwater Noise on Marine Mammals, in The Effects of Noise on Aquatic Life,* A. Popper and A. Hawkins, Editors. 2012, Springer New York.**

6. **Wind, D.W. Block Island Wind Farm. 2013; Available from: http://dwwind.com/block-island/block-island-project-overview.**

7. **Reinhall, P.G. and P.H. Dahl. *Acoustic radiation from a submerged pile during pile driving*. in OCEANS 2010. 2010.**

8. **OCEANSAMP. Rhode Island Ocean Special Area Management Plan Available from: http://seagrant.gso.uri.edu/oceansamp/documents.html.**

9. **Ravi Sharma, J.H., Christopher D.P. Baxter, Sau-Lon James Hu, *Development of a Technology Type Factor for Jacket Structures for Offshore Wind Turbines in Rhode Island,* in OCEAN SPECIAL AREA MANAGEMENT PLAN VOLUME 2 2010.**

10. **OceanSAMP GIS Data Download: *Bathymetry*. Available from: http://www.narrbay.org/physical_data.htm.**

11. Simulia, *2.9.1 Coupled acoustic-structural medium analysis, in Abaqus 6.11* PDF Documentation Theory manual 2.9 Coupled fluid-solid analysis2011.

12. Miller, J.H., G.R. Potty, and H. Kim, *Pile driving pressure and particle velocity at the seabed: Quantifying effects on crustaceans and ground fish.* The 3rd International Conference on the Effects of Noise on Aquatic Life, 2013.

13. Potty, G.R. and J.H. Miller and J.F. Lynch, *Inversion for sediment geoacoustic properties at the New England Bight.* Journal of Acoustical Society of America, 2003. 114(4).

MANUSCRIPT – IV

Intended for submission to the Journal of the Acoustical Society of America-Express Letter

Finite Element modeling of offshore impact pile driving noise mitigation with an air bubble curtain in the water column

Corresponding Author:

Huikwan Kim

Department of Ocean Engineering, University of Rhode Island, Narragansett, Rhode Island 02882, hkkim524@my.uri.edu

Contributing Authors:

James H. Miller, Gopu R. Potty

Department of Ocean Engineering, University of Rhode Island, Narragansett, Rhode Island 02882

Abstract: Impact pile driving noise has the potential to be intense enough to harm marine life in the near field and the radiated noise from the pile propagates well along water column in the far field. Researchers investigated and tested different types of noise mitigation technologies such as pile sleeve, the ABC (Air Bubble Curtain), and the HSD (Hydro Sound Damper) etc. Some systems are placed surrounding the pile in the near field and these systems are efficient and relatively low cost but have difficulties covering acoustic energy from ocean bottom. Hence, this study focuses on the relationship between the location of the ABC and acoustic attenuation in the water column assuming the ABC is not affected by ocean current and the same size air bubbles are equally spaced. To accomplish this, we used implicit dynamic analysis in the commercial FE (Finite Element) code Abaqus/CAE 6.11 assuming loading and structural/ acoustical responses are independent of azimuthal angle which enables us to use axisymmetric element with significantly reduced computation cost. We compared SEL (Sound Exposure Level) depending on the location of the ABC system.

PACS numbers: 43.30.Jx, 43.30.Ky, 43.30.Nb

4.1 INTRODUCTION AND BACKGROUND

A. Introduction

Offshore wind turbines are being used by a number of countries to harness the energy of strong, consistent winds that are found over the oceans. Offshore winds tend to blow harder and more uniformly than on land. The potential energy produced from wind is directly proportional to the cube of the wind speed. As a result, increased wind speeds of only a few kilometers per hour can produce a significantly larger amount of electricity. This is one reason that developers are interested in pursuing offshore wind energy resources [1]. However, noise generated by offshore impact pile driving for wind turbine construction radiates into and propagates through the air, water, and ocean bottom. Noise and vibration increase with pile size (diameter and wall thickness) and hammer energy [2-4]. In the United States, offshore wind farms are being planned and construction could begin in the near future along the east coast of the U.S. and one of the offshore wind turbines project, Block Island Wind Farm is a 30-megawatt offshore wind farm to be located approximately three miles southeast of Block Island Rhode Island consisting of 5 turbines. The company will begin transmission construction as early as 2014 and offshore construction in 2015 [5]. Hence it is necessary to investigate how we can mitigate the noise due to these huge offshore wind farm construction planned in the near future.

B. Background

European firms have developed a number of offshore wind turbines and associated noise mitigation technologies which can be classified into two main categories. The primary noise reducing methods with changing the excitation (active method) such as adjusting the parameters of the pile stroke and prolonging the impulse contact time and

using vibrators for small piles instead of impact hammers. The secondary noise reducing methods consist of changing the transmission path (passive method) such as using a pile sleeve or curtain of air bubbles around the pile and putting a foam coated tube as noise barrier over the pile [6, 7]. For the case of pile sleeve system, a pile is surrounded by a sleeve that is made of material with acoustic impedance that is different from that of the medium [7]. This method blocks generated noise due to offshore impact pile driving in the near field and needs relatively low cost. However, it passes noise reflected from the ocean bottom into water because large portion of noise is generated from the part of the pile driven into the sediment. As the depth driven increases and as the bottom gets harder, more acoustic energy propagates through the water from the bottom. To treat this weakness, the ABC system can be used by placing holed hose with larger radius which can trap some amount of acoustic energy from the ocean bottom. Sound propagating in water with air bubbles is subject to a stronger sound attenuation than in pure water because of scattering from resonant bubbles [7]. However air bubbles are easily dispersed by ocean currents and the ABC system is expensive because high pressure air compressor on a ship is required to generate bubbles. Würsig et al [8] did sound testing of the bubble curtain in regard to broadband pulse levels, effects of frequency, and potential reactions of dolphins. Lucke et al [9] placed an air bubble curtain in front of harbor porpoise pool and observed received sound levels and three harbor porpoises' behavioral reaction. More recently, Kuhn et al [10] developed new system called HSD (Hydro Sound Damper) [11]. Their system uses spherically shape forms or air balloons attached on the fishing net instead of natural air bubble from holed hose placed on the ocean bottom. Their prototype

model covering near field from the pile structure as shown in Figure 6 (reproduced from [10]) has been tested during real pile driving and showed large sound attenuation.

This study focuses on one of the passive method for reducing noise from offshore impact pile driving by blocking the noise within the region of the ABC. We observed from our earlier studies that significant amount of acoustic energy propagates into water from the part of the pile driven into the ocean bottom. Furthermore, it increases with increased length of the pile penetration into the bottom. In our FE model, we placed thin solid air medium in the water domain at the distance of 5 m from the outer surface of the pile and observed that the acoustic energy generated from the pile in contact with water can be trapped and showed large attenuation right behind solid air medium. However, the acoustic energy generated by the part of the pile in the ocean bottom and the peak SPL at 15 m from the pile remains intense enough at water-bottom interface. To make the FE model more realistic, we developed vertically located and equally spaced air bubbles in the water column instead of solid air medium, we used environmental data such as approximate water depth and sound speed profile from the measurement off Block Island Rhode Island in summer 2009. The previous studies motivated this quantitative investigation to explore relationship between different locations of the ABC and the corresponding received level. Reinhall and Dahl's FE model with Comsol Multiphysics [12] and our previous FE model with the different location of the ABC considered the sediment as acoustic medium which accounts for the propagation of compressional waves. We extended this approach using elastic sediment which can support propagation of shear and interface waves in addition to compressional waves. We applied reasonable values of attenuation coefficient on the elastic bottom based on the previous study by

Potty et al [13]. Overall conclusion is that the results of our FE model verified the hypothesis that we can achieve more attenuation as we place the ABC further from the outer surface of the pile structure.

4.2 FE MODELING OF IMPACT PILE DRIVING WITH THE ABC

We modeled offshore impact pile driving using the commercial FE code, Abaqus/CAE 6.11. To verify our model is reliable, we developed benchmark model by reproducing Reinhall and Dahl's FE model [12] developed by another commercial FE code Comsol Multiphysics. The major assumption in this study is axisymmetric loading and associated outputs which reduces significant amount of computation cost. Our benchmark model is verified by comparing with Reinhall and Dahl's measured data [12, 14] as described in the Manuscript III. We developed new FE models which includes equally spaced small size air bubbles along the water depth simulating the ABC. The radius of air bubble is 0.02 m and the spacing between adjacent air bubbles is 0.01 m. New FE models simulate offshore impact pile driving noise around Block Island Rhode Island. An approximate water depth of 26 m [15] and average sound speed [16] measured in summer 2009 were used to make this model more realistic. The depth of the pile driven in the bottom is 10 m and we placed vertically spaced 518 air bubbles at 5, 10 m from the outer surface of the pile structure and observed acoustic pressure amplitude time history at 20 m from the pile. The outer edge of numerical boundary, 30 m from the pile is considered as rigid by default. That is to say, the waves are reflected at the outer edge which is condition against non-reflecting boundary as in the liquid bottom. Thus, we limited our total time duration to avoid reflection of propagating waves from outer edges. We applied $0.025\ dB/m$ as attenuation coefficient in the elastic ocean bottom by

inputting Rayleigh damping coefficients $\alpha = 0$ and $\beta = 5 \times 10^{-6}$ when we define material properties of the ocean bottom in property module of Abaqus/CAE 6.11. This paper presents quantitative prediction of acoustic pressure due to impact pile driving without and with the ABC at 5, 10 m. We used implicit dynamic analysis and maximum time duration was set to 0.0377 second and time increment was set to 6.7535e-5 second. We applied pressure impact loading on top of the pile with the expression given by Reinhall and Dahl's published paper [12] as shown in equation (4.3) and t is time after impact and time constant τ is equal to 0.004 second.

$$p(t) = 2.1 \times 10^8 \exp\left(-\frac{t}{\tau}\right) Pa \tag{4.1}$$

The field output request was set to calculate acoustic pressure in Pascal in addition to default setting such as displacement, velocity, acceleration and so on. The history outputs were set to record acoustic pressure time series at the predefined nodes located at ranges of 20 m from the surface of the pile simulating the VLA in the water column and water depths of 6.5, 13, 19.5, and 26 m simulating the HLA. We used 8-node quadratic axisymmetric acoustic quadrilateral element for the air, water domain and 8-node biquadratic axisymmetric quadrilateral element for steel pile and ocean bottom domain. Total number of 271,962 elements and 827,210 nodes are used for the ABC FE models. To prevent reflection from the numerical boundaries from air and water domain, non-reflecting boundary condition was defined along the boundary. This is an acoustic structure interaction problem and the velocity outputs at the nodes on the pile structure in contact with acoustic medium can be converted associated acoustic pressure at the nodes in the acoustic medium. Specific details about FE theory are well described in the manual

[17]. To solve this interaction problem, tie constraints were applied all the contacts in the FE model. For example, the surface of the steel pile interacts with three acoustic media and acoustic media interact at the air-water and water-bottom interface region. To define elastic bottom we did input Young's modulus (E), Poisson's ratio (ν), and density (ρ) because this modeling supports propagation of shear and interface waves due to impact pile driving in addition to compressional waves. We observed this phenomenon in our previous work [18]. Using equation (4.1), we applied Young's modulus of 1,147,000,000 Pa and Poisson's ratio of 0.463 and density of 1,866 kg/m^3 for the elastic sediment to achieve compressional wave speed of 1,750 m/s. The material properties for the other domains are summarized in Table 4.1.

$$C_{p\_elastic} = \sqrt{\frac{E(1-\nu)}{\rho(1+\nu)(1-2\nu)}} \tag{4.2}$$

We placed the ABC at 5 m and 10 m from the surface of the pile. This setting is motivated from the question that how much attenuation we can achieve when we place the ABC at full and half the pile length driven into the ocean bottom. We compared the SEL outputs case by case at different locations of virtual VLA and HLA using the equation (4.3). The expression $\widehat{p_i}(t)$ is acoustic pressure amplitudes time history at pre-defined nodes of interest.

$$SEL = 10\log_{10}\left(\frac{\int_0^{T_0}|\widehat{p_i}(t)|^2 dt}{1\mu Pa^2}\right) \tag{4.3}$$

4.3 RESULTS OF NEW FE MODELS WITH THE ABC SYSTEM

Implicit dynamic analysis available in the commercial FE code Abaqus/CAE 6.11 solves acoustic-structure interaction problem with time dependent pressure loading applied on top of the pile structure [17]. Figure 4.1 shows propagation of Mach wave from the pile in contact with air and water as acoustic medium and ocean bottom as elastic medium. The dynamic ranges for acoustic pressure in Pa and velocity in m/s are consistently applied as legends in the first panel. Four panels show the Mach wave generation and propagated in three different media as time step increases at 6, 12, 18, 14 milliseconds. To extract time history of pressure and velocity amplitudes, the node sets are defined at water depth of 6.5, 13, 19.5, and 26 m and range of 20 m from the surface of the pile with 1 m spacing. Figure 4.2 shows the field outputs when the ABC is located at 5 m from the pile. Overall, the ABC enables to mitigate acoustic energy in the water column.The length of the pile driven into the ocean bottom is 10 meter and the ABC is located at half distance of it. Hence it is observed that the acoustic pressure amplitude of Mach wave reflected from the pile's lower end remains high and it is propagating in the water column. It is contribution of compressional wave in the ocean bottom. It is also observed that high acoustic pressure amplitudes close to the bottom by the contribution of interface wave as shown in the fourth panel of Figure 4.2. The acoustic energy can't be well trapped by the ABC located at 5 m from the pile. In contrast, Figure 4.3 is showing the results of the case that the ABC is located at 10 m from the pile and it is observed that more acoustic energy can be trapped within the range of the ABC. The field output in the third panel in Figure 4.3 shows reduction of acoustic energy in the domain behind the ABC. Overall field outputs show that we can achieve more attenuation when we place the ABC range of the same distance the pile is driven in the bottom.

The field outputs are useful understanding transient phenomenon of the entire domain but these are not showing specific values of the outputs. Thus, we extracted acoustic pressure amplitude time history at the pre-defined nodes of interest. At first, we investigated mitigation of noise with the ABC at mid-water depth (13 m) and water-bottom interface (26 m) as function of ranges. The left panel in Figure 4.4 is showing the SEL outputs with the ABC located at 5 m from the pile. The solid lines with blue and red color show the SEL outputs without the ABC at water depth 13 and 26 m respectively. Blue Square and red circle show the SEL outputs with the ABC located at 5 m from the pile. The SEL is approximately 3 dB re 1 μPa^2 higher within the range of the ABC at 5 m than the one without the ABC because reflected waves by the ABC are superposed with consecutive Mach waves generated from the pile. The SEL output at water depth 13 m is attenuated more than 30 dB in the region right behind the ABC and it is increasing with increased ranges. It is also observed that the SEL in mid-water depth is greatly affected by the existence of the ABC but the SEL extracted along the water-bottom interface remains high with the ABC. This phenomenon is also happening in case of the ABC located at 10 m as shown in the right panel in Figure 4.4.

Lastly, we explored the relationship between noise mitigation and the location of the ABC as shown in Figure 4.5. It is clearly seen that the SEL curves with the ABC located at 5 m and 10 m obtain at least 10 dB re 1 μPa^2 attenuation comparing to the case without the ABC. The highest attenuation (additional 3 dB re 1 μPa^2 more attenuation than the SEL from the results of ABC located at 5 m) can be achieved by placing the ABC at 10 m for this case study. Also, we can observe that the SEL curve without the ABC shows approximately 195 dB re 1 μPa^2 entire water column and the attenuation is

increasing as water depth is shallower for the ABC at 5 m and 10 m. In other words, acoustic energy remains high close to the ocean bottom even if the ABC system for the offshore impact piling location.

4.4 CONCLUSIONS

We have quantitatively investigated the effect placing the ABC to mitigate noise generated by offshore impact pile driving. We developed benchmark FE model using Abaqus/CAE 6.11 in manuscript III and compared our results with measured data in the published paper by Reinhall and Dahl [12]. We extended the benchmark model adding equally spaced sphere shape air medium in the water column with the environmental data off Block Island Rhode Island. Total numbers of 518 spaced air bubbles are placed vertically in the water domain. We modeled cases such as no ABC and the ABC is located at the distance of 5, 10 m from the outer surface of the steel pile structure. To watch how much acoustic energy can be generated from the portion of pile driven into the bottom and reduced by the different locations of ABC, the depth of pile in the bottom is set to 10 m. We watched acoustic pressure field outputs for different time steps showing transient phenomenon of Mach wave propagation by the existence of the different locations of the ABC in the entire domain. We simulated virtual HLA at water depth 13 m and 26 m and VLA at range 20 m to investigate details about the results. The SEL outputs at simulated HLA show that noise attenuation by the ABC at mid-water depth 13 m is more effective than the one on the water-bottom interface (26 m). The SEL at range 20 m shows that noise attenuation can be obtained at least 10 dB re 1 μPa^2 with the ABC in between the pile and receiver location. In this study, the attenuation by the ABC at 10 m gets approximately 3 dB re 1 μPa^2 more than the one located at 5 m.

We found that the distance of the ABC is important to get significant reduction of noise in the water column. The better performance can be achieved by placing the ABC further distance from the piling spot, however, tradeoff study for the cost and feasibility extending the distance of the ABC system should be considered. Also, as the distance is increasing, the region of trapped acoustic energy is increasing. It causes more damage to marine life staying within the region of the ABC system. In addition, we found that the SEL outputs remain high at the water-bottom interface regardless of the location of the ABC system and bottom properties. This gives an idea that the ABC itself which contains vertically spaced small air bubbles has limitation mitigating noise impact along the water-bottom interface. It is necessary to investigate extensively to mitigate the acoustic energy in this region because lots of marine life such as lobsters and flounders live on the ocean bottom.

ACKNOWLEDGEMENTS

I would like to acknowledge the financial support of the Republic of Korea Navy and the Link Foundation Ocean Engineering and Instrumentation PhD Fellowship Program which enabled me to carry out this work at the University of Rhode Island.

TABLES

Table 4.1 Material properties of the FE model without and with ABC located at 5 m and 10 m

Parameters	Air	Water	Bottom	Steel
Density ($\rho, kg/m^3$)	1.21	1,025	1,866	7,831
Bulk Modulus (K, Pa)	117,650	2,358,821,225	-	-
Young's Modulus (E, Pa)	-	-	1,147,000,000	206,800,000,000
Poisson's Ratio(ν)	-	-	0.463	0.3
Compressional wave speed (m/s)	311	1517.1	1,746	5,962
Shear wave speed (m/s)	-	-	458	3,187

FIGURES

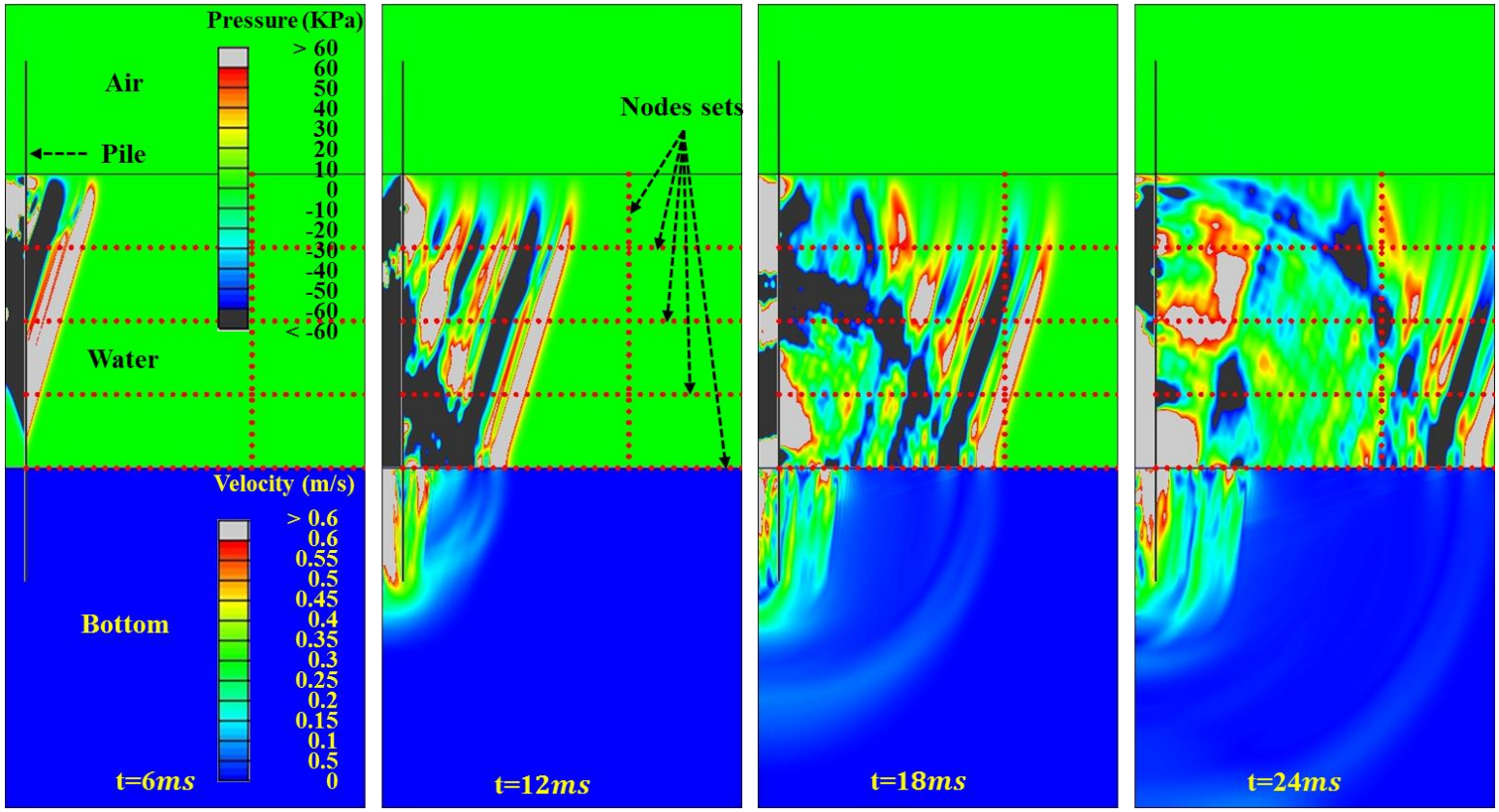

Figure 4.1 **Acoustic pressure and velocity field outputs for evolution of Mach waves due to offshore impact pile driving. There is no ABC placed for this FE model. Same dynamic ranges applied all for panel for consistency.**

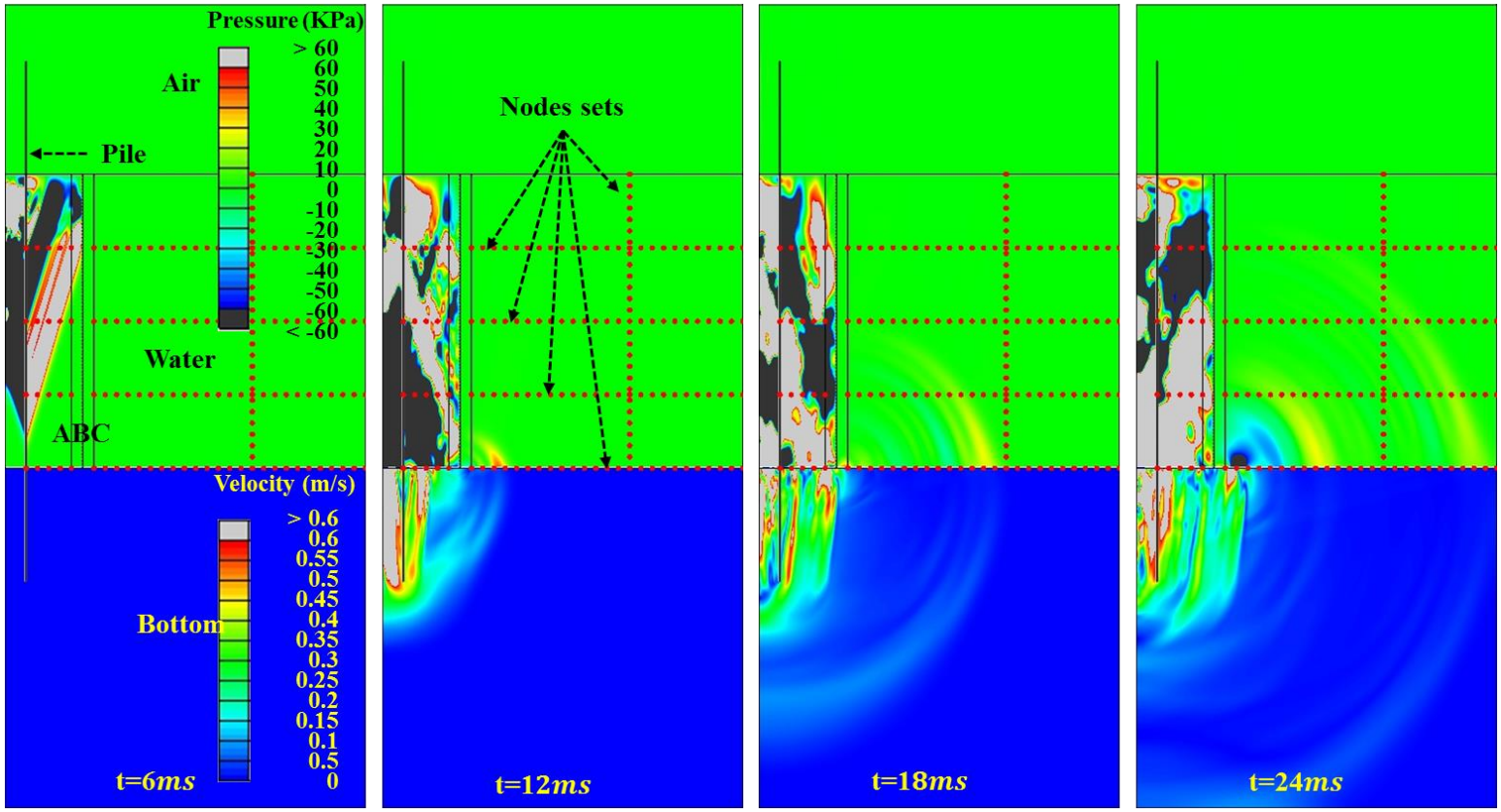

Figure 4.2 **Acoustic pressure and velocity field outputs for evolution of Mach waves due to offshore impact pile driving. The ABC is placed at range 5 m from the pile for this FE model. Same dynamic ranges applied all for panel for consistency**

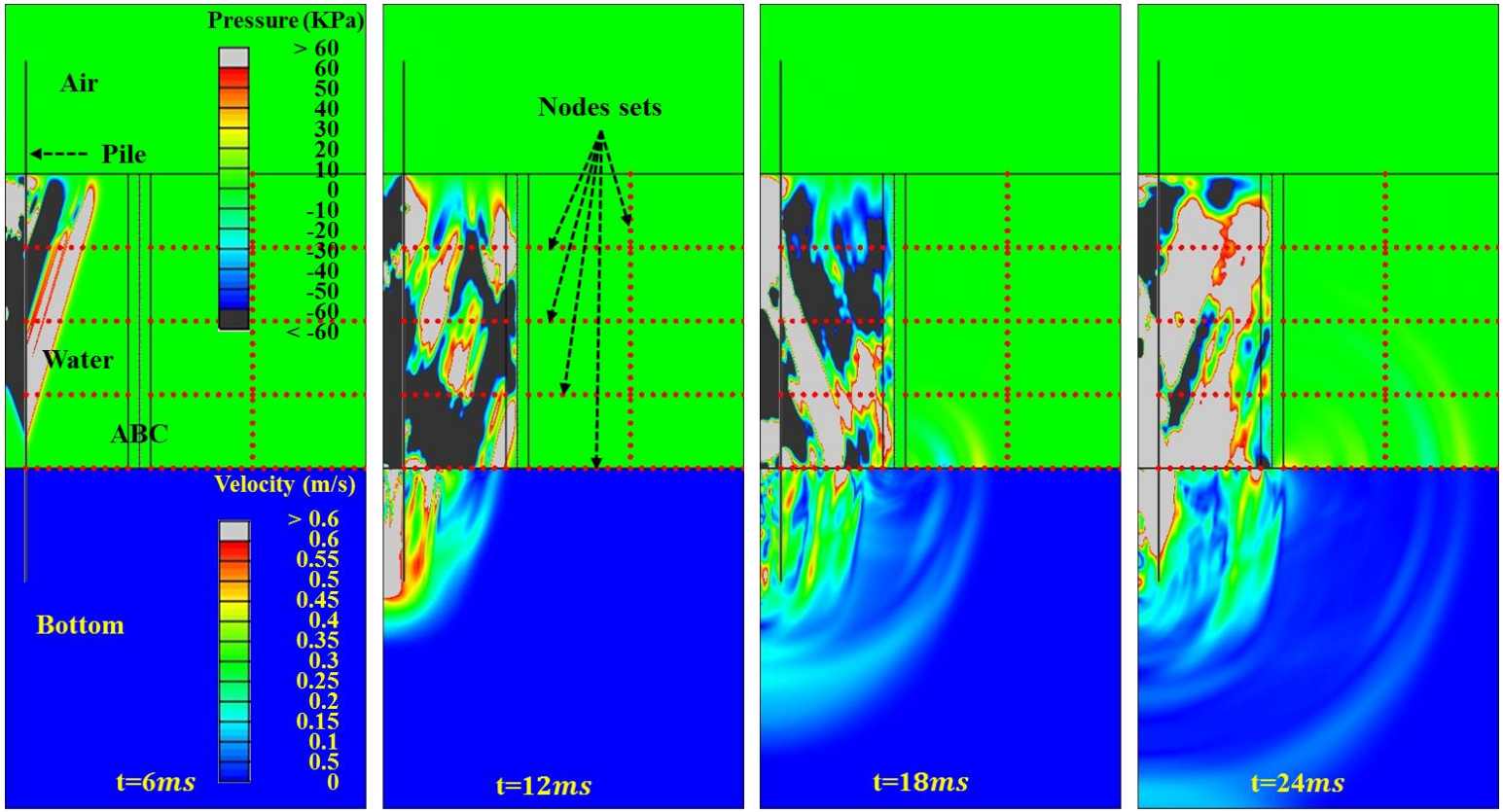

Figure 4.3 **Acoustic pressure and velocity field outputs for evolution of Mach waves due to offshore impact pile driving. The ABC is placed at range 10 m from the pile for this FE model. Same dynamic ranges applied all for panel for consistency**

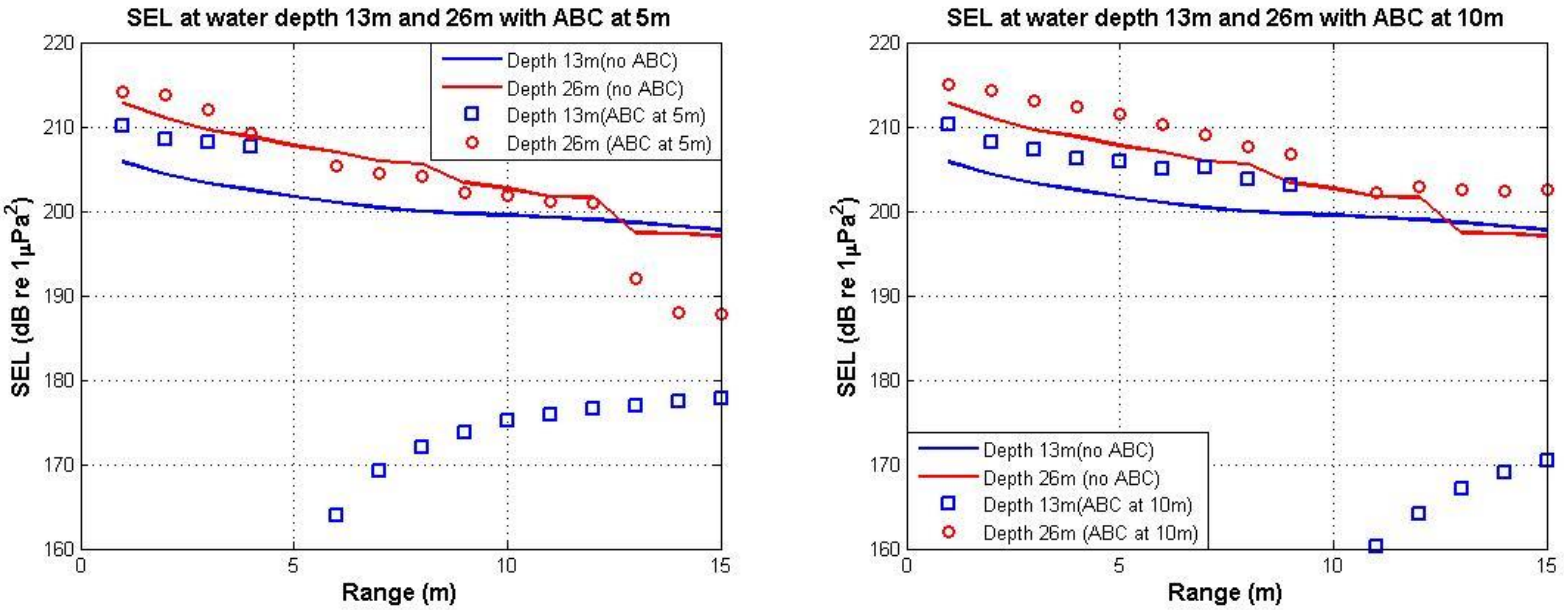

Figure 4.4 **SEL outputs for the case of ABC at 5 m as function of range from simulated HLA located at water depth 13 m and 26 m (left panel). The right panel shows the SEL outputs for the case of the ABC at 10 m.**

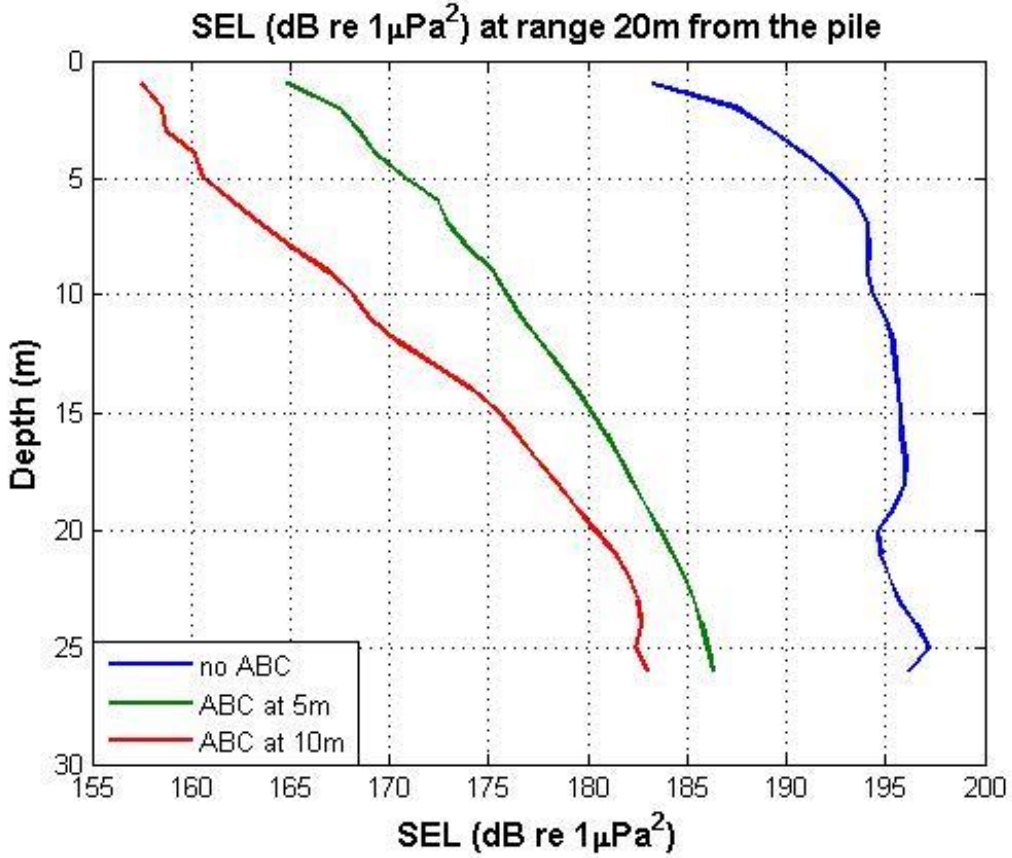

Figure 4.5 **SEL outputs for the case with the ABC at 5 m and 10 m and without the ABC from simulated VLA located at range 20 m**

REFERENCES AND LINKS

1. ***Bureau of Ocean Energy Management*. Offshore Wind Energy Resources; Available from: http://www.boem.gov/Renewable-Energy-Program/Renewable-Energy-Guide/Offshore-Wind-Energy.aspx.**

2. **Erbe, C., *UNDERWATER NOISE FROM PILE DRIVING IN MORETON BAY, QLD.* Acoustics Australia;Dec2009, Vol. 37 Issue 3, p87, 2009.**

3. **Erbe, C., *Underwater acoustics: Noise and the effects on marine mammals, 3rd edn. Pocketbook*2010: JASCO Applied Sciences.**

4. **Erbe, C., *Effects of Underwater Noise on Marine Mammals*, in *The Effects of Noise on Aquatic Life*, A. Popper and A. Hawkins, Editors. 2012, Springer New York.**

5. **Wind, D.W. *Block Island Wind Farm*. 2013; Available from: http://dwwind.com/block-island/block-island-project-overview.**

6. **Elmer, K.H., et al., *Measurement and Reduction of Offshore Wind Turbine Construction Noise*, in *DEWI Magazin Nr. 30, Februar 2007*.**

7. **Matuschek, R. and K. Betke. *Measurements of construction noise during pile driving of offshore research platforms and wind farms*. in *NAG/DAGA 2009 International Conference on Acoustics* 2009.**

8. **Würsig B, G.C.J., Jefferson TA, *Development of an air bubble curtain to reduce underwater noise of percussive piling.* Marine Mammal Research, 2000**

9. **Lucke, K., et al., *The use of an air bubble curtain to reduce the received sound levels for harbor porpoises (Phocoena phocoena)*. The Journal of the Acoustical Society of America, 2011. 130(5): p. 3406-3412.**

10. **Kuhn, C., Bruns, B., Fischer, J., Gattermann, J., Elmer, K.H. *Development of a New Underwater Piling Noise Mitigation System - Using Hydro Sound Dampers (HSD)*. in *31st International Conference on Ocean, Offshore and Arctic Engineering (OMAE2012)*. 2012.**

11. **Kuhn, C., et al.** ***Development of a New Underwater Piling Noise Mitigation System: Using Hydro Sound Dampers (HSD)*****. in** ***ASME 2012 31st International Conference on Ocean, Offshore and Arctic Engineering*****. 2012.**

12. **Reinhall, P.G. and P.H. Dahl,** ***Underwater Mach wave radiation from impact pile driving: Theory and observation.*** **The Journal of the Acoustical Society of America, 2011. 130(3): p. 1209-1216.**

13. **Gopu R. Potty, J.H.M.,** ***Inversion for sediment geoacoustic properties at the New England Bight.*** **The Journal of the Acoustical Society of America, 2003. 114(4).**

14. **Huikwan, K., et al.** ***Long range propagation modeling of offshore wind turbine construction noise using Finite Element and Parabolic Equation models*****. in** ***OCEANS, 2012 - Yeosu*****. 2012.**

15. ***OceanSAMP GIS Data Download: Bathymetry*****. Available from: http://www.narrbay.org/physical_data.htm.**

16. **Crocker, S.E.,** ***Geoacoustic inversion using the vector field*****, in** ***Ocean Engineering*****2011, University of Rhode Island: Narragansett.**

17. **Simulia,** ***2.9.1 Coupled acoustic-structural medium analysis*****, in** ***Abaqus 6.11 PDF Documentation Theory manual 2.9 Coupled fluid-solid analysis*****2011.**

18. **Miller, J.H., G.R. Potty, and H. Kim,** ***Pile driving pressure and particle velocity at the seabed: Quantifying effects on crustaceans and ground fish.*** **The 3rd International Conference on the Effects of Noise on Aquatic Life, 2013.**

APPENDIX A. THEORY OF THE FINITE ELEMENT MODEL

A.1 Motivation and general concepts

The Finite Element Method (FEM) is a powerful computational technique for the solution of differential and integral equations that arise in various fields of engineering and applied sciences. It is useful in many real problems which are defined on geometrically complex domains and may have different boundary conditions on different portions of the boundary. Therefore, it is usually impossible (or difficult) to find a solution analytically and to generate approximation functions required in the traditional variational methods. Main concept of the FEM is that a given domain can be viewed as an assemblage of simple geometric shapes, called finite elements, for which it is possible to systematically generate the approximation functions. The approximation functions are also called shape function or interpolation functions since they are often constructed using ideas from interpolation theory. For a given boundary value problem, it is possible to develop different finite element approximations depending on the choice of a particular variational and weighed-residual formulation [1].

A.2 Major steps of finite element analysis

Finite element analysis includes the following steps and specific derivation of finite element equation for the model problem is described in Zielinski's work [1].

- Discretization of the domain into a set of finite elements (mesh generation).
- Weighted-integral weak formulation of the differential equation over a typical finite element (subdomain)

- Development of the finite element model of the problem using its weighted-integral or weak form. The finite element model consists of a set of algebraic equations among the unknown parameters (degrees of freedom) of the element.
- Assembly of finite elements to obtain the global system (i.e. for the total problem) of algebraic equations – for the unknown global degrees of freedom.
- Imposition of essential boundary conditions.
- Solution of the system of algebraic equations to find (approximate) values in the global degrees of freedom.
- Post-computation of solution and quantities of interest.

A.3 Transient and steady state dynamic analysis

To solve acoustic-structure interaction problems of interest, implicit dynamic analysis using direct integration and direct-solution steady-state dynamic analysis were used in one of the commercial FE codes Abaqus. Implicit dynamic analysis calculates transient response of acoustic-structure interaction problems. In this study, a hydraulic hammer strikes offshore wind turbine support structure. Associated transient pressure, $p(t) = 2.1 \times 10^8 e^{-t/0.004}$, provided by Reinhall and Dahl [2] were applied on top of the pile. The pile is tied with air, water, and ocean bottom media and the FE code calculates structural and acoustical response of coupled system. Transient responses such as, displacement, velocity, acceleration, force, stress in the elastic medium and acoustic pressure in the acoustic media were calculated depending on field/history output requests. In contrast, steady state dynamic analysis calculates the harmonic response of the coupled system. Loading in this analysis type is the frequency dependent pressure amplitude, $P(f) = \int_{-\infty}^{\infty} p(t) e^{-j2\pi ft} dt$, which is calculated by taking the Fourier

transform of transient pressure, $p(t)$. The acoustic pressure outputs on the surface of the pile are complex and they can be used as starting field of long range propagation model, MMPE (Monterey-Miami Parabolic Equation) [3]. Because the MMPE model accepts frequency dependent starting field to initialize the marching algorithm. The transient and steady-state dynamic analysis type can be easily modeled in the GUI environment of finite element commercial code. It is necessary to understand finite element theory on the acoustic-structure interaction problem. Hence, the following section describes the governing equation of the coupled system and the derivation of the variational statement to construct finite element equation for implicit dynamic analysis. Derivation of variational statement for steady state dynamic analysis is similar to transient analysis and details can be obtained in the theory manual [4].

A.4 Acoustic-structure interaction problems using finite element method

One of the commercial finite element codes, Abaqus, provides a set of elements for modeling a fluid medium undergoing small pressure variations and interface conditions to couple these acoustic elements to a structural model. These elements are provided to model a variety of phenomena involving dynamic interactions between fluid and solid media. The equilibrium equation for small motions of a compressible, adiabatic fluid with velocity-dependent momentum losses is taken to be

$$\frac{\partial p}{\partial \boldsymbol{x}} + \gamma(\boldsymbol{x}, \theta_i)\dot{\boldsymbol{u}}^f + \rho_f(\boldsymbol{x}, \theta_i)\ddot{\boldsymbol{u}}^f = 0 \qquad \text{(A.1)}$$

where, p is the excess pressure in the fluid; $\boldsymbol{x}$ is the spatial position of the fluid particle; $\dot{\boldsymbol{u}}^f$ is the fluid particle velocity; $\ddot{\boldsymbol{u}}^f$ is fluid particle acceleration; ρ_f is the density of the

fluid; γ is the volumetric drag; and θ_i are i independent field variables such as temperature, humidity of air, or salinity of water on which ρ_f and γ may depend. The constitutive behavior of the fluid is assumed to be inviscid, linear, and compressional

$$p = -K_f(\boldsymbol{x}, \theta_i)\frac{\partial}{\partial \boldsymbol{x}} \cdot \boldsymbol{u}_f \tag{A.2}$$

where K_f is the bulk modulus of the fluid

A.5 Physical boundary conditions in acoustic analysis

Acoustic fields are strongly dependent on the conditions at the boundary of the acoustic medium. The boundary of a region of acoustic medium that obeys equation (A.1) and (A.2) can be divided into sub-regions S on which the following conditions are imposed:

S_{fp} , where the value of the acoustic pressure p is prescribed.

S_{ft} , where we prescribe the normal derivative of the acoustic medium. This condition also prescribes the motion of the fluid particles and can be used to model acoustic sources, rigid walls (baffles), incident wave fields, and symmetry planes.

S_{fr} , the "reactive" acoustic boundary, where there is a prescribed linear relationship between the fluid acoustic pressure and its normal derivative. Quite a few physical effects can be modeled in this manner: in particular, the effect of thin layers of material, whose own motions are unimportant, placed between acoustic media and rigid baffles. An example is the carpet glued to the floor of a room or car interior that absorbs and reflects acoustic waves. This thin layer of material provides a "reactive surface," or impedance

boundary condition, to the acoustic medium. This type of boundary condition is also referred to as an imposed impedance, admittance, or a "Dirichlet to Neumann map."

S_{fi} , the "radiating" acoustic boundary. Often, acoustic media extend sufficiently far from the region of interest that they can be modeled as infinite in extent. In such cases it is convenient to truncate the computational region and apply a boundary condition to simulate waves passing exclusively outward from the computational region.

S_{fs}, where the motion of an acoustic medium is directly coupled to the motion of a solid. On such an acoustic-structural boundary the acoustic and structural media have the same displacement normal to the boundary, but the tangential motions are uncoupled.

S_{frs}, an acoustic-structural boundary, where the displacements are linearly coupled but not necessarily identically equal due to the presence of a compliant or reactive intervening layer. This layer induces an impedance condition between the relative normal velocity between acoustic fluid and solid structure and the acoustic pressure. It is analogous to a spring and dashpot interposed between the fluid and solid particles. As implemented in Abaqus, an impedance boundary condition surface does not model any mass associated with the reactive lining; if such a mass exists, it should be incorporated into the boundary of the structure.

S_{ff}, a boundary between acoustic fluids of possibly differing material properties. On such an interface, displacement continuity requires that the normal forces per unit mass on the fluid particles be equal. This quantity is the natural boundary traction in Abaqus, so this condition is enforced automatically during element assembly. This is also true in one-dimensional analysis (i.e., piping or ducts), where the relevant acoustic properties

include the cross-sectional areas of the elements. Consequently, fluid-fluid boundaries do not require special treatment in Abaqus.

A.6 Formulation for direct integration transient dynamics

To derive the partial differential equation used in direct integration transient analysis, dividing equation (A.1) by ρ_f, taking its gradient with respect to $\boldsymbol{x}$, neglect the gradient of γ/ρ_f, and combining the result with the time derivatives of equation (A.2) to obtain the equation of motion for the fluid in terms of the fluid pressure:

$$\frac{1}{K_f}\ddot{p} + \frac{\gamma}{\rho_f K_f}\dot{p} - \frac{\partial}{\partial \boldsymbol{x}} \cdot \left(\frac{1}{\rho_f}\frac{\partial p}{\partial \boldsymbol{x}}\right) = 0 \tag{A.3}$$

An equivalent weak form for the equation of motion, equation (A.3), is obtained by introducing an arbitrary variational field, δp, and integrating over the fluid:

$$\int_{V_f} \delta p \left\{\frac{1}{K_f}\ddot{p} + \frac{\gamma}{\rho_f K_f}\dot{p} - \frac{\partial}{\partial \boldsymbol{x}} \cdot \left(\frac{1}{\rho_f}\frac{\partial p}{\partial \boldsymbol{x}}\right)\right\} dV = 0 \tag{A.4}$$

Green's theorem allows this to be rewritten as

$$\int_{V_f} \left\{\delta p\left(\frac{1}{K_f}\ddot{p} + \frac{\gamma}{\rho_f K_f}\dot{p}\right) + \frac{1}{\rho_f}\frac{\partial \delta p}{\partial \boldsymbol{x}}\frac{\partial p}{\partial \boldsymbol{x}}\right\} dV + \int_S \delta p\left(\frac{1}{\rho_f}\boldsymbol{n}^- \cdot \frac{\partial p}{\partial \boldsymbol{x}}\right) dS = 0 \tag{A.5}$$

Assuming that p is prescribed on S_{fp}, the equilibrium equation, equation (A.1), is used on the remainder of the boundary to relate the pressure gradient to the motion of the boundary:

$$\boldsymbol{n}^{-} \cdot \left(\frac{1}{\rho_f} \frac{\partial p}{\partial \boldsymbol{x}} + \frac{\gamma}{\rho_f} \dot{\boldsymbol{u}}^f + \ddot{\boldsymbol{u}}^f \right) = 0 \quad on \quad S - S_{fp} \tag{A.6}$$

Using this equation, the term $\boldsymbol{n}^{-} \cdot \frac{\partial p}{\partial \boldsymbol{x}}$ is eliminated from equation (A.5) to produce

$$\int_{V_f} \left\{ \delta p \left(\frac{1}{K_f} \ddot{p} + \frac{\gamma}{\rho_f K_f} \dot{p} \right) + \frac{1}{\rho_f} \frac{\partial \delta p}{\partial \boldsymbol{x}} \frac{\partial p}{\partial \boldsymbol{x}} \right\} dV + \int_{S - S_{fp}} \delta p(T(\boldsymbol{x})) dS = 0 \tag{A.7}$$

where, for convenience, the boundary "traction" term

$$T(\boldsymbol{x}) = \boldsymbol{n}^{-} \cdot \left(\frac{\gamma}{\rho_f} \dot{\boldsymbol{u}}^f + \ddot{\boldsymbol{u}}^f \right) = -\boldsymbol{n}^{-} \cdot \left(\frac{1}{\rho_f} \frac{\partial p}{\partial \boldsymbol{x}} \right) \quad on \quad S - S_{fp} \tag{A.8}$$

Except for the imposed pressure on S_{fp}, all the other boundary conditions described above can be formulated in terms of $T(\boldsymbol{x})$ which can be referred in Abaqus theory manual [4]. Different definitions for the boundary term, $T(\boldsymbol{x})$ to give the final variational statement for the acoustic medium:

$$\int_{V_f}\left\{\delta p\left(\frac{1}{K_f}\ddot{p}+\frac{\gamma}{\rho_f K_f}\dot{p}\right)+\frac{1}{\rho_f}\frac{\partial\delta p}{\partial \boldsymbol{x}}\frac{\partial p}{\partial \boldsymbol{x}}\right\}dV-\int_{S_{ft}}\delta p T_0 dS$$

$$+\int_{S_{fr}}\delta p\left(\frac{\gamma}{\rho_f c_1}p+\left(\frac{\gamma}{\rho_f k_1}+\frac{1}{c_1}\right)\dot{p}+\frac{1}{k_1}\ddot{p}\right)dS$$

$$+\int_{S_{fi}}\delta p\left(\frac{1}{c_1}\dot{p}+\frac{1}{1_1}p\right)dS-\int_{S_{fs}}\delta p\boldsymbol{n}^{-}\cdot\ddot{\boldsymbol{u}}^{m}dS \qquad \text{(A.9)}$$

$$+\int_{S_{frs}}\delta p\left(\frac{\gamma}{\rho_f c_1}p+\left(\frac{\gamma}{\rho_f k_1}+\frac{1}{c_1}\right)\dot{p}+\frac{1}{k_1}\ddot{p}-\boldsymbol{n}^{-}\right.$$

$$\left.\cdot\ddot{\boldsymbol{u}}^{\boldsymbol{m}}\right)dS=0$$

In this appendix, the procedures defining the variational problem for the coupled field $\boldsymbol{u}^{\boldsymbol{m}}$ and p has been covered. The problem is discretized by introducing interpolation functions: in the fluid $p = H^P p^P$, $P = 1,2,$ ... up to the number of pressure nodes and in the structure $\boldsymbol{u}^{\boldsymbol{m}} = N^N u^N$, $N= 1,2,$ ... up to the number of displacement degrees of freedom. Galerkin method for the structural system; the variational field has the same form as the displacement: $\delta u^m = N^N \delta u^N$. For the fluid, $\delta p = H^p \delta p^P$ has been used but with the subsequent Petrov-Galerkin substitution. This appendix covered derivation of variational statement for direct integration transient dynamics and formulation for finite element equation is described in Abaqus theory manual [4]. A formulation for steady state dynamic analysis is also covered in Abaqus manual [4].

REFERENCES AND LINKS

1. **Zielinski, T.G. *Introduction to the Finite Element Method (Introductory Course on Multiphysics Modelling).* Available from: http://bluebox.ippt.pan.pl/~tzielins/doc/ICMM_TGZielinski_IntroFEM.slides.pdf.**

2. **Reinhall, P.G. and P.H. Dahl, *Underwater Mach wave radiation from impact pile driving: Theory and observation.* The Journal of the Acoustical Society of America, 2011. 130(3): p. 1209-1216.**

3. **Smith, K.B., *Convergence, Stability, and Variability of Shallow Water Acoustic Predictions Using a Split-Step Fourier Parabolic Equation Model.* Journal of Computational Acoustics, 2001. 9(1): p. 243.**

4. **Simulia, 2.9.1 *Coupled acoustic-structural medium analysis, in Abaqus 6.11* PDF Documentation Theory manual 2.9 Coupled fluid-solid analysis2011.**

APPENDIX B. PARABOLIC EQUATION MODEL

B.1 Introduction

The parabolic equation method was introduced into underwater acoustics in the early 1970s by Hardin and Tappert [1], who devised an efficient numerical solution scheme based on fast Fourier transforms. Since then, interest in PE techniques has grown steadily within the acoustic modeling community, to the point that the PE method has now become the most popular wave-theory technique for solving range-dependent propagation problems in ocean acoustics. The description about the standard parabolic equation model in this appendix follows the derivation presented in Jensel et al. [2].

B.2 Derivation of parabolic equations

The starting point is the 3-D Helmholtz equation for a constant-density medium in cylindrical coordinates (r, φ, z),

$$\frac{1}{r}\frac{\partial}{\partial r}\left(r\frac{\partial p}{\partial r}\right)+\frac{1}{r^2}\frac{\partial^2 p}{\partial \varphi^2}\frac{\partial^2 p}{\partial z^2}+\frac{\omega^2}{c^2(r,\varphi,z)}p=0 \tag{B.1}$$

Assuming azimuthal symmetry and hence no dependence on the φ-coordinate, this reduces to the standard 2-D Helmholtz equation,

$$\frac{\partial^2 p}{\partial r^2}+\frac{1}{r}\frac{\partial p}{\partial r}+\frac{\partial^2 p}{\partial z^2}+{k_0}^2 n^2 p=0 \tag{B.2}$$

where, $p(r,z)$ is the acoustic pressure, $k_0=\omega/c_0$ is reference wavenumber, and $n(r,z)=c_0/c(r,z)$ is the index of refraction and ω is the angular frequency and c_0 is the reference sound speed.

There are several ways to arrive at the standard form of the 2-D parabolic wave equation and this section follow Tappert [3] by assuming the solution of equation (B.2) to take the form

$$p(r,z) = \psi(r,z)H_0{}^{(1)}(k_0 r) \tag{B.3}$$

The envelop function $\psi(r,z)$ is assumed to be slowly varying in range and the Hankel function, which satisfies the Bessel differential equation

$$\frac{\partial^2 H_0{}^{(1)}(k_0 r)}{\partial r^2} + \frac{1}{r}\frac{\partial H_0{}^{(1)}(k_0 r)}{\partial r} + k_0{}^2 H_0{}^{(1)}(k_0 r) = 0 \tag{B.4}$$

is generally replaced by its asymptotic form for $k_0 r \gg 1$,

$$H_0{}^{(1)}(k_0 r) \cong \sqrt{\frac{2}{\pi k_0 r}}\, e^{i(k_0 r - \pi/4)} \tag{B.5}$$

Substituting trial solution equation (B.3) into the 2-D Helmholtz equation and making use of the Hankel-function property given in equation (B.4),

$$\frac{\partial^2 \psi}{\partial r^2} + 2ik_0\frac{\partial \psi}{\partial r} + \frac{\partial^2 \psi}{\partial z^2} + k_0{}^2(n^2 - 1)\psi = 0 \tag{B.6}$$

Finally, introducing the crucial paraxial approximation in order to arrive at the standard parabolic equation. Small-angle approximation is expressed by

$$\frac{\partial^2 \psi}{\partial r^2} \ll 2ik_0 \frac{\partial \psi}{\partial r} \tag{B.7}$$

By making use of the paraxial approximation in equation (B.7), the following wave equation is obtained.

$$2ik_0 \frac{\partial \psi}{\partial r} + \frac{\partial^2 \psi}{\partial z^2} + {k_0}^2 (n^2 - 1)\psi = 0 \tag{B.8}$$

This is the standard parabolic equation introduced into underwater acoustics by Hardin and Tappert [1].

B.3 Solution of the standard PE by FFTs

The principal advantage of the parabolic wave equation is that it constitutes an initial-value problem in range and hence can be solved by range marching numerical technique, given a source-field distribution over depth at the initial range. It is started by transforming the entire parabolic equation, under the assumption that the refraction index n is constant. With the forward transform given by equation (B.9) and making use of the transform property in equation (B.10),

$$\begin{aligned} \psi(r, z) &= \int_{-\infty}^{\infty} \psi(r, k_z) e^{ik_z z} dk_z \\ \psi(r, k_z) &= \frac{1}{2\pi} \int_{-\infty}^{\infty} \psi(r, z) e^{-ik_z z} dz \end{aligned} \tag{B.9}$$

where, k_z is the vertical wavenumber.

$$\int_{-\infty}^{\infty} \frac{\partial^2 \psi(r,z)}{\partial z^2} e^{-ik_z z} dz = -{k_z}^2 \psi(r,k_z) \tag{B.10}$$

the transformed wave equation in $\psi(r,z)$ takes the form

$$2ik_0 \frac{\partial \psi}{\partial r} - {k_z}^2 \psi + {k_0}^2 (n^2 - 1)\psi = 0 \tag{B.11}$$

Or by rearranging the terms

$$\frac{\partial \psi}{\partial r} - \frac{{k_0}^2 (n^2 - 1) - {k_z}^2}{2ik_0} \psi = 0 \tag{B.12}$$

Equation (B.12) is linear first-order differential equation with the solution

$$\psi(r,k_z) = \psi(r_0,k_z) e^{-\frac{{k_0}^2 (n^2-1) - {k_z}^2}{2ik_0}(r-r_0)} \tag{B.13}$$

Now if we transform (B.12) back to the z-domain, the field solution becomes

$$\psi(r,z) = e^{\frac{ik_0 (n^2-1)(r-r_0)}{2}} \int_{-\infty}^{\infty} \psi(r_0,k_z)\, e^{-\frac{-i(r-r_0){k_z}^2}{2k_0}} e^{ik_z z} dk_z \tag{B.14}$$

Denoting the range increment $(r - r_0)$ by Δr and introducing the symbol $\mathcal{F}$ for the Fourier transform from the z-domain to the $k_z -$ domain and $\mathcal{F}^{-1}$ as the inverse transform, the field solution can then be written in the compact form

$$\psi(r,z) = e^{\frac{ik_0\{n^2(r_0,z)-1\}\Delta r}{2}}\mathcal{F}^{-1}\left[e^{-\frac{i\Delta r}{2k_0}k_z{}^2\mathcal{F}\{\psi(r_0,z)\}}\right] \quad \text{(B.15)}$$

Equation (B.15) is the split-step marching algorithm proposed by Hardin and Tappert [1] for solving the standard parabolic equation. This study used standard MMPE (Monterey Miami Parabolic Equation) model developed by Kevin Smith [4] and more details can be found in the webpage [5].

B.4 Examples of MMPE results

Based on theoretical background in the previous section, Kevin Smith developed the Monterey- Miami Parabolic Equation (MMPE) model and this model is available in the public domain. Instructions to prepare the input files and post-processing routines are also provided along with the model. This appendix shows two example results of MMPE model which reproduces Fig. 6.11 and Fig 6.12 of Computational Ocean Acoustics [2].

The first example modeled the study of wave phenomena such as mode conversion and mode cutoff during upslope propagation in a wedge-shaped ocean represents one of the earliest successful applications of PE techniques to practical ocean acoustics problems [2]. In this example, a homogeneous ocean with a sound speed of 1500 m/s overlying a homogeneous bottom with a speed of 1700 m/s was considered. The source frequency is 25 Hz and the source depth is 180 m. The principal feature of interest in top panel of Figure B.1 is the radiation of sound into the bottom, both at short ranges and on the slope and bottom panel shows associated input parameters such as sound speed profile in water and bottom and bottom properties.

The second example shown in Figure B.2 modeled long range propagation in deep water at a frequency of 230 Hz. The source depth is 18 m, a prominent seamount blocks propagation via deep refracted paths within the initial 20 km. The seamount has a slope of around 14°, with its peak reaching a depth of just 500 m below the sea surface. The bottom is taken to be homogeneous with a sound speed of 1800 m/s and a density of 1500 kg/m^3 [2].

FIGURES

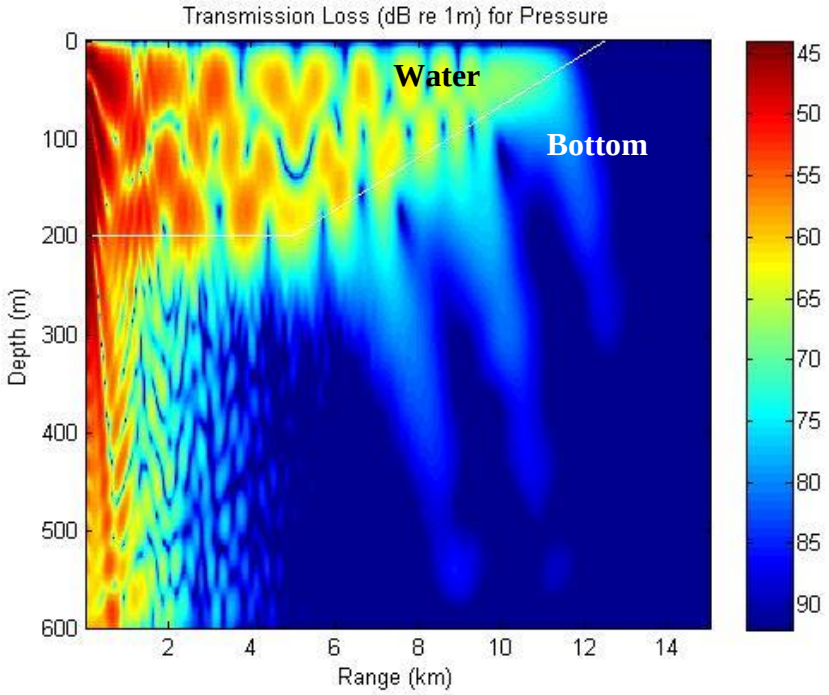


```
SOUND SPEED PROFILE AT RANGE =     0.00 km
    DEPTH(m)    SSPD(m/s)
       0.00      1500.00
    1200.00      1500.00




BOTTOM DEPTH
    RANGE(km)   DEPTH(m)
       0.00       200.00
      12.50         0.00

BOTTOM PROPERTIES
RNG(km) VEL(m/s) GRAD(1/s) DENS LOSS(dB/km/Hz) SHR(m/s) SHRLOSS(dB/km/Hz)
 0.00   1700.00    0.00    1.50     0.2900      0.00    0.0000

DEEP BOTTOM DEPTH
    RANGE(km)   DEPTH(m)
       0.00       600.00

DEEP BOTTOM PROPERTIES
RNG(km) VEL(m/s) GRAD(1/s) DENS LOSS(dB/km/Hz) SHR(m/s) SHRLOSS(dB/km/Hz)
 0.00   3000.00    0.00    3.00     0.2900      0.00    0.0000

FFT size, nz =  1024  and depth mesh, dz =  2.34375000  m.
Range step, dr =  1.00000007E-02  km.
Outputting  1000  points from  0.00000000E+00  km to  15.0000010  km in range
Outputting  256  points from  1.17187500  m to  598.828125  m in depth.
Outputting  1  radials separated by  0.00000000E+00  deg.
```

Figure B.1 Upslope sound propagation in a wedge-shaped ocean with a penetrable bottom (top) and associated input parameters (bottom)

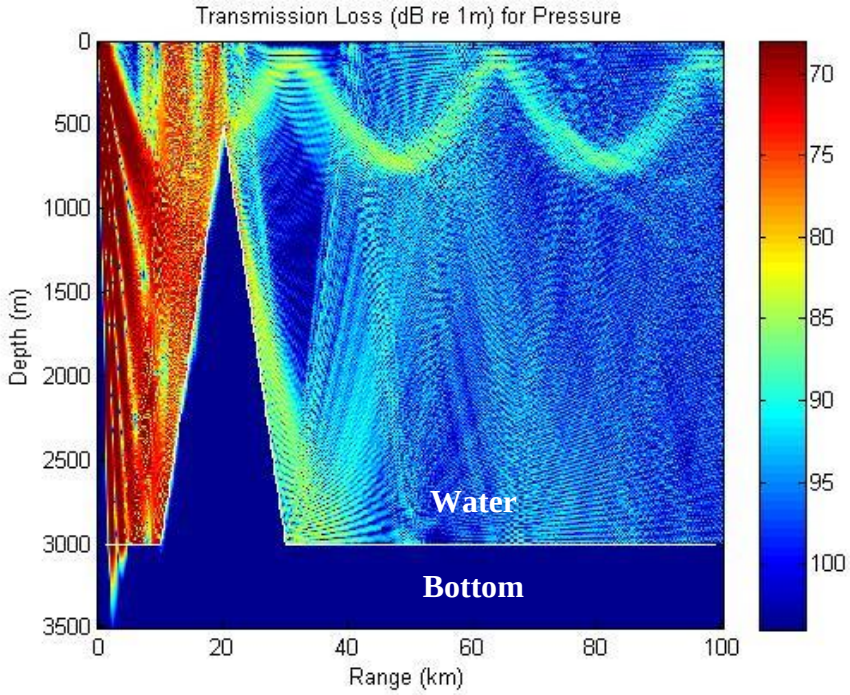


```
SOUND SPEED PROFILE AT RANGE =     0.00 km
    DEPTH(m)    SSPD(m/s)
       0.00      1476.00
      20.00      1478.00
      50.00      1476.00
      80.00      1466.00
     160.00      1473.00
     300.00      1471.00
     800.00      1475.00
    3000.00      1490.00
    7000.00      1517.27

BOTTOM DEPTH
    RANGE(km)   DEPTH(m)
       0.00      3000.00
      30.00      3000.00

BOTTOM PROPERTIES
RNG(km) VEL(m/s) GRAD(1/s) DENS LOSS(dB/km/Hz) SHR(m/s) SHRLOSS(dB/km/Hz)
 0.00   1800.00     0.00    1.50      0.2800      0.00     0.0000

DEEP BOTTOM DEPTH
    RANGE(km)   DEPTH(m)
       0.00      6000.00

DEEP BOTTOM PROPERTIES
RNG(km) VEL(m/s) GRAD(1/s) DENS LOSS(dB/km/Hz) SHR(m/s) SHRLOSS(dB/km/Hz)
 0.00   3000.00     0.00    3.00      0.2800      0.00     0.0000

FFT size, nz =  32768  and depth mesh, dz =  0.427246094  m.
Range step, dr =  6.52173953E-03  km.
Outputting  500  points from  0.00000000E+00  km to  100.000008  km in range.
Outputting  911  points from  0.213623047  m to  3499.35913  m in depth.
Outputting  1  radials separated by  0.00000000E+00  deg.
```

Figure B.2 Sound propagation across a seamount (top) and associated input parameters (bottom)

REFERENCES AND LINKS

1. **Hardin, R.H. and F.D. Tappert, *Application of the split-step Fourier method to the numerical solution of non-linear and variable coefficient wave equation.* SIAM Rev, 1973. 15(423).**

2. **Jensen, F.B., Kuperman W.A., Porter M.B. Schmidt H., *Computational Ocean Acoustics*. 2nd ed, 2011: Springer.**

3. **Tappert, F.D., *The parabolic approximation method in wave propagation in underwater acoustics*, ed by J.B. Keller, J.S. Papadakis (Spinger, New York), pp. 224-287, 1977.**

4. **Smith, K.B., *Convergence, Stability, and Variability of Shallow Water Acoustic Predictions Using a Split-Step Fourier Parabolic Equation Model.* Journal of Computational Acoustics,. 9(1): p. 243, 2001**

5. **Smith, K.B. *MONTEREY-MIAMI PARABOLIC EQUATION.* Available from: http://oalib.hlsresearch.com/PE/MMPE/.**